Optimal Fiber Yield Strength for Concrete Reinforcement

by

Nathan Shapiro

Bachelor of Science
Rutgers The State University of New Jersey
College of Engineering
(1993)

Submitted to the Department of Civil and Environmental Engineering
in partial fulfillment of the requirements for the degree of
Master of Science in Civil and Environmental Engineering
at the

MASSACHUSETTS INSTITUTE OF TECHNOLOGY

February 1995

Author .....
Department of Civil and Environmental Engineering
January 20, 1995

Certified by .....
Christopher K. Y. Leung
Assistant Professor
Thesis Supervisor

Accepted by .....
Joseph M. Sussman
Chairman, Departmental Committee on Graduate Students

Optimal Fiber Yield Strength for Concrete Reinforcement

by

Nathan Shapiro

Submitted to the Department of Civil and Environmental Engineering on January 20, 1995,in partial fulfillment of the requirements for the degree of Master of Science in Civil and Environmental Engineering

ABSTRACT

Steel fibers are the most common type of fiber used to reinforce cementatious materials. They impart ductility and energy absorption to a brittle material. Fibers act to bridge cracks in a matrix and hold it together. Energy is absorbed by yielding the fiber or pulling it out of the matrix. The main objective of this study is to investigate the effect of fiber yield strength on reinforcement efficiency.

An experimental study was carried out on the performance of ductile-fiber reinforced mortar while varying; 1) the fiber yield strength, from the lowest value of 39,900 psi (0.275 GPa) to the highest,170,000 psi (1.171 GPa), 2) matrix strength from 5,000 psi (34.5 MPa) to 12,000 psi (82.7 MPa) and 3) fiber angle, including 0°, 30°, and 60°. A procedure was developed for conducting fiber pull-out tests on specimens embedded with a fiber at an angle. An existing computer code was modified to allow simulation of the experimental results.

The experimental procedure which was developed yielded results which were repeatable, showing that it is an appropriate procedure for the measurement of crack bridging behavior of fibers in a cementitious matrix. Results from fiber optimization experiments showed that a fiber with a yield strength of 138,500 psi was more efficient during pull-out than a commercial fiber with a yield strength of 170,000 psi, in terms of the work needed to fully extract a fiber from a matrix. The computer model predicted pull-out behavior very well for fibers at 0° but underestimated the response for both the 30° and 60° specimens. It is suggested that other mechanisms related to angled fibers need to be incorporated into the simulation to provide a better quantitative prediction.

Thesis Supervisor: Christopher K. Y. Leung
Title: Professor of Civil and Environmental Engineering

ACKNOWLEDGMENTS

There are many people whom I'd like to thank for their moral support, their ingenuity, and for helping me with materials procurement and testing equipment.

First I would like to thank Chris Leung, my advisor and teacher, for having confidence in me to undertake this project and for having ultimate patience while I wrote the paper, I hope he finds this work beneficial.

I'd like to thank my parents and family for giving me their support.

To my two roommates James and Roy for diverting my attention by playing Doom all night long. For proofreading and making themselves available, and for dinner every time I finished two chapters.

Special thanks to Yiping Geng who showed me the ropes and helped with everything.

To Steven and Arthur Rudolph who manufactured the testing devices and always had time to address those last minute, ASAP, rush jobs.

To Uwe Trende and Darmadi Darmawangsa for making the summer enjoyable.

To my friends at home; Lina, Jeff, Alex and Lily who just wanted me to finish my "paper" and come home.

To my friends whom I have worked and studied with this year; Julio Maldonado-Mercado, Kotaro and Megumi Tanaka, Pete Pheeraphan, Numer Ybanez, and Gail Kelly.

To Dr. Germain, Professor Gibson and Chris Swan from Civil engineering; Professor Backer, Yiping and Lotta from Mechanical engineering; and Professor Dunand in Material Science for their expertise and testing equipment.

To the many representatives and their companies whom I bothered and annoyed for months just to get sample wire and materials; Peter Tatnall from Bekaert, Robert Mitchell from Baird Industries, Mike Campbell from Central Wire, Charles Hill from Loos & Co. Inc., Glenn Schaefer from W.R. Grace and the people at Boston Sand and Gravel.

Dedicated to my family with all my love

TABLE OF CONTENTS

LIST OF TABLES

LIST OF FIGURES

1.0 INTRODUCTION

1.1 MOTIVATION

Fiber reinforcement of building materials has been used for hundreds of years. Horsehair and straw were the early additives in bricks to strengthen them against failure. The mechanics and properties of adding these materials to bricks were not known, the only thing that was known was that they improved the brick's strength. Today man-made materials are specifically designed to provide better performance. Fibers are added to a cement matrix to change and improve its basic characteristics.

The use of fiber materials is meant to reinforce brittle matrices, to improve their mechanical properties. Concrete is a well known brittle material which is strong in compression but weak in tension. Fibers increase the flexural strength by reducing and arresting the development of cracks in concrete and improve toughness by providing energy dissipating mechanisms. Fiber reinforcement influences many other characteristics of concrete including shear and compressive strength. The strength and toughness of fiber reinforced concrete is affected many parameters including: properties of the fiber, the matrix and the fiber/matrix interface as well as the size, geometry and volume fraction of fibers.

By studying the effects of the various parameters, a model may be developed. From this model an optimal design for fiber reinforced concrete can be determined.

1.2 BACKGROUND

Fibers require a strong bond with the mortar in order to function beneficially. There are three basic objectives of reinforcing concrete with fiber materials:

1) Improve flexural strength.

2) Improve impact strength.

3) Control cracking and mode of failure by post cracking ductility.

Moreover, while achieving the above three objectives, desirable characteristics of the material in the "fresh state" needs to be maintained.

Since the strain capacity for concrete is very low, one of the primary objectives of fiber reinforcement is to reduce cracking and keep crack widths to a minimum. When concrete initially cracks the fibers resist the tensile forces which are no longer taken by the concrete. The fibers bridge the cracks and inhibit their propagation. Fibers provide a pinching effect at the crack tips to prevent further propagation and create a slow crack propagation stage. This causes many micro cracks to form which do not severely threaten the integrity of the sample. Due to this behavior, fiber reinforcement improves tensile strength, compressive strength, and provides crack control for concrete. In addition steel fibers in concrete are able to absorb large amounts of energy from fracture

due to impact loading. The energy is absorbed by the fibers due to the high energy needed to debond and pull out the fibers.

Fiber types fall into four categories:

1) Metallic - steel, and stainless steel

2) Polymeric - acrylic, polyester, and polyethylene etc.

3) Mineral - glass

4) Naturally occurring fibers - cellulose.

The effectiveness of fiber reinforcement is dependent on the properties of the fibers, concrete, and aggregate. Fiber properties which affect performance characteristics include: strength, stiffness, % volume, length, aspect ratio, and cross sectional area. Important concrete properties depend on compressive strength and type of aggregate used in the mix. The main variables for aggregate are the size of the particles and the volume.

Many of the disputes over fiber reinforced concrete (FRC) stem from the wide range of results obtained during testing. A major contributor to this inconsistency is the non-uniformity of fibers in the concrete matrix. The uniform distribution of fiber reinforcement is dependent upon the characteristics of the aggregate and fibers as mentioned previously. Large aggregate takes up more volume and limits the volume occupied by the fibers. The less volume available for fibers increases the concentration of fibers and leads to the problem of balling. "Balling" is the formation of a large mass of fibers sticking together.

Smaller sized aggregate particles allow fibers to mix uniformly and create useful bonds. A recommended mix is composed of 70% mortar and 30% aggregate with aggregate size between 5 and 10 mm. Fiber volume percentages have been recommended to be a maximum of about 5%. Long fibers tend to cling to each other and bunch together during mixing This occurs especially at high volumes. The use of shorter, "stubby" fibers and lower fiber volume removes the problem of "balling." Several other solutions have been suggested to prevent mixing problems. Steel fibers which are not straight offer a more efficient answer to the problem of fiber volume. For example, fibers which are hooked at the ends provide equal strength with less volume than straight fibers, thereby reducing the volume of fibers needed in the matrix and eliminating the "balling" process.

The definition of a high-performance concrete material usually emphasizes high strength, high ductility, and long lasting durability. These objectives are achieved by the incorporation of additives such as silica fume and super plasticizers. High-strength concrete forms a much stronger bond with aggregate and fibers than normal concrete. The fiber yielding failure mode thus becomes more common for high-strength samples.

1.3 OBJECTIVES

The main objectives of this thesis are:

1) To conduct a brief literature review concerning effects of fiber reinforcement, types of steel fibers available, and applications of steel fiber reinforced concrete in practice.

2) To study the micromechanical modeling of fiber reinforced concrete including the fiber debonding model, important for fibers perpendicular to cracks, and the fiber bending model, important for fibers inclined to cracks.

3) To develop an experimental procedure for the pull-out testing of fibers lying at various angles to the crack.

4) To study the effect of matrix strength and fiber yield strength on the pull-out behavior of steel fiber in a mortar matrix.

5) To Compare experimental results with simulations from a computer model.

1.4 APPROACH

Steel fibers used to reinforce brittle matrices improve the performance characteristics of the matrix under loading conditions. It has been shown by Morton and Groves that the energy expended on fracture and fiber pull-out passes through a maximum at approximately forty five degrees. [1] Chi has also shown theoretically that crack bridging efficiency is affected by fiber yield strength and matrix compressive strength.[2] This investigation studies the effect of fiber yield strength, matrix strength and fiber angle on fiber pull-out behavior

By controlling the matrix strength and fiber inclination while keeping fiber yield strength constant, the pull-out behavior was first recorded. From this data, matrix

---

[1] Morton, J., Groves, G. W., "The cracking of composites consisting of discontinuous ductile fibres in a brittle matrix - effect of fibre orientation", Journal of Materials Science, vol. 9, 1974, pp. 1436-1445.
[2] Chi, J., "Micromechanical Modeling of Ductile-Fiber-Reinforced Ceramics", Masters Thesis, 1992.

spalling strength and optimal fiber angle was determined. A computer simulation was carried out based upon the spalling strength and material properties of the specimens. The simulation was then used to predict fiber pull-out from a matrix. The results from the model were then compared to tests run on specimens using different fiber yield strengths. The optimal fiber yield strength determined from these tests is then compared to the prediction from the model.

Since the results of the experiments will be compared to a computerized modeling program, material properties have to be determined. Various tests of the matrix, wire, and specimens including: concrete cylinder compression test, elastic modulus test, tensile yield strength test for steel wire, are also carried out.

To explain the results of some parts of the experiment, the scanning electron microscope (SEM) was used to measure the spalling length of the matrix. The SEM was also used to explain any anomalous observations during the course of the tests.

1.5 ORGANIZATION

This thesis includes eight chapters. The following provides a brief summary of the contents of each chapter.

The first chapter is an introduction which covers a brief history and description of FRC, an approach to experimentation, organization of this thesis, and the scope of the research.

Chapter two is a literature review. Theory of fiber reinforced concrete and micromechanical theory of fiber pullout is discussed. Previous research papers will be examined and explained and theory applicable to the present work will be reviewed. The final section will review applications and case studies of steel fibers used as reinforcement in concrete.

Chapter three explains the experimental setup. Material selection, test preparation, and testing procedures will be illustrated.

Chapter four is devoted completely to ductile steel fibers. Topics which are covered include: types of fibers, fiber material, and production techniques.

Chapter five covers the tests and their results. The discussion will cover testing parameters and observations. Results will be shown using test plot results and data charts. Comparisons will be made between observations from test results and actual micrographs taken of test specimens.

Chapter six outlines the theoretical simulation. A brief explanation of the model parameters will be given. Proposed changes in the model will be highlighted.

Chapter seven will compare predicted and experimental results using variable fiber yield strengths.

Chapter eight presents conclusions and results. Focus will be on the success or failure of the simulation and on optimization of the results for steel reinforcing fibers.

2.0 LITERATURE REVIEW

2.1 EFFECTS OF FIBER REINFORCEMENT

The addition of fibers to concrete has shown improvement in concrete flexural strength, toughness, enhanced ductility, impact resistance, fatigue strength and resistance to cracking. In addition composite deformation at peak stresses is much greater than plain mortar. Fibers help to alter the behavior of concrete after cracking has begun. The crack bridging behavior of fibers is what improves the ductility of the matrix.[1]

2.2 MECHANISMS OF FAILURE

Increase in crack opening is inhibited by energy supplied to drive mechanisms of failure such as:

1) Fiber debonding
2) Fiber pull-out against interfacial friction
3) Deformation of fibers which lay at oblique angles to the crack face.[2]

Currently there are two theories for analyzing fiber debonding. First is the strength-based approach which is dependent upon the material interfacial strengths. The second theory

[1] Bentur, A., Mindness, S., "Fibre Reinforced Cementitious Composites", Elsevier Applied Science, 1990, pp.1-15.
[2] Morton, J., Groves, G. W., "The cracking of composites consisting of discontinuous ductile fibres in a brittle matrix - effect of fibre orientation", Journal of Materials Science, vol. 9, 1974, pp. 1436

is the fracture-based approach which is based on the strain energy required to break the interfacial bonds between fiber and matrix.

Interfacial friction during pull-out contributes to the ductility of the composite. Energy is transferred from driving cracks to fiber pull-out which also increases the composite strain at failure.

For fibers lying obliquely to a crack, the pull-out force has two components. One due to debonding and pull-out of the fiber and the other due to the bending of the fiber. As the crack opens the fiber is pulled as well as bent. Debonding and pull-out are a function of interfacial bonding and friction between the fiber and matrix. The bending component is a function of the fiber and matrix stiffnesses and strength. Bending of the fiber can result in fiber yielding or breakage as well as spalling of matrix near the fiber exit point.

2.3 FIBER DEBONDING MODEL

2.3.1 STRENGTH BASED FIBER DEBONDING MODEL

Fiber debonding has been studied by several investigators using strength based theories(Gopalaratnum and Shah, 1985, Stang et al, 1990, Naaman et al, 1991). Normal fiber debonding theory says that interfacial fiber debonding occurs once a maximum interfacial strength, τ_s, is reached. Once debonding begins it is assumed that the fiber slips out with a constant friction, τ_i, (Figure 2.1).

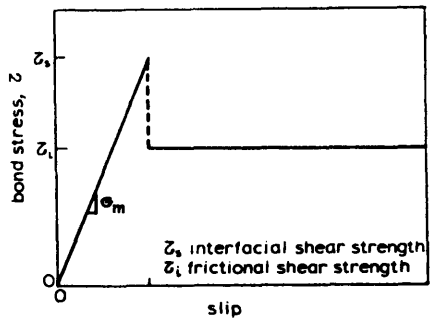

Figure 2.1: Assumed schematic of interface properties for strength based debonding model

2.3.2 FRACTURE BASED FIBER PULLOUT MODEL[3]

Fracture based debonding theory holds that interfacial debonding begins when the interfacial toughness is reached. Debonding continues as a tunnel crack running along the fiber once the interfacial toughness is overcome at the crack tip. From Stang et al a brief explanation of fracture based fiber debonding will follow.

The fracture approach is characterized by the assumption that the propagation of the crack is induced by a certain energy which is associated with the bond between the fiber and the matrix. Thus the energy is proportional to the increase of the debonded zone. This approach is dependent on the idea of the energy release rate which only requires that the loads and deformations be known for the system.

The energy needed to promote crack growth is calculated from the strain energy and the work due to friction at a particular loading and deformation. To calculate the strain energy the system is divided into three parts:

1) The debonded fiber length

[3] Stang, H., Li, Z., Shah, S. P., "Pullout Problem: Stress versus Fracture Mechanical Approach", Journal of Engineering Mechanics, Vol. 116, No.10, October 1990, pp.2136-2149.

2) The bonded fiber length where there is shear lag

3) Strain of the whole system length less than the fiber bonded length

A detailed report on these findings can be found in [Stang, Li, and Shah 1990].

The work due to friction can be calculated assuming that the debonded matrix deformation is constant. Since the force per unit length of the debonded interface is known, assumed constant and is independent of the pull-out history the total work is dependent solely on the relative displacement of the interfaces.

2.3.3 Strength Based vs Fracture Based Theories[4]

The current debonding theories do not make a distinction between strength based and fracture based debonding model, however Leung and Li have proposed conditions to determine when each theory is more appropriate. The debonding theories described above assume that there is a sharp transition between the debonded and undebonded zones of the interface. Leung and Li (1991) proposed that in fact there exists a transition layer between the fiber and the matrix where material breakdown occurs during debonding. Four different cases where determined for combinations of large and small transition zones with large and small ratios of τ_s/τ_i, where τ_s is the interfacial strength and τ_i is the interfacial friction.

Cases I and II are for small τ_s/τ_i ratios. Case I, where a large transition zone exists there is no stress concentration and strength based debonding approach is appropriate. For Case II, with a small transition zone a singularity in the stress field exists therefore a

[4] Leung, C. K. Y., Li, V. C., "Strength-based and Fracture based Approaches in the Analysis of Fiber Debonding", Journal of Material Science Letters, Vol. 9, pp. 1140-1142.

fracture based approach is recommended. Cases III and IV are for large ratios of τ_s/τ_i. Case III and Case IV have a large and small transition zone respectively. A fracture based debonding approach has been recommended for both Case III and IV.

2.4 FIBER BENDING MODEL[5,6]

The crack bridging force of a fiber across a crack can be determined for a given crack opening. Analysis of Leung and Chi (1995) follows results reported by Morton and Groves (1974). Fiber axial force, $F_{db,}$ is determined from axial displacement, u_a. The force, F_l, perpendicular to the fiber can be determined from the fiber end displacement, δ, perpendicular to the fiber axis. To calculate the forces F_{db} and F_l, fiber end displacements must be known. The following equations relate u_a, δ, and l_f to the half crack opening, u, and fiber radius, r, (Figure 2.2):

$$\mathbf{u_a = u\cos\theta} \tag{2.1}$$

$$\mathbf{\delta = u\sin\theta} \tag{2.2}$$

$$\mathbf{l_f = u_a + r\tan\theta = u\cos\theta + r\tan\theta} \tag{2.3}$$

where: l_f is the free fiber length outside the matrix.

θ is the angle the fiber makes with the normal to the crack.

u_a is the axial displacement of the fiber.

δ is the lateral displacement of the fiber.

[5] Morton, J., Groves, G. W., "The cracking of composites consisting of discontinuous ductile fibres in a brittle matrix - effect of fibre orientation", Journal of Materials Science, vol. 9, 1974, pp. 1438

[6] Leung, K. Y., Chi, J., "Derivation of Crack Bridging Force in Random Fiber Reinforced Brittle Matrix Composites through Micromechanics", to appear in ASCE Journal of Engineering Mechanics, 1995.

The fiber was treated as a beam supported on an elastic foundation. The free length, *a*, of the fiber in terms of the crack opening *h* is given by, (Figure 2.3):

$$\mathbf{a = h/2\cos\theta + d/2\tan\theta} \qquad \mathbf{(2.4)}$$

The above equation follows from the equations derived before in terms of half crack opening, u.

where: r = d/2 and a = h/2.

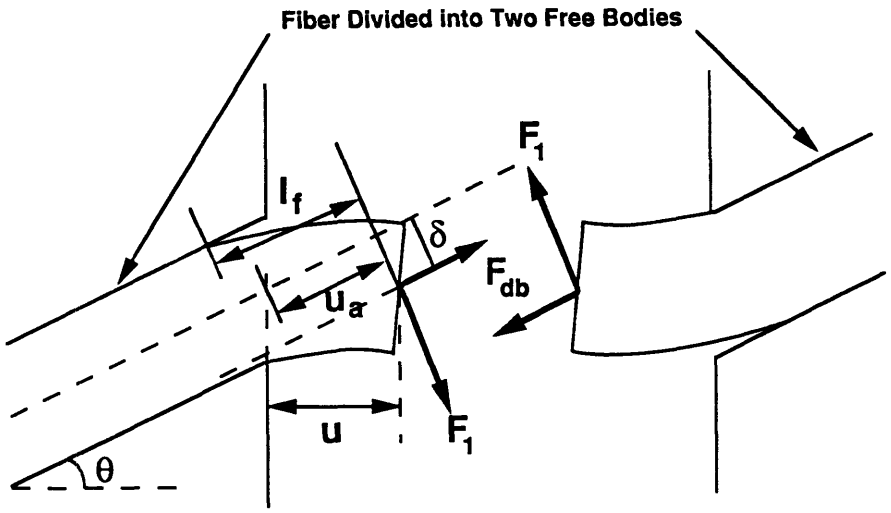

Figure 2.2: Fiber free body diagram bridging a crack, F_1: Bending component of force, F_{db}: Pull-out component of force.

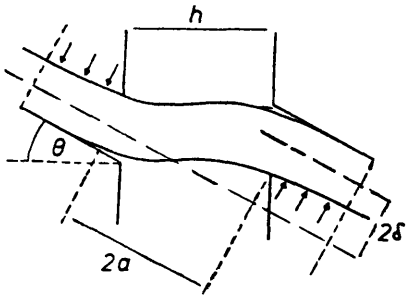

Figure 2.3: Idealization of a fiber bridging a crack at an angle θ when the crack opening is *h*.

Morton and Groves studied metallic fibers embedded in a resin matrix. Fibers were embedded, symmetrically in pairs at an angle 2θ. The force applied to pull out the inclined fibers was compared to that of aligned fibers to propose a theory based on fiber bending and matrix yielding. It was found that a maximum energy input occurred at an angle around 45 degrees. Further more it was observed that for inclined fibers matrix failed in compression at the point of exit thereby removing the assumption that the matrix is rigid. It must also be mentioned that Morton and Groves dealt with a resin matrix which yields, this work is based on a brittle matrix which fails.

2.5 APPLICATIONS OF FIBER REINFORCED CONCRETE (FRC)

Fiber reinforced concrete has many applications due to its increased strength and ductility. However, FRC is not widely used because its long term properties are still being researched. Many contractors are still skeptical of any significant advantages and are uncomfortable with the theoretical and experimental research. Contractors are wary of using new technology in place of widely accepted practices for many reasons including: the need to retrain workers, cost of investment, and liability.

The following is a list of applications for FRC. As structural members, FRC can be used in beams making use of the higher ductility and tensile strength for cracking, and material cost savings. Structural elements can be produced with fibers completely replacing conventional reinforcement. Most uses of steel fiber reinforcement have been for highways, airstrips, repair patching, tunneling, deck slabs and wall panels in

buildings.[7] FRC allows designers to create panels and shell elements which are thinner and lighter for use in apartment buildings and schools thus reducing materials and costs.

2.5.1 SLABS

Fiber reinforced concrete can be used to make slabs for nearly any application including precast slabs, parking garages, slab surface repairs and industrial floor slabs. Significant advantages are realized when conventional reinforcement is completely replaced by the fibers thus reducing cost, time and other logistical problems. Slab thickness can be reduced, which saves material while still retaining or even increasing flexural strength. Slabs can be poured in larger sections with fewer expansion joints and better shrinkage crack control. Since fibers are homogeneously mixed throughout the concrete, reinforcement is present in the entire slab cross-section. The fibers in the upper portion of the slab controls shrinkage cracks. With conventional reinforcement only the lower portion of the slab is reinforced.

Chrysler Jefferson North Assembly Plant: [8]

The new Chrysler Jefferson North Assembly Plant in Detroit, Michigan was designed to cover an area of 1.5 million ft^2(140,000 m^2). Top quality floor slabs are essential for industrial facilities in that they support heavy machinery, resist impact loads

[7] Shah, S. P., Ouyang, C., "Mechanical Behavior of Fiber-Reinforced Cement-Based Composites", Journal of the American Ceramic Society, Vol. 74, #11, November 1991, pp.2727-2738,2947-2953.
[8] Robinson, C., Colasanti, A., Boyd G., "Steel Fibers Reinforce Auto Assembly Plant Floor", Concrete International, April 1991

and must remain stationary and flat to allow equipment to move about easily. Important points to be aware of are shrinkage cracks, joint spacing and slab flexural strength.

The initial slab designs were aimed at reducing cracks resulting from shrinking and reducing the number of expansion joints. Conventional reinforcement was used to control shrinkage cracks in the slab while the joints allow cracks to appear in predetermined locations. However, it is difficult to guarantee that conventional reinforcement will end up in the upper third of the slab where it is needed to control cracks. Fiber reinforced concrete solved many problems with placement and handling, wire mesh was eliminated which reduced labor, workers did not step all over the reinforcement which invariably caused the reinforcement to end up laying on top of the trap rock. Fibers were delivered in special 50 lb (22.7 kg) bags to facilitate easy proportioning, which was one bag of fibers for each truck load. Truck loads were standardized at 10 yd^3 (0.76 m^3) so that each batch contained the same weight in fibers. Fibers were added directly into the truck when it arrived at the site.

The trucks were able to discharge the fiber reinforced concrete directly into the forms inside the plant. If conventional reinforcement was used, rebars would need to be placed in many or all sections ahead of time. This prevented trucks from approaching slab forms in the interior of the building thus creating the need to pump the concrete into position. This type of placement is both time intensive and labor intensive thereby raising costs.

The use of these fibers allowed the contractor to reduce the thickness of the slabs and increase the slab's plan dimensions thereby simplifying finishing details and reducing

maintenance costs. The project was divided into three buildings; The Paint building, Assembly building, and Body shop. In the first two buildings, slab thickness was 5 in. (127 mm) using 50 lb/yd^3 of fibers compared to a normal 6 in. (152.4 mm) depth slab without reinforcement. Expansion joint spacing in the 50 x 50 ft. (15.2 x 15.2 m)bays was increased from $16^2/_3$ x $16^2/_3$ ft. (5.1 x 5.1 m) to 25 x 25 ft. (7.6 x 7.6 m). The Body shop ended up with a $6^1/_2$ in. (165.1 mm) thick slab using 50 lb/yd^3 of fibers compared to a proposed 8 in. slab with #4 rebar @ 12 in. on center or equivalent mesh. Expansion joint spacing in the 70 x 40 ft. (21.3 x 12.2 m) bays was increased from 14 x $13^1/_3$ ft.(4.3 x 4.1 m) to $23^1/_3$ x 20 ft. (7.1 x 6.1 m). The modified joint spacing reduced the amount of control joints by 3 miles (4.8 km).

Costs for the project were not easy to estimate accurately since the use of fiber reinforced concrete in the US was still new. Costs per square foot averaged \$3.20/ft^2. Cost differences can be obtained by comparing with conventional practices. For the Paint building the difference was +\$0.21/ft^2, Assembly building was +\$0.19/ft^2, and the Body shop was -\$0.78/ft^2 yielding a differential of -\$0.38/ft^2. An investigation by the authors of this report concluded that the cost of fibers was less than that to purchase and place wire mesh and addition cost savings were realized due to reduced slab thickness and number of expansion joints.

Parking garages are subjected to some of the worst weather conditions besides marine environments. Parking garages are generally open structures with all surfaces open to the rain, wind and sometimes snow. The interior surfaces suffer from chloride penetration, cracking, spalling and reinforcement corrosion the same as roads and

bridges. Many garages suffer from spalling and corrosion and need to be prepared, however, renovations are hindered by obstacles such as work space limitations, reinforcing bar replacement and cost.

9th & Penn parking garage, Pittsburgh, Pennsylvania: [9]

An example of FRC slabs can be found in use at the "9th & Penn" parking garage in Pittsburgh. Problems encountered at this parking garage included: corroded reinforcement of up to $1^1/_4$ in. diameter, cracking and spalling of deck slabs and separation of deck slabs from underlying 7 x 12 in. (177.8 x 304.8 mm) ribs. Renovation plans called for a complete deck replacement with reinforcement to control shrinkage associated with concrete curing. Designers also wanted to optimize reinforcement to provide for combined flexure strength and crack control to reduce water and chloride penetration. Replacement slabs were reinforced using $^3/_4$ in. steel fibers. This design increased the slab flexural strength by 25-100% over the original design without increasing deadload on the existing structure. Fiber to cement ratio used in the design was 0.152 by weight. The use of short fiber reinforced concrete allowed the garage to operate during restoration and eliminated clumping and "balling" found in mixes with long fibers. The concrete was batch mixed at a plant, pumped into place, finished with a vibratory screed and sealed. Project engineers stated that if the fibers continued to perform as they have, then maintenance costs and crack propagation should decrease.

[9] Mitchell Fibercon, "9th & Penn Parking Garage Renovation", On The Job, CSL 100 2M 0790.

Heathrow Airport parking garage:

FRC has been used in 1971 to construct a multistory parking garage at Heathrow airport. The concrete was cast into slabs 1.1 m^2 (11.8 ft^2) and held together by a steel grid supported by a steel space frame. Problems were encountered due to non-uniformity in fiber distribution and the application was considered impracticable at the time, but today mixing techniques have mostly solved the problem of uniform fiber distribution.

2.5.2 PAVEMENTS

U.S Interstate 10, Louisiana: [10]

End-deformed steel fibers have been used in major highway renovations such as U.S. Interstate 10 between Baton Rouge and New Orleans, LA. The renovation was conducted in three stages starting in 1991. The first stage was a four-lane, five mile long section which used over 25,000 yd^3 (19114 m^3) of cement and 750,000 lb. (340,200 kg) of end-deformed steel fibers. Local construction techniques called for a 10 - 14 in. (254 - 355.6 mm) layer of concrete, sometimes with conventional reinforcement. Site engineers instead used a 4 in. (101.6 mm), fiber reinforced cement overlay on top of an 8 in. (103.2 mm) layer of pavement. Advantages noted due to this project included; material, time, and cost savings. Instead of a full 10-14 in. full depth replacement it was only necessary to lay a 4 in. overlay. Time savings were realized in that similar projects normally take 2-3 years to complete but this project was finished in just six months. Time savings translates into cost savings and shorter time schedule which makes motorists happier.

[10] Mitchell Fibercon, "Fibercon Strengthens I-10", On The Job, CSL 001 8/93.

Costs were also cut because normal renovation practices called for reinforcing bars to be laid every 20 ft thereby increasing labor costs. The roadway was prepared by shotblasting to improve the bonding surface. One hundred and seventy thousand, 5/8 in. holes were drilled to install steel anchoring bars just before the overlay was poured. Ease of construction was so significant that construction averaged 3,000 ft/day with one day recording a full mile.

2.5.3 Marine Structures

The use of FRC in the Marine community is based on the properties of impact resistance and crack control. Impact resistance is needed in jetties, piers, and any place subjected to wear and tear from waves and water borne objects. The main need for FRC in marine structures is for it's ability to control cracks and thereby reducing the possibility of corrosion in the main steel reinforcement. The increased concentrations of salt and water pose a serious threat to concrete especially in the winter months. Salt enters the concrete through cracks at the air-surface interface and migrates to the reinforcement. The salt then corrodes the steel and causes the concrete to crumble and deteriorate. FRC is used in warehouse floors, wharf decking, and jetty armor.

2.5.4 Impact Resistance and Energy Absorption

FRC has a high impact resistance and energy absorption. This is very useful for foundations carrying large machinery which induce large shock and vibratory stresses. For blast structures the fibers resist the complex waves of compression, tension and shear

produced in a blast. These stresses are absorbed by the increased ductility of postcracking and isotropic reinforcement provided by the fibers.

Metal processing yard paving:[11]

Short steel fibers used in slurry infiltrated fiber concrete (SIFCON) have been used for impact resistance in the form of thin panels. To prevent damage to paving around a machine in a metal processing plant, panels were made of SIFCON. The slabs were 1 inch (25.4 mm) thick by 30 inches (760 mm) wide by 10 ft (3.0 m) long. Previous concrete slabs needed to be replaced several times a year due to falling metal, but the SIFCON slabs have not needed to replaced as of the printing of this source

2.5.5 HIGH TEMPERATURE SURFACES

Refractory concrete is concrete specially designed to withstand high temperatures caused by some processes. The proper name for Refractory concretes is "Castables", however "Refractory Concrete" is gaining popularity. [12] Refractory concrete can not be reinforced by conventional steel like normal concrete due to the high temperatures used in the furnaces. Steel fibers can be safely embedded in refractory concrete and have a definite positive effect on its mechanical properties. Both steel and carbon fibers are used as reinforcement. The addition of fibers to castables has an increasing influence on design possibilities, and the control of cracking.[13] Steel fibers added to refractory concretes can

[11] Schneider, B., "Development of Sifcon Through Applications", High Performance Fiber Reinforced Cement Composites, edt. Reinhardt, H. W., Naaman, A. E., RILEM 1992, pp.177-194.
[12] Bakker, W. T., "Refractory Concretes: Past, Present, and Future", ACI Publication SP-57, pp.12.
[13] Robson, T. D., "Refractory Concretes: Past, Present, and Future", ACI Publication SP-57, pp.10.

improve properties including: flexural and impact strength and thermal shock resistance. Resistance to cracking and spalling is significantly increased.[14] Mechanical and thermal stresses needed to cause cracking in refractory materials are higher when fibers are used. Stainless steel fibers are used in most refractories due to their resistance to high temperatures up to 3000° F (1650° C)[15], see Chapter 4. Steel fiber reinforced refractory concrete has been used since 1970 in countries such as France, Germany, England, Australia, and Japan primarily in the steel plants. Applications which use refractory concrete include, foundries, chemical and petroleum processing plants, metallurgical processing, aerospace launching pads, kilns and other related structures. The ability of fibers to inhibit crack propagation make it a useful material for these applications.

Rocket Launch Pad: [16]

Refractory concrete containing steel fibers was used to repair flame exhaust ducts for a launch pad. The concrete was applied by the gunite method using 100 tons of concrete mix to form a 9 in. thick lining. After a launch in 1977 the concrete lining suffered little material loss, reportedly, the concrete lining performed better than any other material previously used. Refractory concretes are subjected to elevated temperatures and environments much more aggressive than what normal portland cements are subjected. For those reasons fibers are used to meet performance requirements. Stainless steel fibers fulfill the requirements for refractory concrete.

---

[14] Lankard, D. R.., "Steel Fiber Reinforced Refractory Concrete", ACI Publication SP-57, pp.241
[15] ACI Committee 506, "State-of the-Art Report on Fiber Reinforced Shotcrete", ACI 506.1R-84, pp.3
[16] Lankard, D. R.., "Steel Fiber Reinforced Refractory Concrete", ACI Publication SP-57, pp.250

Furnace Doors: [17]

Furnace doors and door linings have been produced using fibers for reinforcement. Large doors (20 - 30 ft^2, 6 in. thick) are made for reheat furnaces that operate at temperatures up to 2450 F. Doors made from the fiber reinforced refractory concrete have lasted for two years compared to doors made from normal castables which only last two or three months.

2.5.6 FIBER REINFORCED SHOTCRETE

Fiber reinforced shotcrete is a type of concrete containing discrete fibers applied by a pneumatic or "shooting" method at high velocities to cover a surface. [18] Shotcrete is applied to either plain surfaces or to surfaces lined with reinforcing material such as welded wire mesh or reinforcing bars. Shotcrete containing fibers has been used in applications with and without conventional reinforcement and has proven itself quite capable of performing by itself.

Shotcrete has been and can be used with steel, glass and polypropylene fibers, however, most applications to date use steel fibers. Applications for steel fiber reinforced shotcrete include; slope stabilization, fire protection coatings, refractory linings, dome structures (thin shells), and many underground situations such as, tunnels, mines and other such areas.

---

[17] Lankard, D. R.., "Steel Fiber Reinforced Refractory Concrete", ACI Publication SP-57, pp.246
[18] ACI Committee 506, "State-of-the-Art Report on Fiber Reinforced Shotcrete", ACI 506.1R-84, pp.2

Fiber reinforced shotcrete, like normal fiber reinforced concrete, generally improves material characteristics such as ductility, flexural strength, toughness, impact resistance, and compression resistance; Fibers also reduce rebound losses normally associated with regular shotcrete. Fibers used in shotcrete are produced by the same methods covered in section 4.2, however, some fiber characteristics are crucial for shotcrete. [19] Fiber length and physical deformations are important in that fiber mixing is essential to providing adequate reinforcement. Long fibers cause problems during mixing by clumping together and during the application process they can get caught in the tubing or joints. These problems have been generally eliminated by using shorter fibers to control the mixing problem and plugging in the hoses. joints and elbows in the hoses are eliminated or the angles are lengthened to allow a smooth flow through the hose. The total volume of fibers has been reduced to control clumping. End-deformed, hooked, or otherwise deformed fibers are used to increase toughness and flexure strength losses from using shorter fibers.

Snake River rock slope stabilization - Corps of Engineers: [20]

Steel fiber reinforced shotcrete was used to stabilize a deteriorating rock slope above the Camas Prairie Railroad. The railroad was located near the Little Goose Dam in the State of Washington. The shotcrete was applied to form at least a 2½ in. (63 mm) thick layer covering rock bolts set into the slope. The area involved was approximately

[19] ACI Committee 506, "State-of-the-Art Report on Fiber Reinforced Shotcrete", ACI 506.1R-84, pp.4
[20] ACI Committee 506, "State-of-the-Art Report on Fiber Reinforced Shotcrete", ACI 506.1R-84, pp.7

1550 ft(460 m) long by 15-45 ft(5-14 m) high for a total area of 6900 yd^2. The project was completed in 1974.

Cumberland Gap road tunnel - Parsons Brinckerhoff Quade & Douglas: [21]

The Cumberland Gap road tunnel was designed to relieve the volume traveling along the current, twisting, mountainous, two lane road which services approximately 18,000 vehicles/day. The road is located in the tri-state region between Kentucky, Tennessee and Virginia. This road is the main pass over the mountains between Kentucky and Tennessee. Congestion is a concern for this road especially during the summer when tourists use the road and during the winter in the icy, winter road conditions.

This project is a benchmark for tunneling in the US for several reasons, one among them is that steel fiber reinforced shotcrete was proposed to replace conventional welded wire mesh reinforcement. "Instead of using welded wire mesh for shotcrete reinforcement, we specified the use of fibre reinforcement to meet a given performance specification", explained Bob Leary, geotechnical engineer for the project since 1984. The contractor decided to use 90 lb/yd^3 of 1.5 in. long steel fiber reinforced shotcrete. The fibers were purchased from Bekaert and mixed at a plant to be delivered as a wet mix. Accelerator is added at the nozzle during application.

Steel fiber reinforced shotcrete is used in Norway and other Scandinavian countries, however, it is not widely used in Europe and only recently introduced in the

[21] Wallis, S., "Fibrecrete at Cumberland Gap advances NATM in the US", Tunnels & Tunnelling, June 1992, pp. 23-26

US. Mr. Leary further explains that, "although marginally more expensive at about $100/yd^3$ for unreinforced shotcrete and about $160/yd^3$ for steel fibre shotcrete excluding accelerator ,fibre reinforced shotcrete is much easier to handle than welded wire mesh.", and "it eliminates one labour and time consuming process from the working cycle, reduces rebound, avoids shadows behind the wire mesh, and places where it is needed most to increase the flexural strength of the shotcrete...".

Fire Island Lighthouse: [22]

Fiber reinforced shotcrete has been used in a project to restore the historic Fire Island Lighthouse. The lighthouse was built of brick in 1858 to replace the original built in 1825. A portland cement wash was applied to the brick structure in 1871 and again in 1876, then a protective covering of reinforced concrete was applied in 1912. In 1986 the lighthouse was renovated using shotcrete to cover wire mesh tied to epoxy coated bars. The 1912 coating was removed entirely and then cadmium anchors were installed in the brick. Epoxy coated bars and wire mesh were tied to the anchors. A 2-4" coating of steel fiber reinforced dry mix shotcrete was applied.

[22] Hurd, M. K., "Shotcrete restores Fire Island Light", Concrete Construction, April 1989, pp. 400-401

3.0 EXPERIMENTAL SETUP

3.1 MATERIALS

3.1.1 SAND (FINE AGGREGATE)[1,2,3,4]

Fine aggregates are defined by ASTM to consist of natural sand, manufactured sand, or a combination of both. Both normal and high strength mortar were prepared for these tests. In order to make mortar of sufficient quality the properties of the fine aggregate were tested to see if they compared with requirements. The same fine aggregate was used for all mortar batches, therefore the sand was selected to produce quality high strength mortar.

Workability is a major issue for high strength concrete. Normally water content is reduced to gain higher strength which then requires a water reducer to provide workability. The shape of the sand particles can affect workability, rounded and smooth fine aggregate particles (natural sand) is better for workability than rough jagged edged particles (manufactured sand).

Fine aggregate also have more of an affect on water demand for concrete than coarse aggregate because the fine particles have a greater surface area for a given weight.

---

[1] ASTM C 33 - 92a, "Standard Specification for Concrete Aggregates".
[2] Portland Concrete Association, "High Strength Concrete", PCA Publication EB114, pp.8-9.
[3] ACI Committee 363, "State-of-the-Art Report on High Strength Concrete", ACI 363R-92.
[4] Neville, A. M., Brooks, J. J., "Concrete Technology", Longman Scientific & Technical, 1987, pp.67-70.

The Portland Concrete Association recommends that a coarser fine aggregate be used to produce high strength concrete both for workability and water demand. The PCA suggests a fineness modulus anywhere from 2.7 to 3.2. Other studies have shown that a fineness modulus between 2.5 and 3.1 is adequate, where 2.5 produced a sticky consistency and 3.0 gave the best workability and compaction. Results of the gradation test for the aggregate used in these tests can be found in Table 3.1.

Table 3.1: Grain Size Analysis for Fine Aggregate

Boston Sand and Gravel					
Sieve Size		Mass Retained[c]	Percentage Retained[d]	Cumulative Percentage Passing[e]	Cumulative Percentage Retained[f]
BS[a]	ASTM[b]	(g)			
(1)	(1)	(2)	(3)	(4)	(5)
2.36 mm	8	0	0.0	100.0	0
1.18 mm	16	921	22.8	77.0	23
600 μm	30	1587	39.2	38.0	62
300 μm	50	931	23.0	15.0	85
150 μm	100	436	10.8	4.0	96
<150 μm	>100	171	4.2	---	---
Total = 4046			Total = 266		
Fineness Modulus = 266 / 100 = 2.66					

[a]British Standard sieve opening sizes.

[b]ASTM sieve opening sizes. e.g. #8 sieve has 8 openings per inch therefore opening size = 0.125 in.

[c]Weight of sand retained on each sieve.

[d]Percentage of sand retained on each sieve. e.g. Column 2 divided by the total weight of sand sample.

[e]Taken as 100 percent minus the percent retained on each sieve.

[f]Each cell is the sum of the cells above it and including itself from column 3. e.g. For the cell in column 5, and for sieve #30 it is the sum of the cells in column 3 from sieves #8 to #30 inclusive.

3.1.2 PORTLAND CEMENT[5]

Two different types of Portland cement were used. Type I is a general purpose cement used where special properties are not required. Concrete made with Type I cement is used in pavements, floors, buildings, bridges, pipes and other products. Type I is normal curing cement. Type I was used to mix the 28 day concrete. 28 day concrete yielded concrete with compressive strengths of 10,000 psi and 12,000 psi. Type III cement was used to mix the 7 day concrete. 7 day concrete yielded concrete strengths from 4,300 psi to 6,000 psi. Appendix A, Tables A-1 through A-3 show results from mortar compression tests. Type III cement is early setting cement providing high early strength in the first week. Type III is chemically and physically similar to Type I cement except that the average particle size is ground smaller. Type III is used when forms must be removed quickly, in road repair when service must be restored quickly or in cold weather when it permits a reduction in the controlled curing period.

3.1.3 CONCRETE ADMIXTURES

Finely divided mineral admixtures, powered or pulverized are added to concrete to increase compressive and flexural strength. One such additive is silica fume which is finely ground particles in a liquid form. The small particles help fill the voids in normal concrete to create stronger bonds between the particles.

Another additive is high range water reducer, or superplasticizer. This liquid reduces the amount of water needed in a concrete mix while maintaining workability.

---

[5] Kosmatka, S. H., & Panarese, W. C., "Design and Control of Concrete Mixtures", Thirteenth Edition, 1988, Portland Cement Association, pp. 12 - 24.

3.1.3.1 SILICA FUME[6]

Mineral admixtures are powdered or pulverized material which are added to concrete before or during mixing to improve its plastic or hardened properties. These are generally natural or byproduct materials. They are classified either by their chemical or physical properties as; 1) Cementitious, 2) Pozzolans, 3) Pozzolanic and Cementitious and 4) Nominally inert materials. Silica fume admixture was used in the preparation of the high strength cement mortar mixes. Silica fume is a finely divided mineral admixture.

Adding silica fume greatly increases both compressive and flexural strength of concrete. Force 10,000 is a microsilica based liquid admixture. Concrete produced using silica fume attain strengths greater than 6,000 psi. Silica fume reduces permeability of concrete thus reducing the intrusion of chlorides into the concrete which corrodes reinforcement. Microsilica works in two ways. First, microsilica is essentially pure silica with an average size of ~0.1 μm and hence a high surface to volume ratio. Adding silica fume to cement generally decreases the setting time of concrete therefore requiring a water reducer.

Silica fume is a pozzolanic material, a siliceous material, which, by itself, does not have any cementitious properties. When mixed with water, silica fume reacts with the calcium hydroxide released by the hydration process of the Portland cement, the resulting mix has cementitious properties. Silica fume is a result of high-purity quartz

---

[6] Kosmatka, S. H., & Panarese, W. C., "Design and Control of Concrete Mixtures", Thirteenth Edition, 1988, Portland Cement Association, pp. 67 - 75.

reacting with coal in an electric arc furnace during the production of silicon or ferrosilicon alloy. The fumes from the process condense and are collected in large canvas bags. The silica fume is then processed to remove impurities and control particle size. Surface area is about 20,000 m^2/kg.

Silica fume requires a greater amount of water to be used in the mix, unless a water reducer is used in conjuction with it. Workability is also affected by silica fume thus high range water reducers need to be added. Silica fume can be used as either a replacement for cement or in addition to it from 5% to 10% up to 30% of the total cementitious material weight. Silica fume generally increases concrete strength from 3 to 28 days as compared to control mixes with cement only.

3.1.3.2 HIGH RANGE WATER REDUCER[7]

Water Reducers, or Superplasticizers, reduce the amount of water needed in a concrete mixture and help retain the workability of low water to cement ratio mix. If the amount of water is not reduced then water reducers increase the slump of the concrete from the normal. Water reducers are used in conjunction with admixtures which impart quick setting properties to concrete. The compressive strength of concrete is increased with the use of water reducers due to the decrease in the amount of water. Increases in ultimate compressive strength in excess of 10,000 psi are realized, and increases in high early strength gain are evident. Water reduction can be obtained from 12% to 30%. Reduction in water decreases chloride penetration and steel reinforcement corrosion. Water reducers

---

[7] Kosmatka, S. H., & Panarese, W. C., "Design and Control of Concrete Mixtures", Thirteenth Edition, 1988, Portland Cement Association, pp. 65 - 67.

can be used to make high strength concrete with workability sufficient for consolidation by internal vibration.

Superplasticizers are high range water reducers meeting ASTM C1017 and C494 Types F and G specifications. Water reducers are added to concrete with a low to normal water-cement ratio to make flowing concrete. Flowing concrete is a highly fluid concrete with good workability. Flowing concrete is used in such places as; thin sections, sections with congested and closely spaced reinforcement, pumped concrete to reduce pump pressure, and sections where conventional consolidation techniques are impractical. Flowing concrete is defined by ASTM C1017.

3.1.4 Fiber Types[8]

This research was based on finding the optimal fiber yield strength for fiber reinforced concrete. Wire and fiber samples were gathered from many different sources including an industrial fiber manufacturer, and traditional steel manufacturers. Approximately seven different fiber strengths were collected but only five were included in the experiments. Fiber Yield strengths included: 39.9 ksi, 68.1 ksi, 92. ksi, 138.5 ksi, and 170 ksi. The first four fibers were made from type 304 stainless steel while the fourth was mild carbon steel.

The most common type of stainless steel currently used for fiber reinforcement is type 304 bright basic, in the 300 series. Stainless steel is corrosion resistant, resistant to high temperatures and has good workability.

---

[8] ASTM, "Standard Specification for Steel Fiber Reinforced Concrete", A 820 - 90

3.2 EXPERIMENTAL PREPARATION

3.2.1 OVERVIEW

Several mortar mixes were used as shown in Table 3.2. The material used as the matrix is labeled as "mortar". The mortar had a maximum fine aggregate size of 2.36 mm, the maximum size passing the #8 sieve. The fine aggregate used was sand obtained from a local batch concrete plant and conformed to ASTM specifications C 136 - 92 for sand. The cement used was Type I and Type III Portland cement.

Table 3.2: Details of Matrix Properties

Material	Mix Proportions[a] (cement:sand:water)	Silica fume[b]	High Range Water Reducer[c]	Compressive Strength	Testing Age (days)[d]
(1)	(2)	(3)	(4)	(5)	(6)
Mortar	1.0 : 2.0 : 0.55	----	----	5,000	7
Mortar	1.0 : 2.0 : 0.35	10	1	10,000	28
Mortar	1.0 : 2.0 : 0.28	10	2	12,000	28

[a]Mix proportions by weight
[b]Content is a percent of cement by weight. Calculated amount of silica fume is for solid constituent of liquid silica fume mixture.
[c]Content is a percent of cement by weight.
[d]Curing time for mortar specimens from day of casting to day of testing.

Pull-out specimens were comprised of a mortar matrix with a single steel fiber embedded in it at varying angles. The compressive strength of the matrix, the tensile yield strength of the ductile fibers and the angle of the reinforcing fiber, with respect to the normal of the crack face, were all variable parameters.

Pull-out specimens were cast in brass molds while their companion compression specimens were cast in plastic cylinders, (Figure 3.1). All fibers were embedded 10 mm in the mortar matrix. The first series was comprised of mortar compressive strengths from 5,000 psi to 12,000 psi and were tested at 7 days and 28 days. Specimens were cured from seven to twenty eight days in water storage tanks. The water was saturated with lime to prevent leaching from the mortar.[9] The fibers used were made of mild carbon steel and 304 stainless steel. The second series had specimens made of mortar with a compressive strength of 5,000 psi and were tested at 7 days. The second series used four different fibers all made of 304 stainless steel. The steel fibers in these tests were straight, with a smooth finish, and a round cross section. The pull-out tests were conducted at a monotonic crack opening displacement of roughly 0.00833 mm/sec; each test lasted approximately 20 minutes.

3.2.2 Specimen Preparation

Three concrete mixes with different strengths were used in these experiments; 5,000 psi (34.5 MPa), 10,000 psi (68.9 MPa), and 12,000 psi (82.68 MPa). The 5,000 psi mix was tested at seven days using Type III, quick setting cement. The 10,000 psi and 12,000 psi mixes were tested at 28 days using Type I, normal setting cement. Mixing proportions were taken from [Quang Li 1994], varying the water to cement ratio, silica fume, and high range water reducer. Each batch of mortar yielded twelve to eighteen pull-out specimens and four cylinders. The pull-out specimens were 1" (25.4 mm) by 1/2" (12.7

[9] ASTM C 511 - 85, "Standard Specification for Moist Cabinets, Moist Rooms, and Water Storage Tanks used in the Testing of Hydraulic Cements and Concretes"

mm) by 1/2" (12.7 mm) thick, (Figure 3.2). Fibers were inclined at an angle to the normal of the crack face. Specimens were prepared with fibers inclined at three different angles, 0°, 30° and 60°, (Figure 3.2). The compression specimens were cylinders with a diameter of 3 in. and a height of 6 in. The matrix properties of the pull-out specimens were taken from tests conducted on the cylinders, including the elastic modulus and compressive strength tests. Table 3.3 displays the specifications for the experimental program.

Table 3.3: Pull-out Specimen Specifications

Test Series	Mortar Compressive Strength[a]	Tensile Fiber Yield Strength[b]	Fiber Angle[c]
	(psi)	(psi)	(degrees)
1	5,000	170,000	0°, 30°, 60°
2	10,000	170,000	0°, 30°, 60°
3	12,000	170,000	0°, 30°, 60°
4	5,000	39,900	0°, 30°, 60°
5	5,000	68,100	0°, 30°, 60°
6	5,000	92,200	0°, 30°, 60°
7	5,000	138,500	0°, 30°, 60°

[a]Compression tests on 3 to 4, 3 in. x 6 in. cylinders following ASTM specifications.
[b]Fiber yield strength determined by 2% offset yield.
[c]Fiber angle measured from normal to crack face. See Figure 3.

3.2.2.1 MORTAR MIXING PROCEDURE[10]

For the mixing of mortars and pastes ASTM recommends an electrically driven mechanical mixer. The mixer should be of an epicyclic type, imparting both a planetary

[10] ASTM C 305 - 91, "Standard Practice for Mechanical Mixing of Hydraulic Cement Pastes and Mortars of Plastic Consistency"

and a revolving motion to the mixing paddle with a minimum of two speeds. The mixing bowl should be removable and made of stainless steel. The bowl should be equipped in order to be held firmly during mixing. The paddle should be the type that follows the inside contours of the bowl allowing a clearance of about 4.0 mm. A Kitchen Aid type kitchen mixer met all of the specifications for the mixing apparatus, (Figure 3.3). The mortar mixing procedure was as follows:

1) Mix all of the liquid constituents together first: Add the water, silica fume, and high range water reducer to the mixer, note: for the 5,000 psi mortar, only water was used.
2) Add cement to the liquid and mix on low speed for 30 seconds.
3) Add entire amount of sand to mix over a 30 second period at slow speed.
4) Change speed to medium and mix for 30 seconds.
5) Stop the mixer and let stand for 1.5 minutes. scrape down sides of bowl.
6) Finish by mixing for another 1.5 minutes at medium speed.

The normal strength mortar mixture, had a liquid consistency. The high strength mixtures exhibited very dry conditions during initial stages of mixing. Mortar consistency was that of moist paste after mixing.

3.2.2.2 FIBER PREPARATION

Most of the fibers used in these experiments were hand made from wire. Currently most fibers used in the industry are deformed in some way, either flat and crimped or round and crimped or hook ended. Fiber yield strengths are for the most part constant from

manufacturer to manufacturer. For the purposes of this investigation to study the basic interaction between fiber and mortar, only straight, round fibers were needed. Due to the unavailability of this product in variable tensile yield strengths, it was necessary to make fibers from special order wire. Wire was received on spools which was then cut to length of approximately 22 mm and straightened. The embedded end of the fiber was ground smooth and perpendicular to the longitudinal axis of the fiber. The fibers were then dipped in acetone to clean off any oil or impurities which might affect mortar curing and interfacial bonding between the fiber and matrix. The unfinished end of the fibers were inserted in the plexiglass pieces so that the finished end was left to be cast in the mortar.

3.2.2.3 MOLD PREPARATION

The brass molds are separated into six sections, each section was one inch square, (Figure 3.4). Plexiglass dupes were made to hold the fibers in the desired configuration for the specimens. The dupes were the same size as the specimens, 1 in. by 1/2 in. by 1/2 in. thick, (Figure 3.5). Each plexiglass piece was fitted with a steel fiber, (Figure 3.6). The face of the plexiglass block was coated with form release oil to facilitate specimen separation. The inside surfaces of the mold were also coated with form release oil in order to remove the specimens with out damaging them. Care was taken to make sure that the fiber surface was not contaminated with the form release oil. Plexiglass pieces were placed in the mold prepared for specimen casting, (Figure 3.7). During casting the molds were placed on a vibrating table to expel entrapped air. The molds were then allowed to cure for 24 hours before placing the specimens in the curing tanks.

3.3 TESTING PROCEDURES

3.3.1 FIBER PULL-OUT TEST

The rig for the pull-out test was comprised of two loading chains perpendicular to each other, (Figure 3.8), and was originally designed for the mix mode pull-out test. Here, only one chain was required for the direct pull-out experiments. The chain long the pull-out direction is referred to as the pulling chain and the one perpendicular to it is the lateral chain. the experimental set-up procedure was as follows:

(1) Mortar specimens were first attached to a vice corresponding to the fiber angle being tested, (Figure 3.9).

(2) The vice was then screwed together and a set screw was tightened to further clamp the fiber in position.

(3) A target was then screwed to the top of the vice to be used in conjunction with the displacement transducer mentioned later.

(4) An "L" shaped support bracket was attached to the lateral chain, (Figure 3.10).

(5) The vice was then mounted onto the end of the pulling chain by four symmetric screws, (Figure 3.11). Both the vice and bracket were checked so that they were orthogonal to the planes of the testing rig.

(6) The sides of the pull-out specimen were coated with 5-minute epoxy.

(7) The pulling and lateral chains were slid toward each other until the specimen was firmly held in place, (Figure 3.12). The "L" bracket, in the top portion of the figure and the block in the bottom of the figure provided lateral support for the specimen. The pulling chain was adjusted so that the back face of the specimen was in contact with the bracket.

(8) The epoxy was left to dry for 30 minutes.

(9) Another bracket was then screwed to the back of the "L" support bracket in order to setup the linear voltage displacement transducer(LVDT).

(10) The LVDT was positioned so that the tip touched the target on top of the vice, (Figure 3.13). The LVDT was capable of measuring a displacement of .25 in.

(11) The motor, visible in the upper right corner of Figure 3.8, was attached to the cog on the pulling chain and turned on. The applied force from the motor pulled the fiber out of the specimen.

(12) The displacement of the target was recorded by an automatic data acquisition system. The tensile force applied on the fiber was measured using a 50 lb load cell placed as part of the pulling chain.

3.3.2 Elastic Modulus[11]

The mortar cylinders were put in a pair of collars as seen in (Figure 3.14). The two collars were 57 mm apart and parallel to each other. They were connected by three

[11] ASTM C 469 - 87a, "Standard Test Method for Static Modulus of Elasticity and Poisson's Ratio of Concrete in Compression"

vertical "pins" which were fastened to the lower collar and unrestrained with respect to the upper collar. Each of the collars were firmly attached to the cylinder by three "set screws" equally spaced around the cylinder in order to provide a uniform attachment. Two direct current displacement transducers (dcdt's), were attached to the upper collar. The dcdt's were placed diametrically opposed to each other. The two displacement readings were then averaged to obtain the shortening of the cylinder under compression. The cylinders were first loaded to about 10% of their compressive strengths several times to initialize the dcdt's. Following the initialization, two trials were conducted up to 40% of the cylinders' compressive strength. The load was applied at a rate of approximately 35±5 Psi/s (241±34 kPa/s) on a 70 kip Baldwin machine. Using the displacement and loading data, stress-strain curves were constructed. The average of the slopes of the linear regions were taken as the elastic modulus for the cylinder. Within each batch the average value was calculated following ASTM specifications. The elastic modulus was calculated to the nearest 50,000 Psi as follows:

$$E = (S_2 - S_1)/(\varepsilon_2 - 0.00005) \qquad (3.1)$$

Where E is the chord modulus of elasticity in Psi, S_2 is the stress corresponding to 40% of the ultimate load, S_1 is the stress, in Psi, corresponding to a longitudinal strain, ε_1, equal to 50 millionths, and ε_2 is the longitudinal strain produced by stress S_2. Results of elastic modulus tests are presented in Appendix B, as well as some sample plots of linear elastic regions of stress-strain diagrams.

3.3.3 COMPRESSIVE STRENGTH[12]

This test was used to evaluate the compressive strength of the cement mortar cylinders in this test. Mortar cylinders were cast in plastic molds with a diameter of 3 in. and height of 6 in.. Tests were conducted within six hours after removing the specimens from the curing tanks and capping. During capping, the specimens were kept moist by covering them with a wet towel. Compression tests for the high strength mortar cylinders were conducted using a 200 kip Baldwin machine with a digital control and automatic data acquisition system, (Figure 3.15). The tests were monotonic displacement controlled at 0.01 in/min. as prescribed by section 7.5 of the ASTM guidelines.

3.3.4 SAND ANALYSIS[13]

Sieve analysis is used to determine the distribution of particle sizes in fine and coarse aggregate. The sand must first be dried adequately by an oven capable of maintaining a uniform temperature of 110 ± 5° C (230 ± 9° F). A suitable range of sieves was selected to determine suitability for mixing concrete and conformity with specifications for sand and fine aggregate. The sieves were stacked from the coarsest on top to the finest on the bottom. A sample was weighed and poured into the stack of sieves. The amount of aggregate in each sieve was weighed and the sum was compared with the original value. The total weight of the sample after sieving cannot be more than 0.3% off the original

---

[12] ASTM C 39 - 86, "Standard Test Method for Compression Strength of Cylindrical Concrete Specimens"

[13] ASTM C 136 - 92, "Standard Test Method for Sieve Analysis of Fine and Coarse Aggregates"

weight, if so then the procedure must be redone with a new sample. Calculate the percentage of the sample retained and passing each sieve.

The fineness modulus of fine aggregate is important when mixing high strength concrete. To calculate the fineness modulus take the sum of the cumulative percentage retained for each sieve. The cumulative percentage retained is the sum of the percentage retained on the sieve and those of sieves more coarse. The sum of the cumulative percentage retained is then divided by 100.

3.3.5 TENSION TEST OF METALLIC WIRE[14]

The following guidelines from ASTM cover the tension testing of metallic materials in any form, specifically, the methods of determination of yield strength, yield point, tensile strength, elongation, and reduction of area. Tension tests provide information on the strength and ductility of materials under uniaxial tensile stresses.

Testing equipment used to conduct tension testing must conform to guidelines in ASTM E 4. Any type of gripping device may be used so far as it transmits the measured load applied by the machine to the test specimens, (Figure 3.16). The axis of the test specimen must match the center line of the heads of the testing machine. Any deviation may cause bending stresses to be induced which are not included in the normal calculation, $\sigma = \frac{P}{A}$. Grips such as the wedge or the snubbing types as shown in Figures 3.16 and 3.17, or flat wedge grips may be used.

---

[14] ASTM E 8M - 93, "Standard Test Methods for Tension Testing of Metallic Materials [Metric]"

To determine the yield strength by the offset method, it is first necessary to gather data from tests with which to create a stress-strain diagram. On the stress-strain diagram draw a line Om equal to the value of the "offset", (Figure 3.18). The offset is a value of strain for which a certain amount of error is accounted for. Plot a line parallel to the linear elastic range of the stress-strain diagram from the end of line Om. The intersection of this line and the diagram is point r, the yield strength at the specified offset. When reporting the values of yield strength found in this manner it is necessary to state the offset in parentheses following the words "Yield Strength", thus for a 0.2% offset:

Yield Strength (offset = 0.2%) = 400 MPa.

Tension testing of wire, especially wire of the diameter used in these experiments, is very difficult. A great deal of effort was put into gathering and preparing testing machines and devices suitable for the testing of this wire. However, due to the lack of finely sensitive extensometers, it was not possible to gather precise strain data to determine elastic modulus. Strain data used to create the stress-strain diagrams in Appendix C were taken from the initial separation of the gripping devices and the displacement of the crosshead during testing. Appendix C presents stress-strain diagrams from tensile tests performed on each wire sample including tables of collected data.

Figure 3.1: Plastic molds used to cast 3 in. x 6 in. mortar cylinders

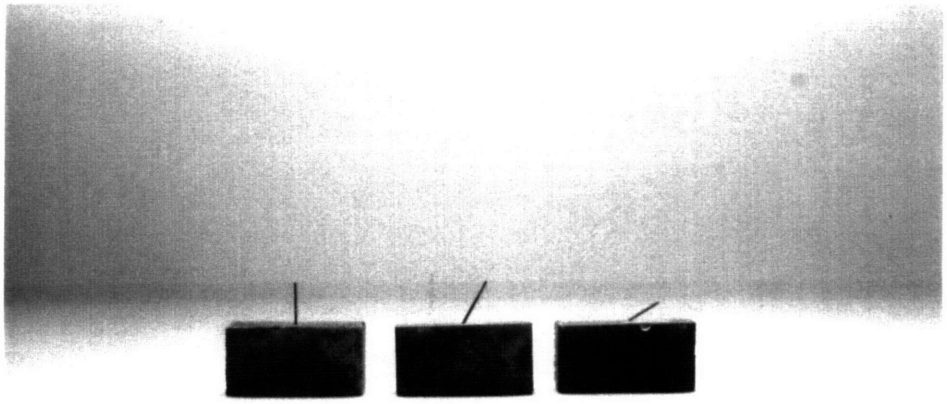

Figure 3.2: Specimens cast with fibers at 0°, 30°, and 60°

Figure 3.3: Mechanical Mixer and Removable Bowl

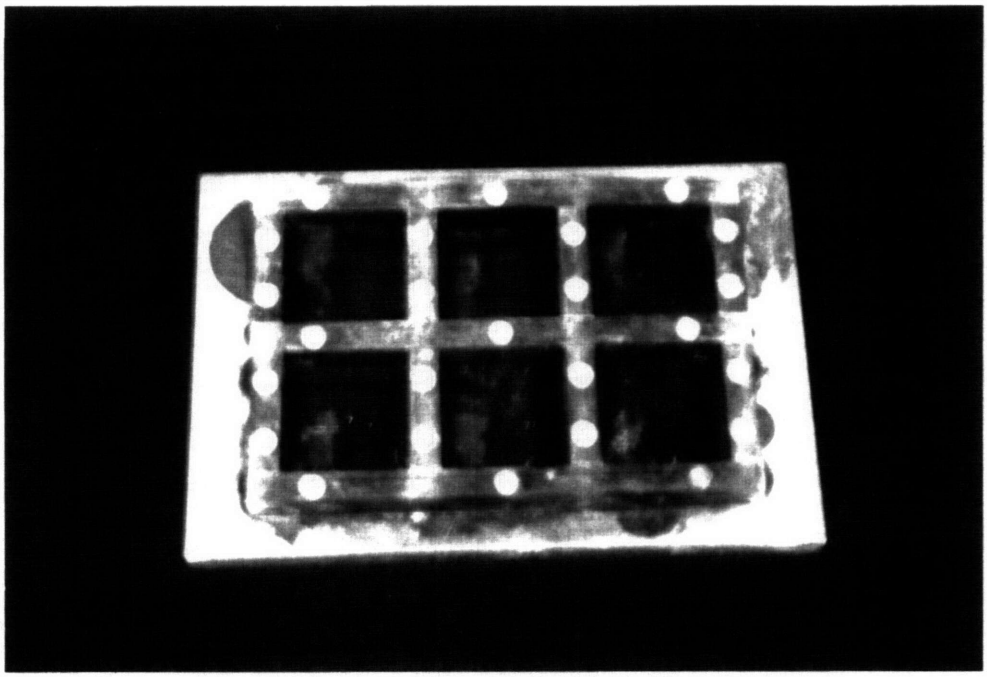

Figure 3.4: Brass mold used to cast specimens, divided into six sections

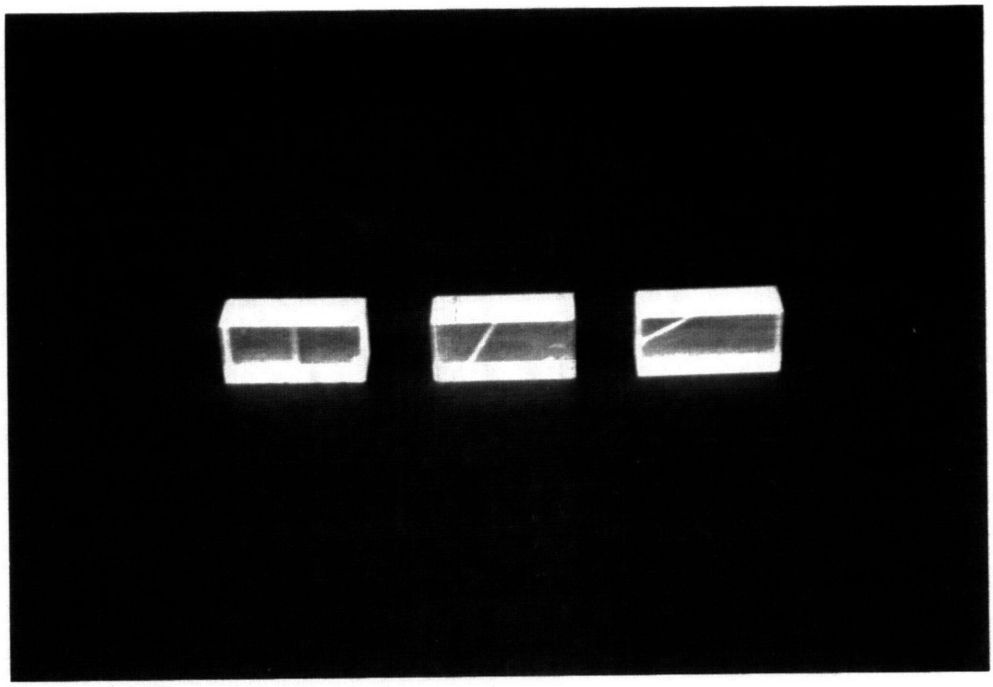

Figure 3.5: Plexiglass blocks used to cast specimens, 0°, 30°, 60°

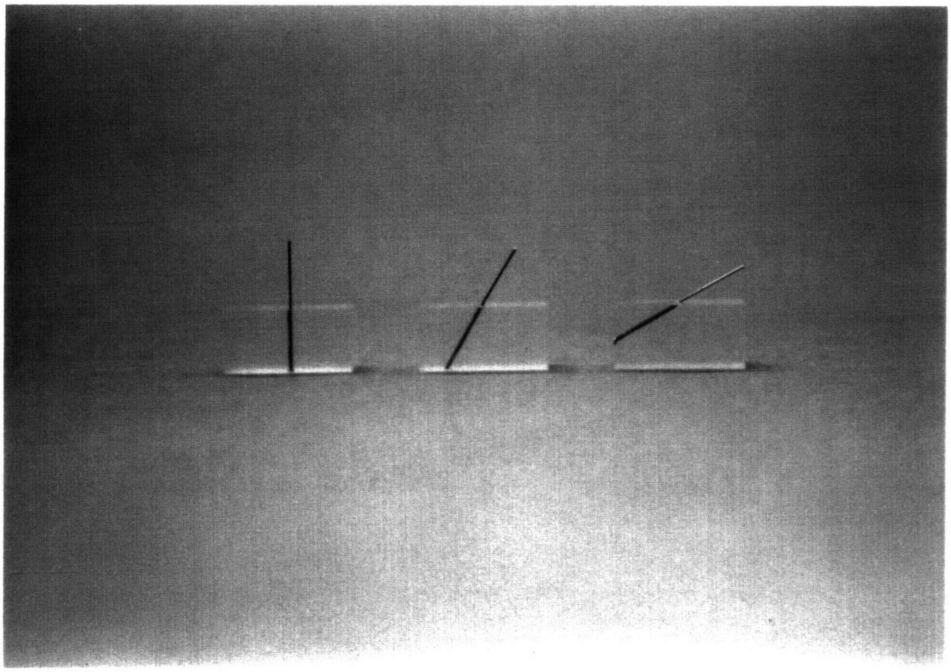

Figure 3.6: Plexiglass blocks with fibers at 0°, 30° and 60°

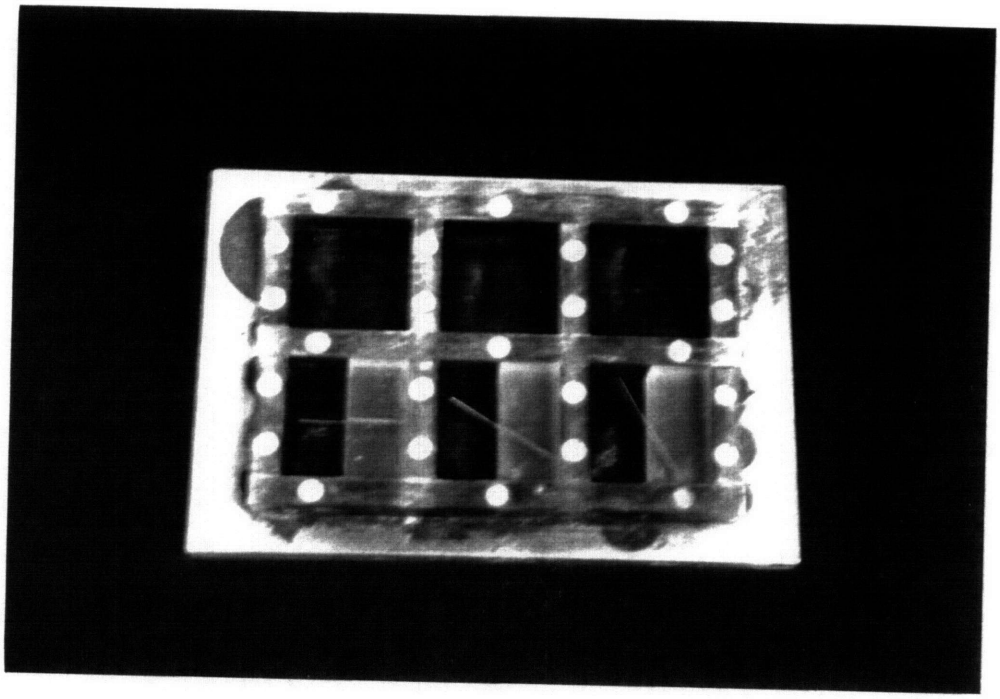

Figure 3.7: Mold with plexiglass blocks prepared for specimen casting

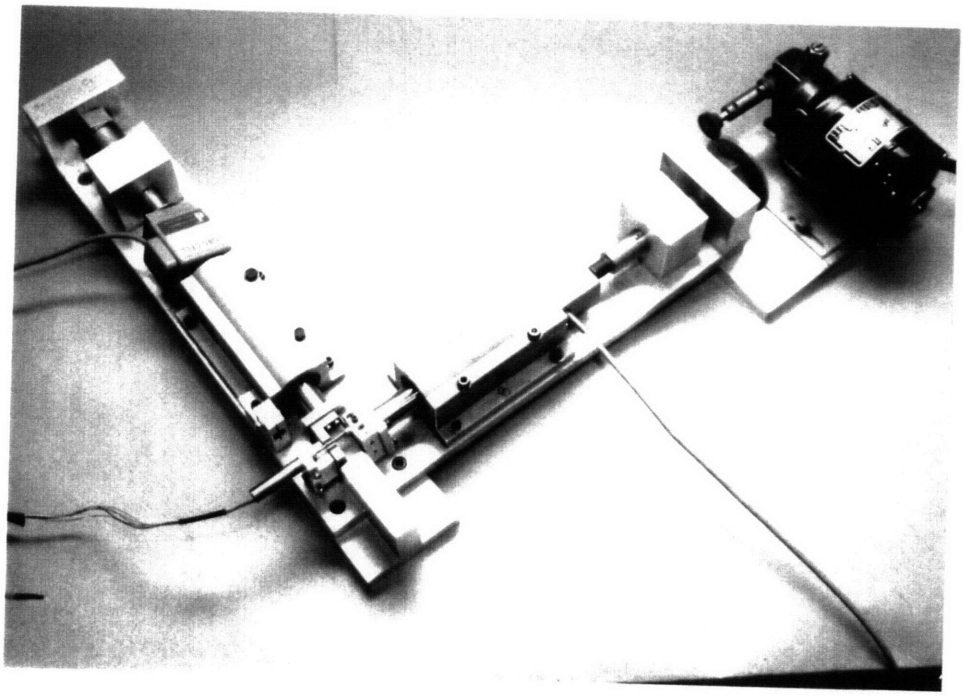

Figure 3.8: Pull-out Test rig

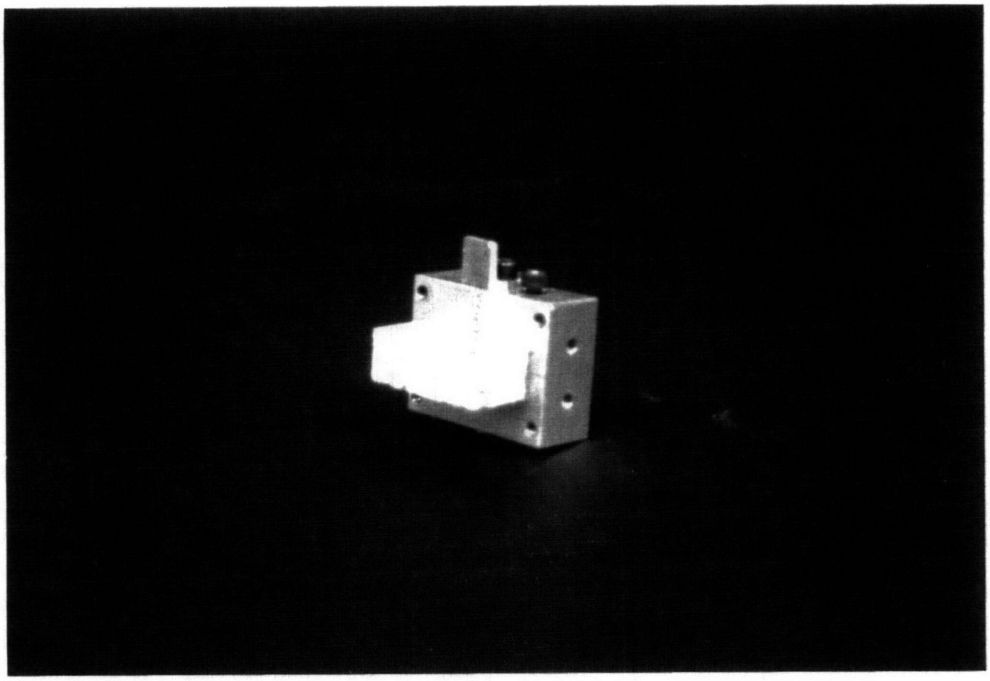

Figure 3.9: Specimen attached to pull-out vice

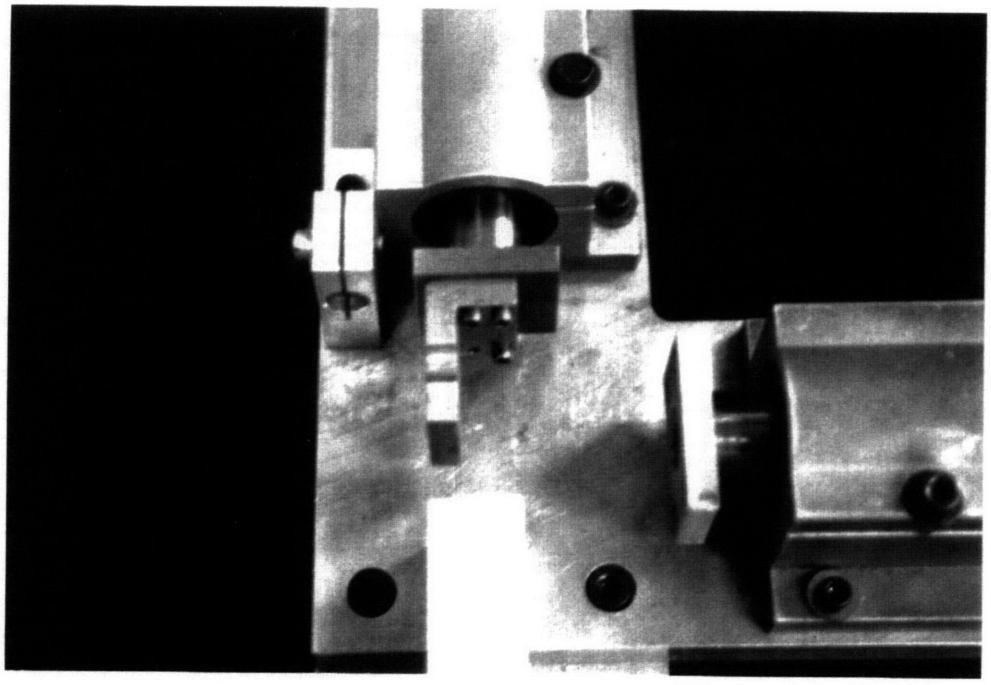

Figure 3.10: Pull-out test rig with support bracket attached

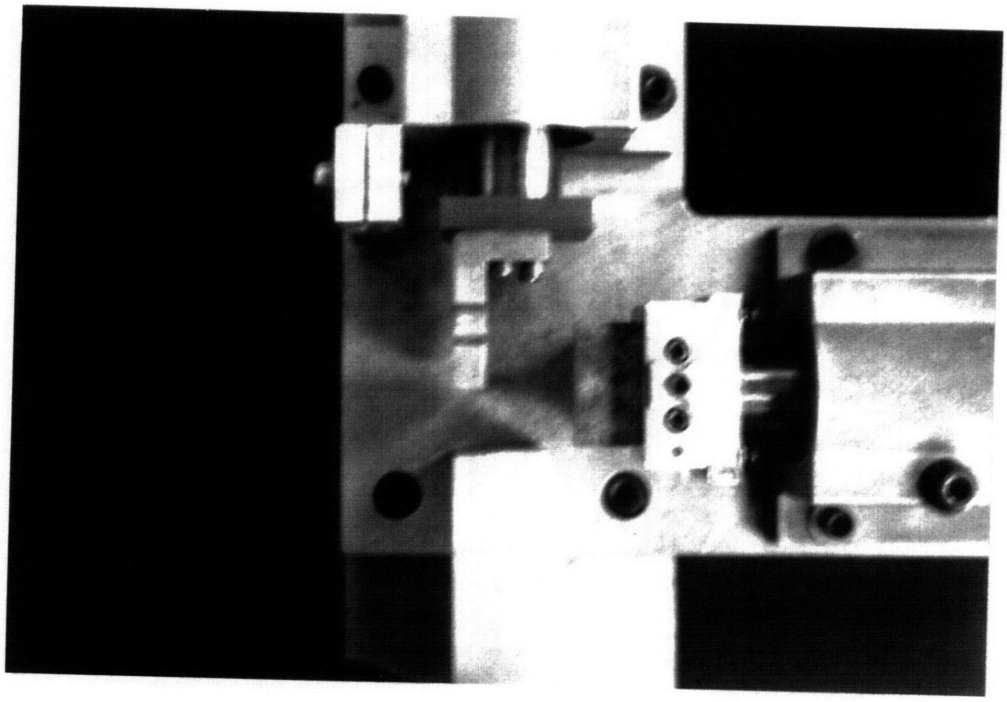

Figure 3.11: Pull-out test rig with vice and specimen attached

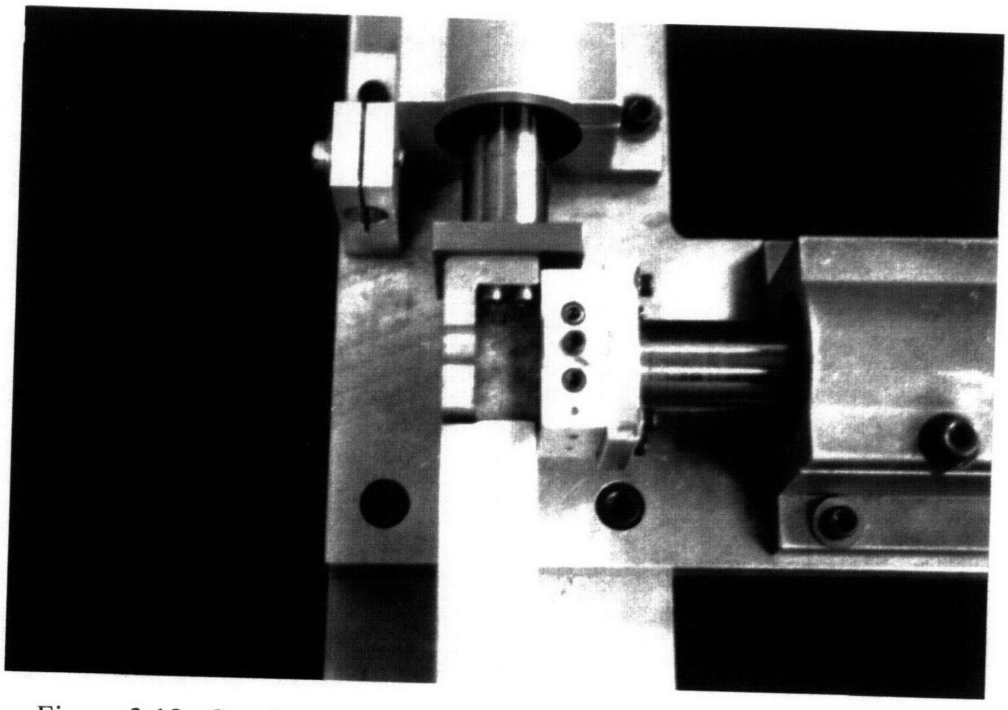

Figure 3.12: Specimen set in Pull-out Test rig

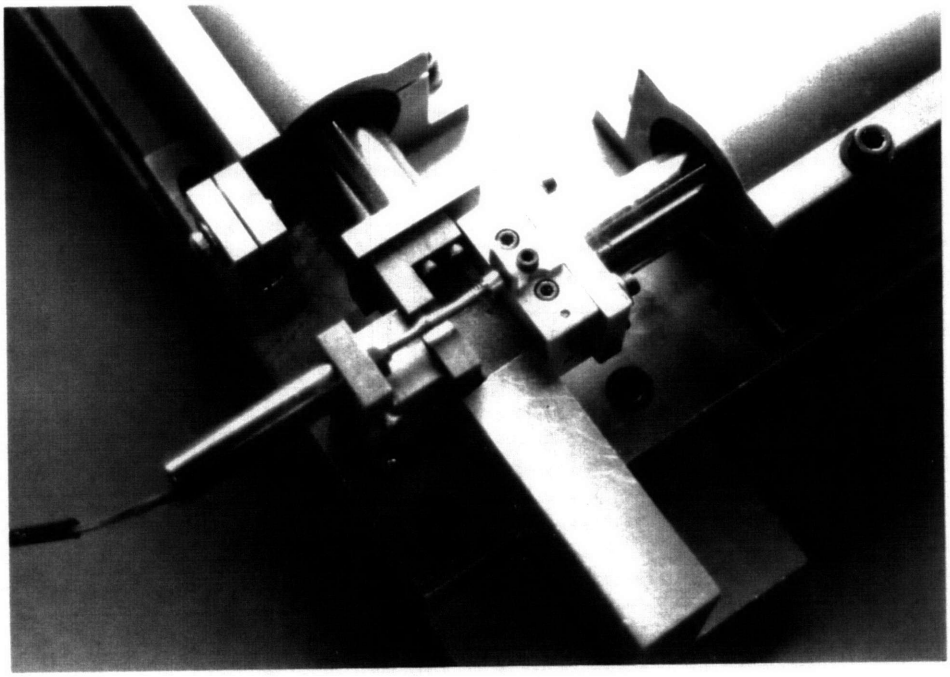

Figure 3.13: LVDT and bracket attached to Pull-out Test rig

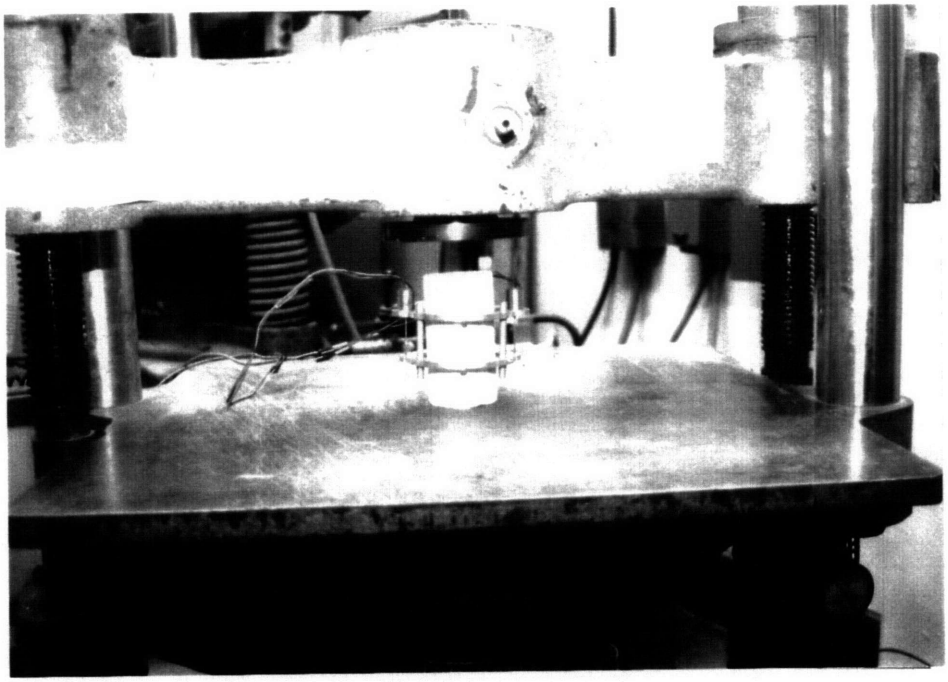

Figure 3.14: Elastic Modulus test setup

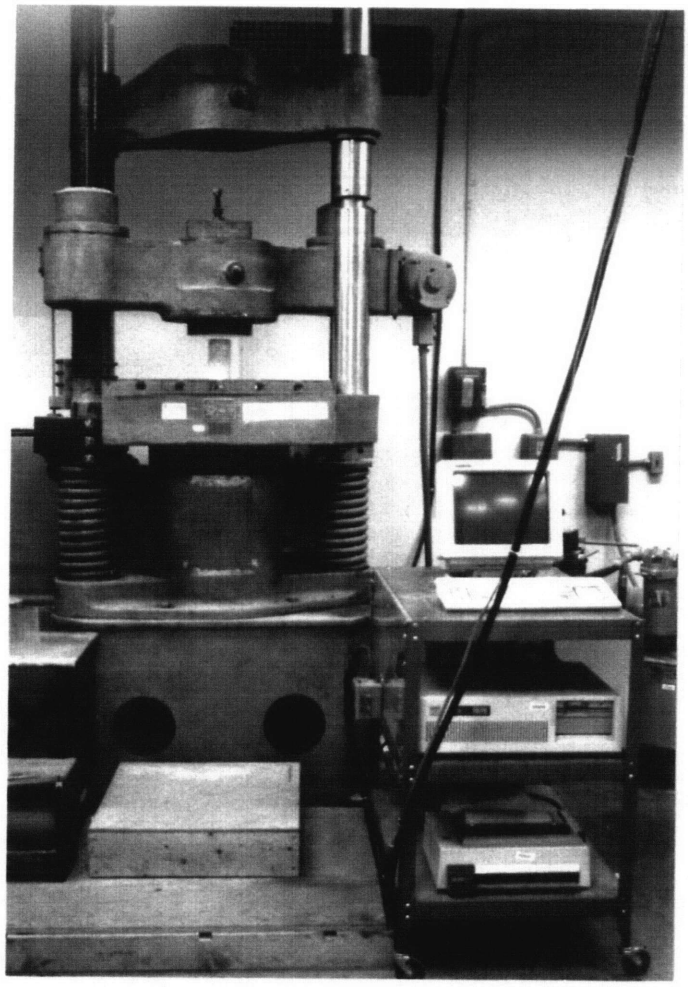

Figure 3.15: Cylinder Compression test setup

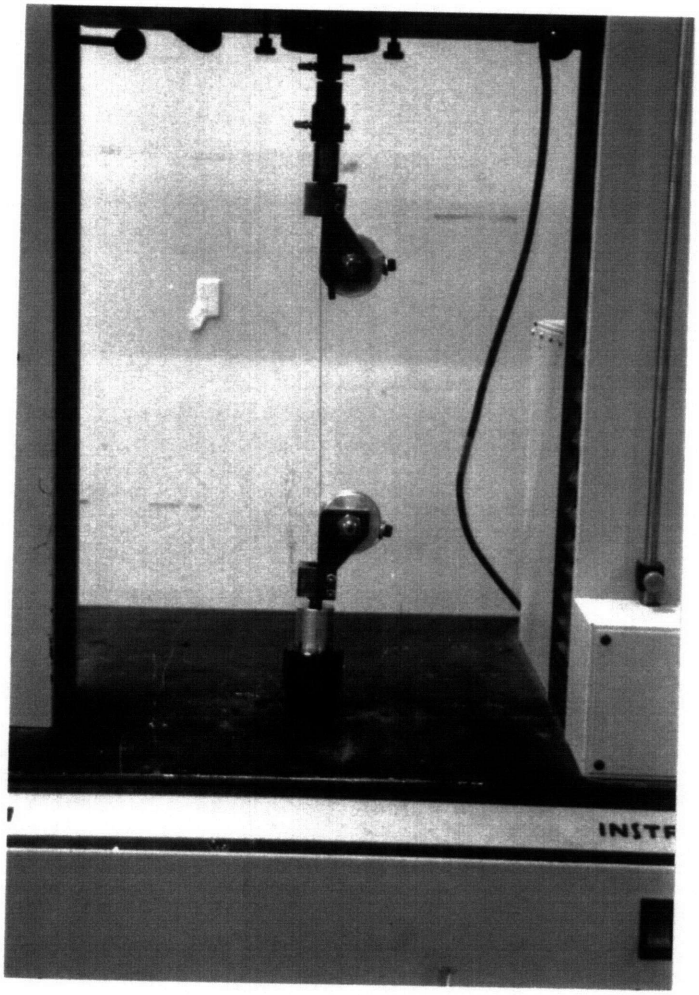

Figure 3.16: Wire Tensile test setup

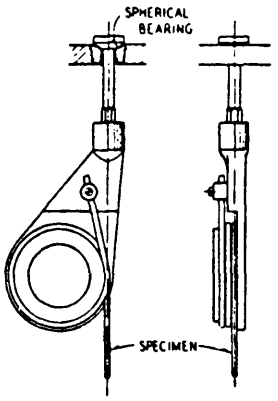

Figure 3.17: Snubbing Type Wire Grips

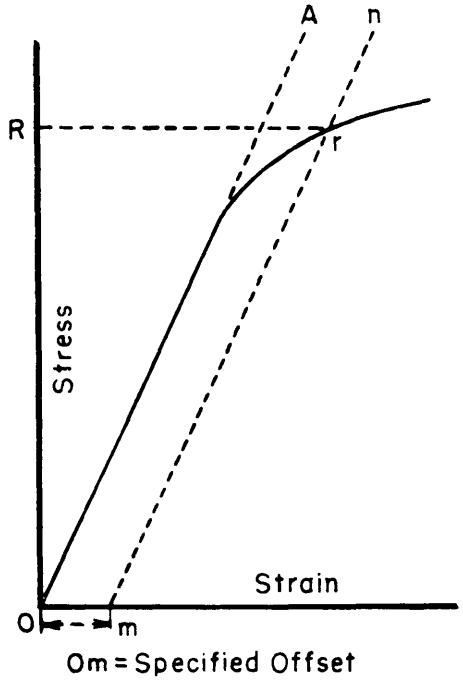

Figure 3.18: Diagram of stress-strain curve to determine yield strength

4.0 DUCTILE STEEL REINFORCING FIBER

4.1 INTRODUCTION

This section covers types of steel fiber currently being manufactured for use in industry. Then the production methods of steel fibers and different treatments given to the steel will be discussed. Types of steel and their properties will be reviewed as well as current fibers, shapes, and cross-sections. Steel fibers were only introduced as concrete reinforcement since the 1950's. Since then their usefulness has been realized in many areas of concrete use.

Different types of steel are used to make fibers for use in different application. For concrete used in areas of extreme temperatures, caustic and corrosive environments stainless steel is used. There are many grades of stainless steel and they each have different properties which make them suitable for harsh environments. Mild and carbon steels are used most often in normal civil engineering type applications such as, slabs, roadway pavements and shotcrete.

4.2 CURRENT TYPES OF FIBERS IN USE[1]

Various types of steel fiber are available and used in industry for reinforcing concrete. These fibers are made from mild carbon steel, corrosion resistant steel and stainless steel.

[1] Information gathered from Bekaert Corporation, Ribtec, and Mitchell Fibercon, Inc.

They are produced in different sizes, shapes, lengths and configurations. They may be flat, round or having a specialized shape. Fibers are generally deformed in some way to enhance the mechanical bond between it and the surrounding matrix material. Some deformation types are crimped, hook ended, and flare ended. Fibers are classified by the process by which they were manufactured.

1) Type I: cut from cold drawn wire

2) Type II: cut from cold rolled sheet metal

3) Type III: melt-extracted

4) Type IV covers other fibers

Fibers must conform to ASTM A 820 - 90 "Standard Specification for Steel Fibers for Reinforced Concrete". ASTM defines steel fiber for concrete reinforcement as "...pieces of smooth or deformed cold drawn wire; smooth or deformed cut sheet; melt-extracted fibers; or other steel fibers that are sufficiently small to be dispersed at random in a concrete mixture".[2] Steel wire can be produced in almost any shape and size. Generally wire drawing dies range in size from 0.004 in. (0.1016 mm) to 0.999 in. (25.37 mm) in diameter. Die shapes include full round (circle), square, hexagonal, elliptical, triangular, half oval, flat, tear shaped, and grooved.

4.3 PRODUCTION OF DUCTILE FIBERS

This section briefly describes the process by which wire is produced. The wire is, in turn, cut into fibers where they are given a finishing treatment such as mechanical

[2] ASTM A 820 - 90, "Standard Specification for Steel Fibers for Fiber Reinforced Concrete".

deformations. Wire drawing is outlined starting from hot rolled rod, then the process of wire drawing is explained. Finally, several wire treatments will be discussed.

4.3.1 STEEL WIRE DRAWING[3]

The first step in the production of wire is the preparation of the rod. Wire is made from hot rolled rod. Typically 7/32 in. (0.2188 mm) is the smallest diameter rod used in wire production. The hot rolled rod is covered with iron oxide or "scale" which must be removed to give the wire a clear finish and protect it from hazardous environmental conditions. There are two ways of removing scale from the rod; mechanically and chemically. The mechanical method involves reverse bending to break off the "scale". Reverse bending is accomplished by pulling the rod through a series of shieves, (or pulleys). The second method, the chemical method, entails the use of a sulphuric or hydrochloric acid bath. The rod is immersed in a hot, dilute sulphuric acid or hydrochloric acid bath. This is followed by a rinsing with water. The rod is then coated with phosphate, hot lime or hot borax. This step does three things:

1) Protects the rod from rust and the environment
2) The coating acts as a carrier for the lubricant used to cold draw the rod in later steps
3) Neutralizes any leftover acid from the baths.

Drawing the rod is the next step in the process of producing wire. Wire drawing is the process whereby hot rolled rod or wire is slowly pulled through either a single or a

[3] American Iron and Steel Institute, "Designers Handbook: Steel Wire Committee of Rod and Drawn Wire Producers".

series of wire drawing dies. Wire drawing dies are blocks with a through hole of a specific diameter. For a series of wire drawing dies the diameter of the holes decrease from start to finish. The inside edges of dies are typically made from tungsten carbide or diamond. Figure 4.1 depicts a typical tungsten carbide die. It can be seen that the die diameter will increase over its lifetime whenever the reducing edge wears out. Diamond is used for most alloys and stainless steel. Wire drawing dies uniformly reduce the cross-sectional area of the wire and leaves a clean finish. The reduction in wire size changes the physical properties of the steel by work hardening the metal which increases its yield and ultimate strength.

Figure 4.1: Tungsten Carbide wire drawing die, 0.020 in. diameter

Drawing is started by tapering one end of the rod or wire and fitting it through the first die. The die is filled with lubricant so that the wire is not damaged and exits with a

smooth finish. The wire is grasped by a gripping device or a draw block. The draw block pulls the wire through the die. As the wire exits the die it is either fed to another die or is rolled onto the draw block for storage or shipment. If the wire requires more reduction it is accomplished in a continuous flow operation from die to die. Wire is pulled through a die where it is taken up by a draw block and is then fed into another die until the desired wire properties are reached. The wire is coiled onto the last draw block. Thermal or other wire treatments are implemented during or at the end of the drawing stage. Desired wire properties determine the drawing process.

4.3.2 THERMAL TREATMENT[4]

Some thermal treatments used in the wire industry include annealing, patenting, and oil tempering. Annealing is the heating of the metal which softens the wire. This is done to improve the ductility of the wire for further processing or to give the final product a desired property. Patenting is used only by the wire drawing industry to give wire rod, or intermediate wire, a structure in high carbon steel to withstand further cold working, also to obtain a uniform cross section and to improve the mechanical properties of the wire. Oil tempering improves the straightness of the wire, and allows closer control over the tensile strength.

[4] American Iron and Steel Institute, "Designers Handbook: Steel Wire Committee of Rod and Drawn Wire Producers".

4.3.3 RESULTS OF WIRE DRAWING

Wire drawing serves many purposes. Steel wire may be elongated and reduced in area greater than by other means. Drawing allows greater dimensional accuracy, provides a smooth uniform surface which may be coated by another material. It also affects the mechanical properties of steel, making it possible to produce wire of different mechanical properties from the same steel. Cold working increases the hardness, the tensile strength, and yield strength of the steel.

4.3.4 MECHANICAL PROPERTIES

Mechanical properties of the finished product depend upon: (*i*) chemical composition of the metal, (*ii*) the degree of reduction of area imposed on the steel during cold drawing, (*iii*) any thermal treatment of the wire at any time, and (*iv*) the size of the finished wire. For many wire drawing plants specific information and processes are highly proprietary. It may take several attempts to arrive at a process which yields the required results which makes this information very valuable.

4.4 STAINLESS STEEL COMPOSITION[5]

Normal steel rusts and corrodes in an ionized environment. It was found that by adding chromium to steel, it takes on a protective quality to corrosion. By adding 13% of chromium (Cr) to normal steel it imparts both aqueous corrosion resistance and oxidation resistance to the steel. Basic stainless steels vary in the Fe-Cr binary system. With the

[5] Collings, E.W., King, H. W., "The Metal Science of Stainless Steels", The Metallurgical Society of AIME, Conference Proceedings, March 2, 1978.

addition of certain elements to this basic system, the properties of the stainless steel can be manipulated. Some of the properties which can be altered are:

1) high temperature resistance

2) cryogenic temperature resistance

3) increased corrosion resistance.

Elements which are added to the Fe-Cr system to make stainless steel, consist of some major constituents (e.g. Ni, Mn etc.) and minor constituents (e.g. C, N etc). Stainless steel is produced in three grades: Ferritic stainless, Martensitic stainless and Austenitic stainless.

4.4.1 FERRITIC STAINLESS STEELS[6]

Ferritic stainless steel has a bcc (α) grain structure in the Fe-Cr system. The typical amount of Chromium is between 11 and 30 percent by weight. This alloy has less effective corrosion resistance than austenitic steel. Ferritic stainless steel lacks ductility, is susceptible to embrittlement, is notch sensitive, lacks heat treatability and have poor weldability. However, Ferritic stainless, is economic because it does not use any Nickel (Ni), which is the reason for its continued use as a commercial binary alloy. Figure 4.2 lists some ferritic stainless steels. The first number is the AISI type, the numbers in parenthesis represent the range of chromium content by weight.

[6] Bernstein, I. M., Peckner, D., "Handbook of Stainless Steels", McGraw Hill, Inc., 1977, pp. v

AISI types:	409 (11-12% Cr)
	430 (16-18% Cr)
	446 (23-27% Cr)

Figure 4.2: AISI Ferritic Stainless Steels

4.4.2 MARTENSITIC STAINLESS STEEL[7]

Martensitic stainless steels essentially have a deformed body centered cubic (bcc) grain structure. They typically contain chromium of an amount between 12 and 18 percent by weight. The heated alloy is quenched into the α phase from high temperatures. Martensitic stainless steel exhibits corrosion resistance less than Ferritic and Austenitic Stainless steel. The advantages of this type of stainless steel is that it is able to be hardened and strengthened through tempering of martensite. Figure 4.3 lists some martensitic stainless steels.

AISI types:	403 (12-13 wgt % Cr)
	416 (12-14 wgt % Cr)
	440A (16-18 wgt % Cr)
	440B (16-18 wgt % Cr)
	440C (16-18 wgt % Cr)

Figure 4.3: AISI Martensitic Stainless Steels

[7] Bernstein, I. M., Peckner, D., "Handbook of Stainless Steels", McGraw Hill, Inc., 1977, pp. v

4.4.3 AUSTENITIC STAINLESS STEEL[8]

The addition of nickel to the iron-chromium system creates austenitic stainless steel. Nickel improves the aqueous corrosion resistance of the steel and stabilizes the face centered cubic (fcc), or γ, structure. Austenitic stainless steels form the largest group of stainless steels. They encompass a wide choice of compositions and material properties. The advantages of austenitic stainless steel include:

1) stability at cryogenic temperatures

2) retained strength at elevated temperatures

3) excellent corrosion resistance and the absence of ferromagnetism.

Figure 4.4 lists some typical austenitic steels. By adding different elements the properties of the wire can be changed. For a more detailed listing of AISI types and composition see [Marshall 1984].

AISI types:[9]	301 Cr(16-18 %), Ni(6-8 %)
	302 Cr(17-19 %), Ni(8-10 %)
	304 Cr(18-20 %), Ni(8-12 %)
	310 Cr(24-26 %), Ni(19-22 %)
	316 includes Mo(2-3 %)
	321 includes Ti(5x %C min.)
	347 includes Nb(10x %C min.)

Figure 4.4: AISI Austenitic Stainless Steels

[8] Bernstein, I. M., Peckner, D., "Handbook of Stainless Steels", McGraw Hill, Inc., 1977, pp. v

[9] Marshall, P., "Austenitic Stainless Steels: Microstructure and Mechanical Properties", Elsevier Applied Science publishers, New York, 1984, pp.423.

Type 304 stainless is one of the most widely produced alloys and finds use at elevated and cryogenic temperatures.[10] From 304 many variations of steel can be produced as listed in figure 4.4. As an example, with the addition of Molybdenum (Mo), to 304 stainless, type 316 is created which exhibits better corrosion resistance, higher corrosion oxidation and higher strength. It has been determined that a minimum of ~13 % by weight of Chromium (Cr) is required for a substantial increase in aqueous and oxidation resistance. The high Cr content creates a hydrated oxide film of about 10-50 Å thick which is required for passivity in an aqueous solution. This Cr_2O_3 is the base oxide scale which provides protection against continuous high temperature oxidation.

4.5 TESTING STEEL WIRE

Five types of steel wire were used in the present testing program. Samples were provided by Bekaert, Loos & Co. Inc, Central Wire, and Baird Industries. A range of tensile yield strengths was obtained to conduct the experiments. Tensile test results for the 68,100 and 98,200 psi wire were supplied by Baird Industries therefore stress-strain graphs are not available. Stress-strain graphs and tensile test results for all wire specimens are displayed in Appendix C.

[10] Bernstein, I. M., Peckner, D., "Handbook of Stainless Steels", McGraw Hill, Inc., 1977, pp. vi

5.0 PARAMETRIC STUDIES AND DISCUSSION

5.1 INTRODUCTION

This chapter describes in detail the observations and analysis made of the experiments. Section one of the testing program will be detailed first. Plots and observations from section one will be explained and analyzed. Results gathered from this series can then be enumerated. Pertinent information needed for the simulation of pull-out behavior will be shown. Next, section two of the testing program will be described. Analysis and results from this section will be covered as well. The comparison of the simulation with section two will be discussed in Chapter Six. For conservation and flow of information, sections one and two will be discussed in the same chapter.

5.2 SECTION ONE OF EXPERIMENTAL PROGRAM

The first section consisted of three series of specimens, all embedded with the same type of steel fiber with a fiber yield strength of 170,000 psi. Each series was characterized by a different mortar strength of approximately, five , ten and twelve thousand pounds per square inch. Within each series three fiber angles were used, zero, thirty, and sixty degrees. Specific information as to mortar mix ratios can be found in Chapter Three. Results from cylinder Compressive Strength tests can be found in Appendix A. Results from Elastic Modulus tests can be found in Appendix B Fiber specifications and tensile

testing results can be found in Chapter Four. Pull-out tests were conducted on these specimens and the data was recorded by a computer data acquisition system. Each test was plotted as pull-out load versus fiber pull-out displacement.

Figure D-1 to Figure D-4 depict pull-out test responses for series one. Figure D-1 is a plot of all legitimate test results for 5,000 psi mortar specimens with a fiber angle of zero degrees. Figure D-2 is a plot of all legitimate test results for 5,000 psi mortar specimens with a fiber angle of thirty degrees. Figure D-3 is a plot of all legitimate test results for 5,000 psi mortar specimens with a fiber angle of sixty degrees. Figure D-4 shows a plot of the average response curves for each fiber angle in series one. Average load-displacement curves were created by averaging load values at specific displacement values.

Figure D-5 to Figure D-8 depict pull-out test responses for series two. Figure D-5 is a plot of all legitimate test results for 10,000 psi mortar specimens with a fiber angle of zero degrees. Figure D-6 is a plot of all legitimate test results for 10,000 psi mortar specimens with a fiber angle of thirty degrees. Figure D-7 is a plot of all legitimate test results for 10,000 psi mortar specimens with a fiber angle of sixty degrees. Figure D-8 shows a plot of the average response curves for each fiber angle in series two.

Figure D-9 to Figure D-12 depict pull-out test responses for series three. Figure D-9 is a plot of all legitimate test results for 12,000 psi mortar specimens with a fiber angle of zero degrees. Figure D-10 is a plot of all legitimate test results for 12,000 psi mortar specimens with a fiber angle of thirty degrees. Figure D-11 is a plot of all legitimate test results for 12,000 psi mortar specimens with a fiber angle of sixty degrees.

Figure D-12 shows a plot of the average response curves for each fiber angle in series three.

5.2.1 MAXIMUM PULL-OUT LOAD

Maximum pull-out load was affected by a change in mortar compressive strength. We can see that the maximum pull-out load generally increased with increasing mortar strength which we might take as academic. This is due to the increased strength of the bond between the fiber and the matrix, (Figure 5.4a). As the fiber angle increased from zero to sixty degrees there was a general downward trend in pull-out load, (Figure 5.1a).

The bending component of the pull-out force was affected as the fiber angle changed. the pull-out force for a fiber at an angle to the crack face can be broken into two components as described in Chapter two, "Bending Model". The first component is aligned with the fiber and provides the debonding and pullout force. The second component is perpendicular to the fiber and provides the force necessary to bend the fiber across the crack opening. We can say that the debonding/pull-out component for angled fibers will be the same as the pull-out force for the cases with aligned fibers. Therefore the bending force component of the pull-out load can be determined by:

$$\mathbf{F_{bending} = F_{\theta} - F_{\theta=0}(\cos \theta)} \qquad \mathbf{(5.1)}$$

Where: $F_{bending}$ = bending component of pull-out force

F_{θ} = pull-out force at an angle θ

$F_{\theta=0}$ = pull-out force at an angle $\theta = 0$

The bending component of the pull-out force increased with the increase in fiber angle, (Figure 5.1b).

5.2.2 PULLOUT WORK

Work done to pull-out fibers peaked at approximately 30 degrees, (Figure 5.2a). The work done to pull out a fiber completely was calculated as the area under the load-displacement curve using the trapezoidal method. These results are comparable to those obtained by Morten and Groves, where it was reported that work done passed through a maximum at approximately 45 degrees.

Pull out work also increased with increasing mortar strength, (Figure 5.4b). As the mortar strength increased it is safe to say that more energy was needed to debond the fiber and cause spalling. This can be seen in Figure 5.2b, where the bending component of the work increased with increasing matrix strength. For the high strength cases work due to bending passed through a maximum at $\theta = 30°$ and decreased at $\theta = 60°$. This is due to the increased spalling which will be discussed below.

5.2.3 SPALLING LENGTH

Spalling length is defined as the length along the fiber direction where the matrix breaks away. Spalling is caused by the lateral force applied by the fiber pullout force for fibers laying obliquely to a crack.

For increasing fiber angle there was an increase in spalling length, (Figure 5.3). This is expected as the volume of matrix under an inclined fiber decreases with increasing

fiber angle. As the volume of matrix decreases so does the cross section through which the force must act to cause spalling.

Spalling length also decreased for all cases with respect to increasing mortar strength, (Figure 5.5). It should be noted that there was negligible spalling for cases of aligned fibers.

Spalling length was calculated from load-displacement graphs in Appendix C. Each test was examined and then an average spalling length was calculated for each case. Spalling length was assumed to be evident at a point near the end of the pullout history where the load drops suddenly. It was not taken at a load of zero because that meant that the fiber was completely disengaged from the specimen. Load characteristics were a sudden drop in load followed by a constant low load where it was assumed that the fiber was scraping against the exit wall.

Spalling length was also measured directly from the pullout specimens under a scanning electron microscope which will be discussed later in this chapter.

5.3 SECTION TWO OF EXPERIMENTAL PROGRAM

The second section consisted of four series of specimens, all made from the same 5,000 psi mortar. Each series was characterized by a different fiber yield strength. Within each series three fiber angles were used, zero, thirty, and sixty degrees. For the purposes of a complete discussion concerning fiber yield strength, series one will be included in the following results.

Figure D-13 to Figure D-16 depict pull-out test response for series four. Figure D-13 is a plot of all legitimate test results for 5,000 psi mortar specimens with a fiber a yield strength equal to 39,900 psi at an angle of zero degrees. Figure D-14 is a plot of all legitimate test results for 5,000 psi mortar specimens with a fiber yield strength equal to 39,900 psi at thirty degrees. Figure D-15 is a plot of all legitimate test results for 5,000 psi mortar specimens embedded with a fiber of yield strength equal to 39,900 psi at sixty degrees. Figure D-16 shows a plot of the average response curves for series four for each fiber angle.

Figure D-17 to Figure D-20 depict pull-out test response for series five. Figure D-17 is a plot of all legitimate test results for 5,000 psi mortar specimens embedded with a fiber of yield strength equal to 68,100 psi at zero degrees. Figure D-18 is a plot of all legitimate test results for 5,000 psi mortar specimens embedded with a fiber of yield strength equal to 68,100 psi at thirty degrees. Figure D-19 is a plot of all legitimate test results for 5,000 psi mortar specimens embedded with a fiber of yield strength equal to 68,100 psi at sixty degrees. Figure D-20 shows a plot of the average response curves for series five for each fiber angle.

Figure D-21 to Figure D-24 depict pull-out test response for series six. Figure D-21 is a plot of all legitimate test results for 5,000 psi mortar specimens embedded with a fiber of yield strength equal to 92,200 psi at zero degrees. Figure D-22 is a plot of all legitimate test results for 5,000 psi mortar specimens embedded with a fiber of yield strength equal to 92,200 psi at thirty degrees. Figure D-23 is a plot of all legitimate test results for 5,000 psi mortar specimens embedded with a fiber of yield strength equal to

92,200 psi at sixty degrees. Figure D-24 shows a plot of the average response curves for series six for each fiber angle.

Figure D-25 to Figure D-28 depict pull-out test response for series seven. Figure D-25 is a plot of all legitimate test results for 5,000 psi mortar specimens embedded with a fiber of yield strength equal to 138,500 psi at zero degrees. Figure D-26 is a plot of all legitimate test results for 5,000 psi mortar specimens embedded with a fiber of yield strength equal to 138,500 psi at thirty degrees. Figure D-27 is a plot of all legitimate test results for 5,000 psi mortar specimens embedded with a fiber of yield strength equal to 138,500 psi at sixty degrees. Figure D-28 shows a plot of the average response curves for series seven for each fiber angle.

5.3.1 Maximum Pull-out Load

Results of maximum pullout load with respect to fiber angle were similar to those of section one where the maximum load occurred at an angle of 30°, (Figure 5.6a). For f_y = 138,500 psi the maximum pullout load peaked at $\theta = 30°$, but the load at $\theta = 60°$ was larger than that of $\theta = 0°$. There was a general upward trend in pullout load with respect to fiber yield strength aside from exceptions, (see Figure 5.9). For this series the maximum pullout load peaked at $\theta = 30°$, but the load at $\theta = 60°$ was larger than that of $\theta = 0°$.

Bending force was calculated as stated in the previous section concerning pullout bending component. For the most part bending peaked at $\theta = 30°$ as long as maximum load @ $\theta = 30°$ is greater than pullout load at $\theta = 0°$ & 60°,(Figure 5.6b). The fiber with,

f_y = 138,500 psi had the largest bending component resulting from a combination of high pull-out force and low spalling as compared to other fibers.

5.3.2 Pullout Work

A large distinction was observed for pullout work in terms of fiber angle for fibers. For all fiber angles fiber, f_y = 138,500 psi required the most energy for complete pullout, (Figure 5.7a and Figure 5.9b). As θ goes from 30° to 60°, the pull-out work done by bending undergoes small changes for most cases, (Figure 5.7b). However, the limited experimental points do not allow us to make a definite statement on the actual trend. Again, maximum bending work occurs at f_y = 138,500 psi.

5.3.3 Spalling Length

Spalling length increased with increasing fiber angle for the same reasons as explained in the previous section. Most of the fibers had the same spalling length as can be seen in the fairly flat plot of Figure 5.10. Large differences were observed for fiber, f_y = 170,000 psi. This could explain the low pull-out work attributable to this series. the fiber, f_y = 170,000 psi is a very brittle fiber as well as shown in Appendix D.

5.4 Calculation of Spalling Length

Spalling length was calculated from load-displacement plots and compared to measurements made of SEM photographs. Most comparisons agreed with assumptions made from plots of Pull-out load vs Displacement.

In Figure 5.11, the drop in load is circled. This is from a specimen with a fiber at 60 degrees and a matrix strength of 5,000 psi and a fiber strength of 39,900 psi. The drop in load is important since it indicates that the end of the fiber is no longer confined by the groove. A small amount of load still registers, however, that is due to the fiber end sliding along the outside edge of the exit hole. We cannot take the spalling length at a position when the load is zero since this is misleading. The load is only zero when the fiber has completely broken all contact with the rough surface of the mortar.

Spalling length, from the SEM photograph, was measured on the underside of the fiber, (the side which spalls). It was measured from the crack face to the point where the fiber groove remained intact, (see the arrows in Figure 5.13). The photograph was taken of the specimen from the test depicted in Figure 5.11, it had been cut in half laterally to expose the fiber hole. The spalling length calculated from the plot was 2.35 mm and that from the photograph was 2.31 mm. This compares favorably as do other comparisons made from other specimens. Another plot is shown in Figure 5.12 and the corresponding specimen photograph is in Figure 5.14. This specimen had a fiber angle of sixty degrees with a mortar strength of 5,000 psi and a fiber strength of 138,000 psi, The spalling calculated from the plot was 2.214 mm and measured from the micrograph was 2.22 mm.

5.5 CRACK BRIDGING BEHAVIOR DURING FRICTIONAL PULLOUT

From the pull-out test results of load vs. displacement it is evident that the force bridging the crack increases slightly near the end of the pull out length of the fiber, (Figures 5.15-5.17). This occurrence is absent or negligible at zero degrees but increases in magnitude

relative to the inclination of the fiber. The first explanation seemed to be that the trailing end of the fiber dragged along the wall of the hole as the fiber was pulled completely free of the mortar. This was not, however, a reasonable explanation since simple sliding could not account for the magnitude of the rise in pullout load.

A closer look at some mortar specimens under the SEM showed signs of scraping and gauging of the side wall of the hole of some specimens, (Figure 5.20). Also those fibers analyzed showed that their ends remained straight, (Figure 5.21). This would seem to indicate that the fiber was more stiff than the matrix in order to mar the surface. The evidence is that the end of the fiber is still straight. The fiber was pulled out beyond the point where the bending component of the force creates a plastic hinge in the fiber. From this it can be theorized that at that moment the end of the fiber can no longer be assumed to rigidly encased, where rigidly encased means that there is enough support from the matrix wall to cause plastic bending in the fiber.

It was observed that for pull-out test of aligned fibers, the fiber remained straight. However for specimens of inclined fibers the embedded end of the fiber emerged bent from yielding due to bending about the exit point of the matrix. This is expected, but at a closer look the end of the fiber remained straight. In addition some fibers had relatively large amounts of mortar particles stuck to the "top" side at the end, (Figures 5.18-5.19). It was interesting to note that most of the fibers had very few if any particles attached to the fiber, but several fibers showed these pieces of material on the same side as that which would support this argument. Also the pull-out histories for those tests show an increase in load near the end of the fiber length.

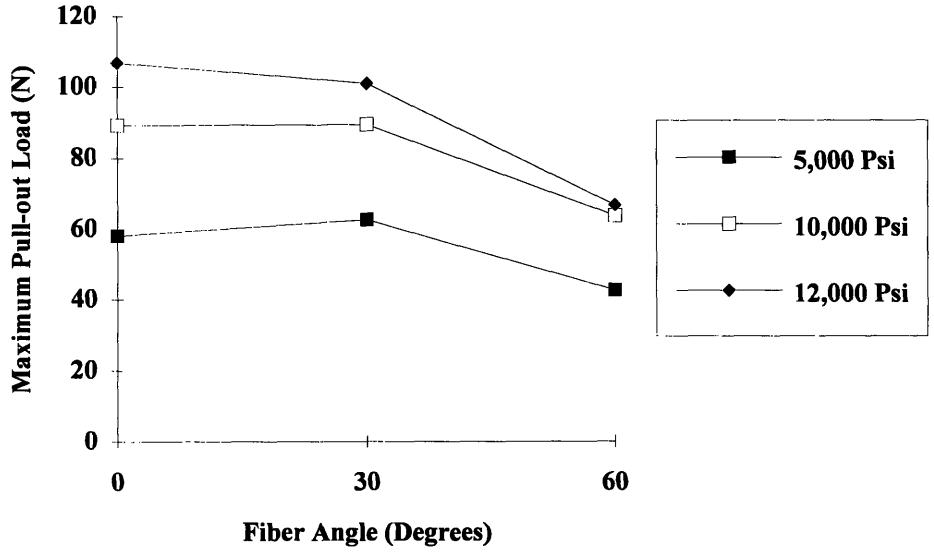

(a)

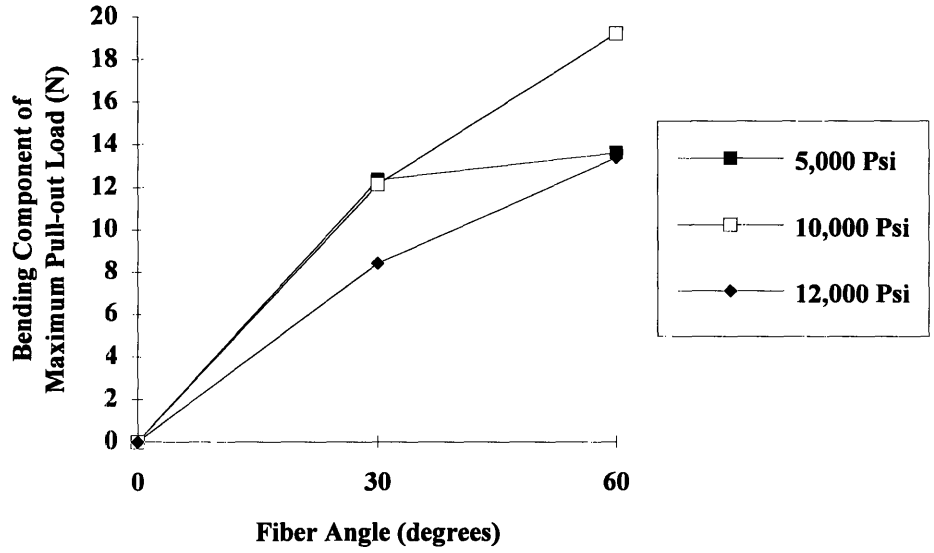

(b)

Figure 5.1: Variation of (a) Maximum Pull-out Load and (b) Bending Component of Maximum Pull-out Load with respect to Fiber Angle in terms of Matrix Compressive Strength. For Series 1-3 embedded with a Steel Fiber, f_y = 170,000 psi (1.171 Gpa).

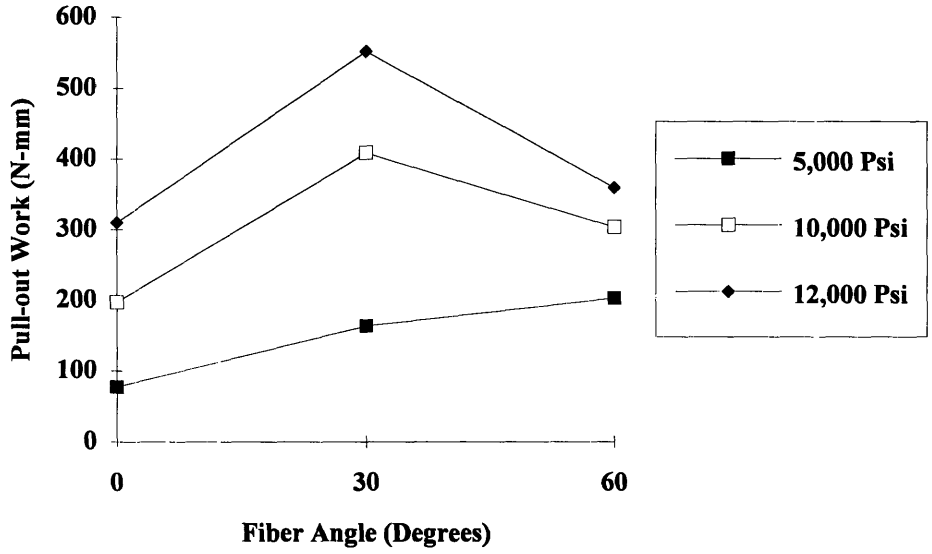

(a)

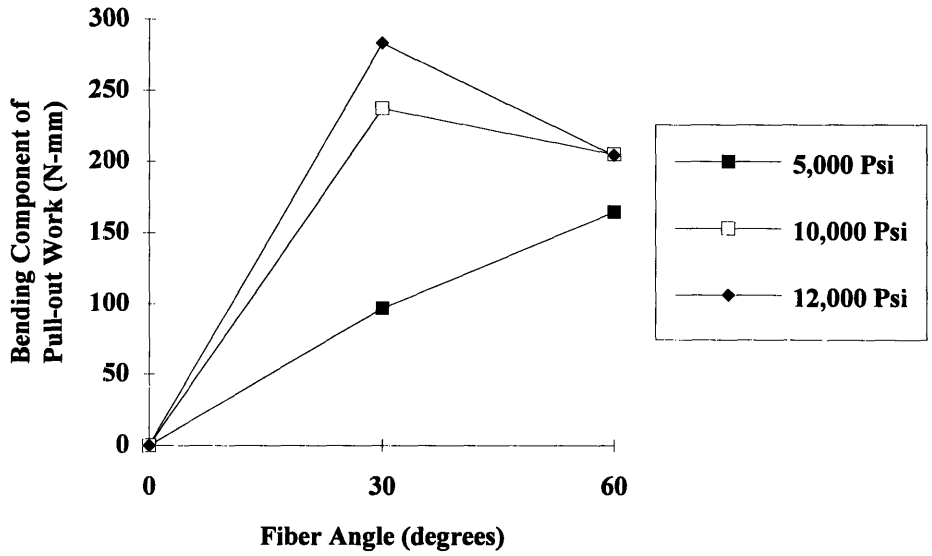

(b)

Figure 5.2: Variation of (a) Pull-out Work and (b) Fiber Bending Component of Work with respect to Fiber Angle in terms of Matrix Compressive Strength. For Series 1-3 embedded with a Steel Fiber, f_y = 170,000 psi (1.171 Gpa).

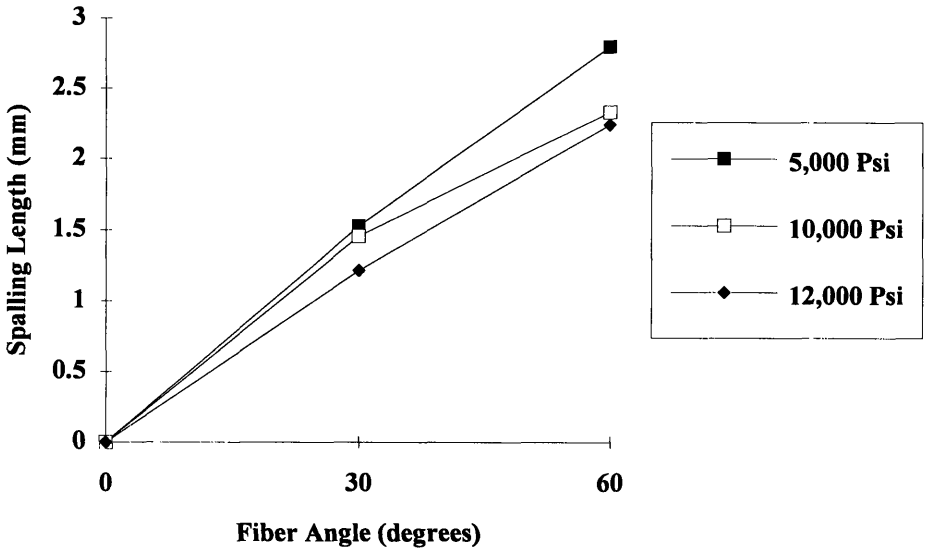

Figure 5.3: Variation of Mortar Spalling Length with respect to Fiber Angle in terms of Matrix Compressive Strength. For Series 1-3 embedded with a Steel Fiber, f_y = 170,000 psi (1.171 Gpa).

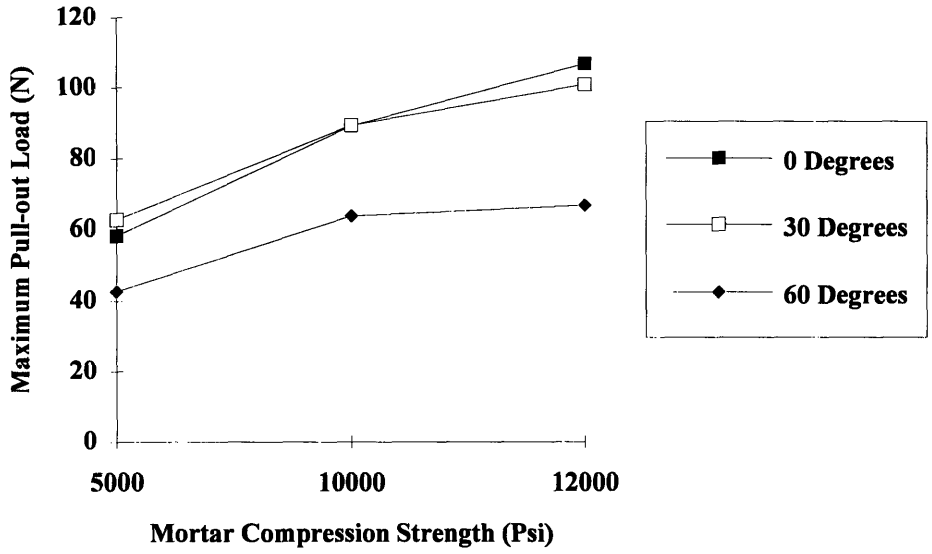

(a)

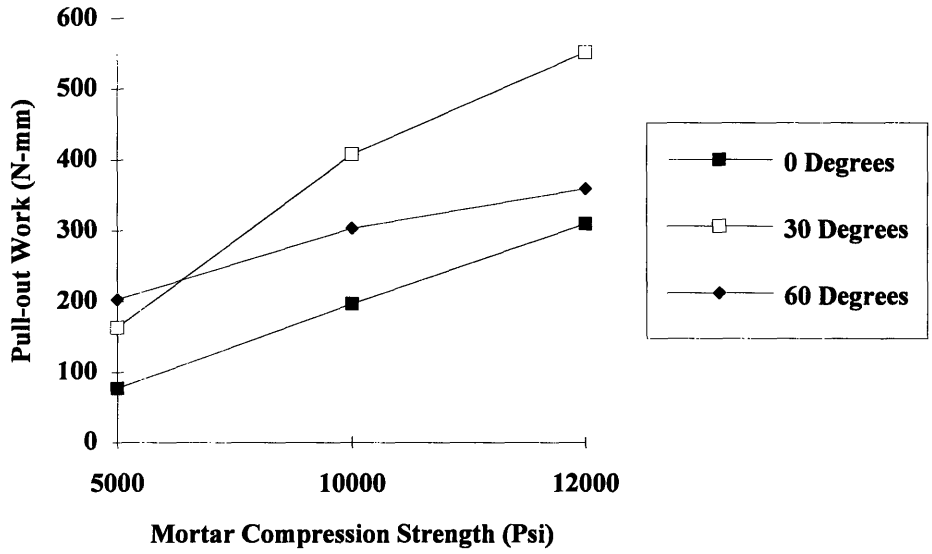

(b)

Figure 5.4: Variation of (a) Maximum Pull-out Force and (b) Pull-out Work with respect to Matrix Compressive Strength in terms of Fiber Angle. For Series 1-3 embedded with a Steel Fiber, f_y = 170,000 psi (1.171 Gpa)

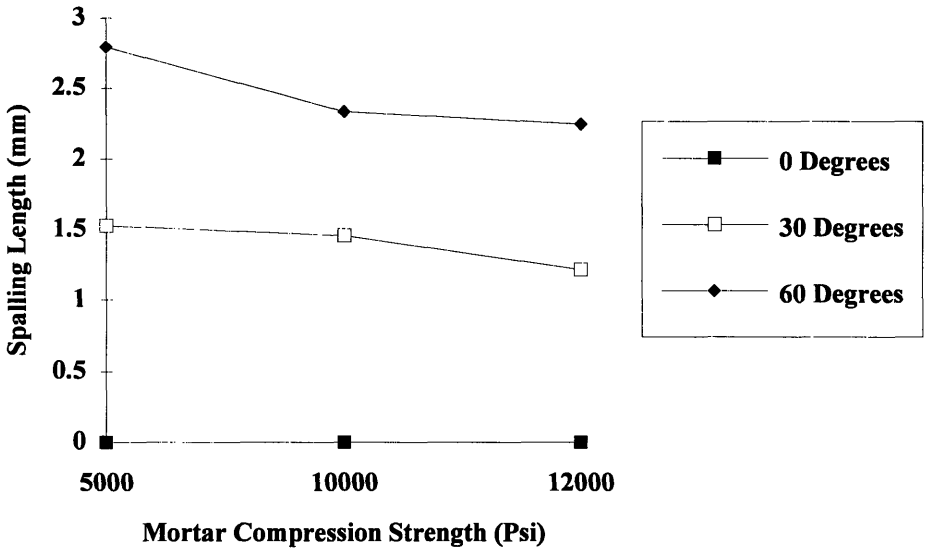

Figure 5.5: Variation of Mortar Spalling Length with respect to Matrix Compressive Strength in terms of Fiber Angle. For Series 1-3 embedded with a Steel Fiber, f_y = 170,000 psi (1.171 Gpa)

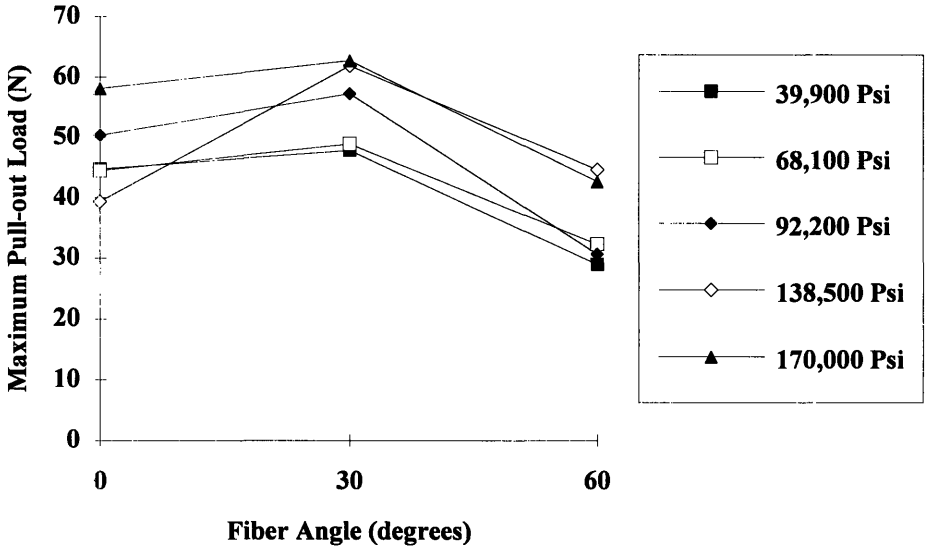

(a)

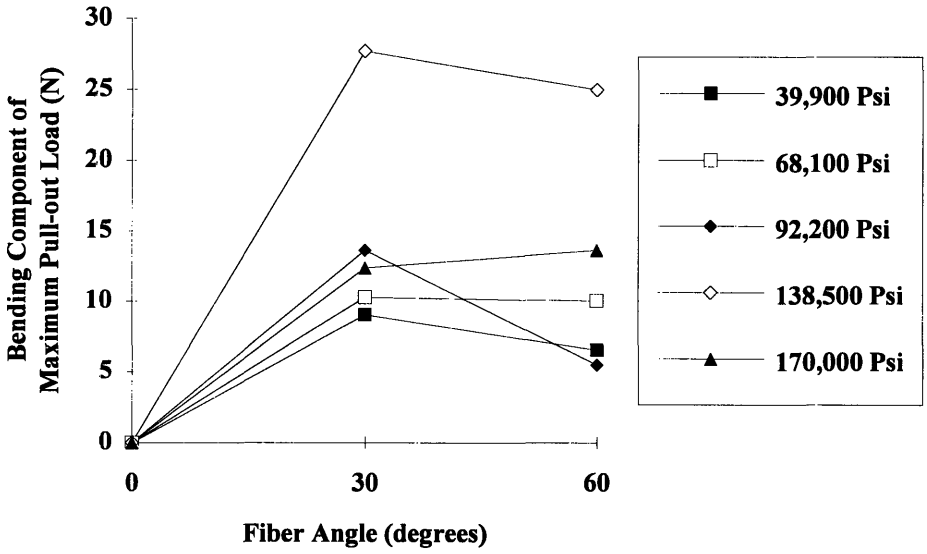

(b)

Figure 5.6: Variation of (a) Maximum Pull-out Load and (b) Bending Component of Maximum Pull-out Load with respect to Fiber Angle in terms of Steel Fiber Yield Strength. For Series 1, 4-7 with Mortar Compressive Strength, f'_c = 5,000 psi (34.5 MPa)

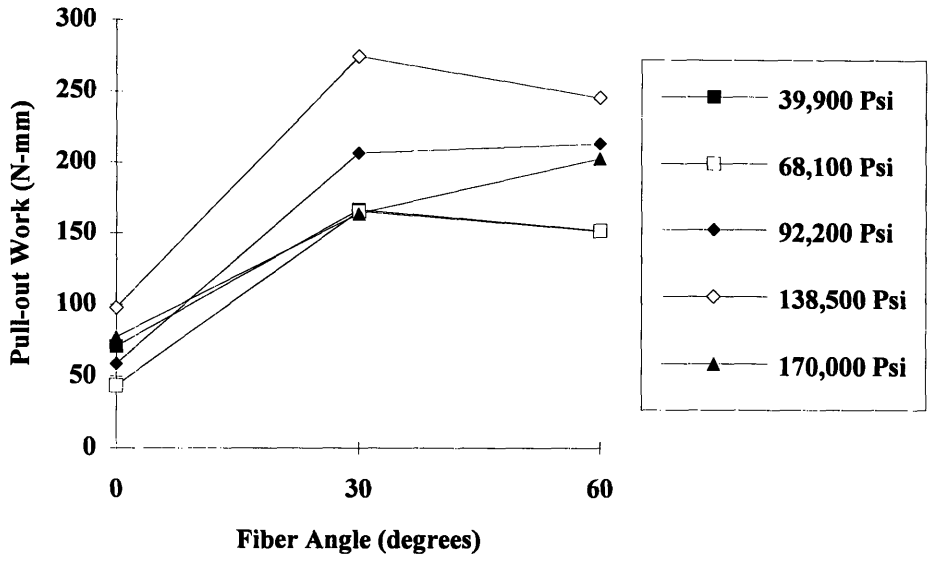

(a)

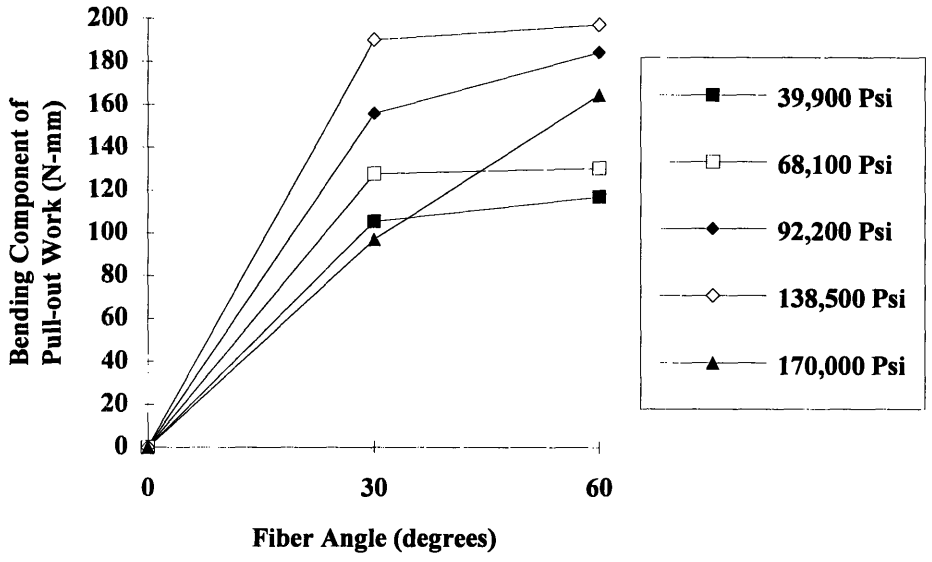

(b)

Figure 5.7: Variation of (a) Pull-out Work and (b) Fiber Bending Component of Work with respect to Fiber Angle in terms of Steel Fiber Yield Strength. For Series 1, 4-7 with Mortar Compressive Strength, f'_c = 5,000 psi (34.5 MPa)

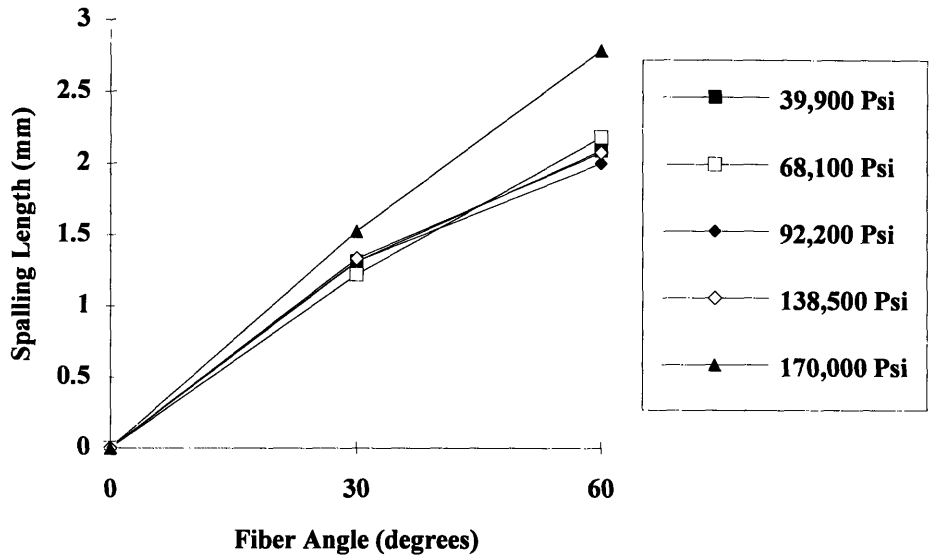

Figure 5.8: Variation of Mortar Spalling Length with respect to Fiber Angle in terms of Steel Fiber Yield Strength. For Series 1, 4-7 with Mortar Compressive Strength, f'_c = 5,000 psi (34.5 MPa)

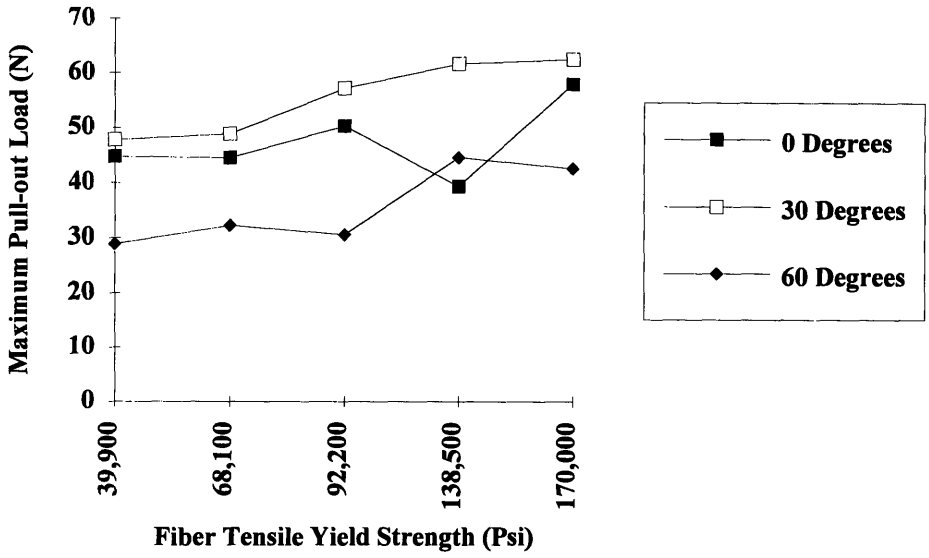

(a)

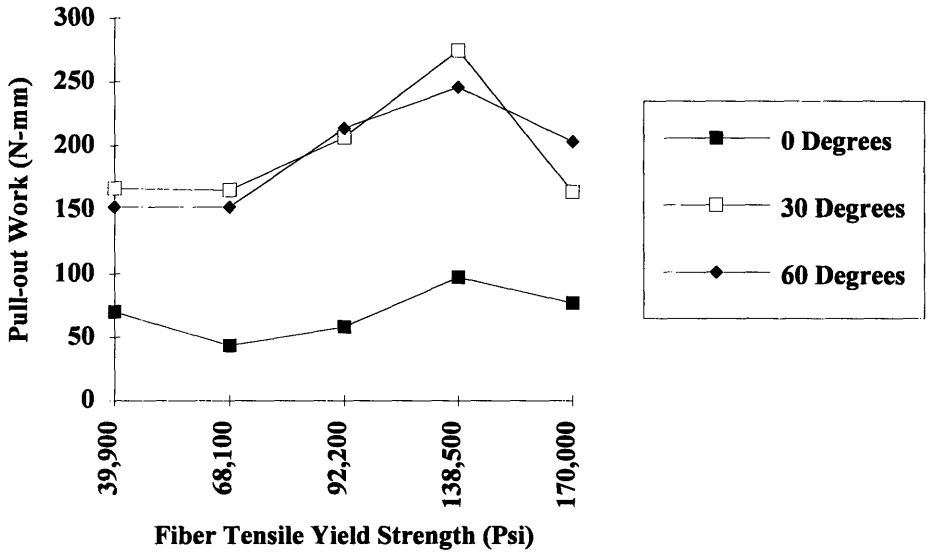

(b)

Figure 5.9: Variation of (a) Maximum Pull-out Force and (b) Pull-out Work with respect to Steel Fiber Yield Strength in terms of Fiber Angle. For Series 1, 4-7 with Mortar Compressive Strength, f'_c = 5,000 psi (34.5 MPa)

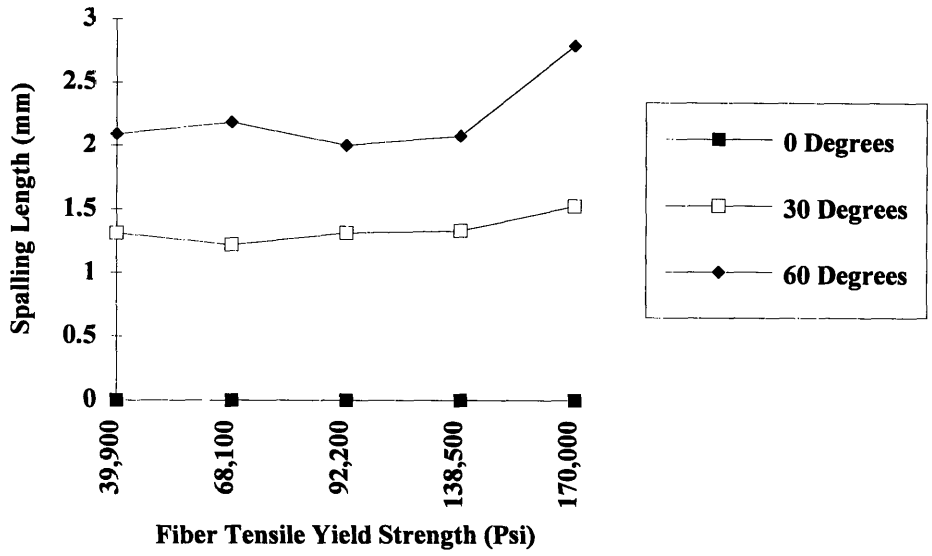

Figure 5.10: Variation of Mortar Spalling Length with respect to Steel Fiber Yield Strength in terms of Fiber Angle. For Series 1, 4-7 with Mortar Compressive Strength, f'_c = 5,000 psi (34.5 MPa)

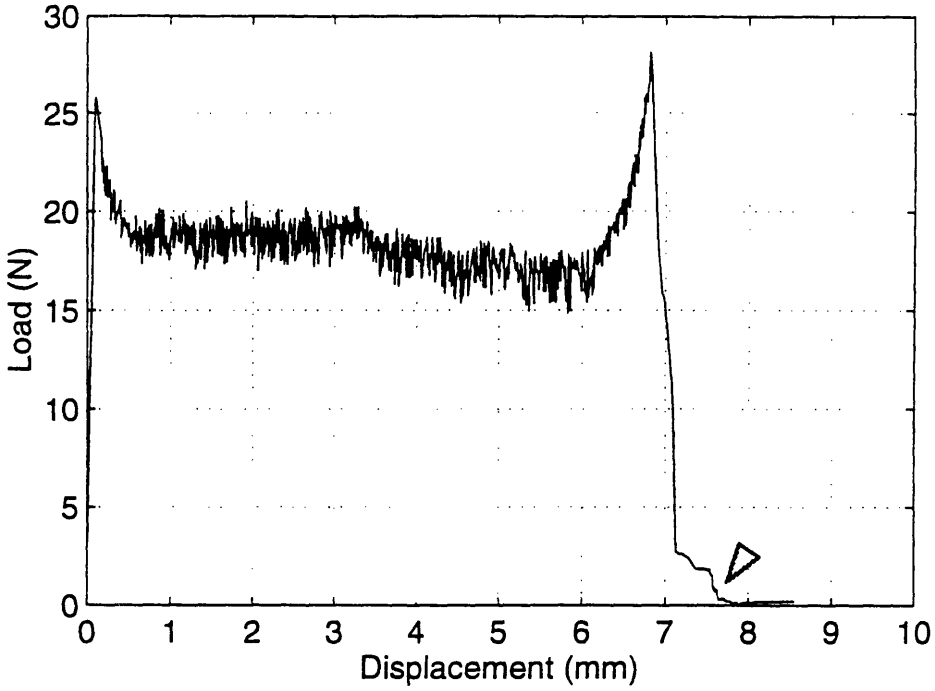

Figure 5.11: Pull-out curve for Series Four, Specimen #4; Matrix: f'c = 5,000 psi, Fiber: F_y = 39,900 psi, Fiber Inclination: θ = sixty degrees

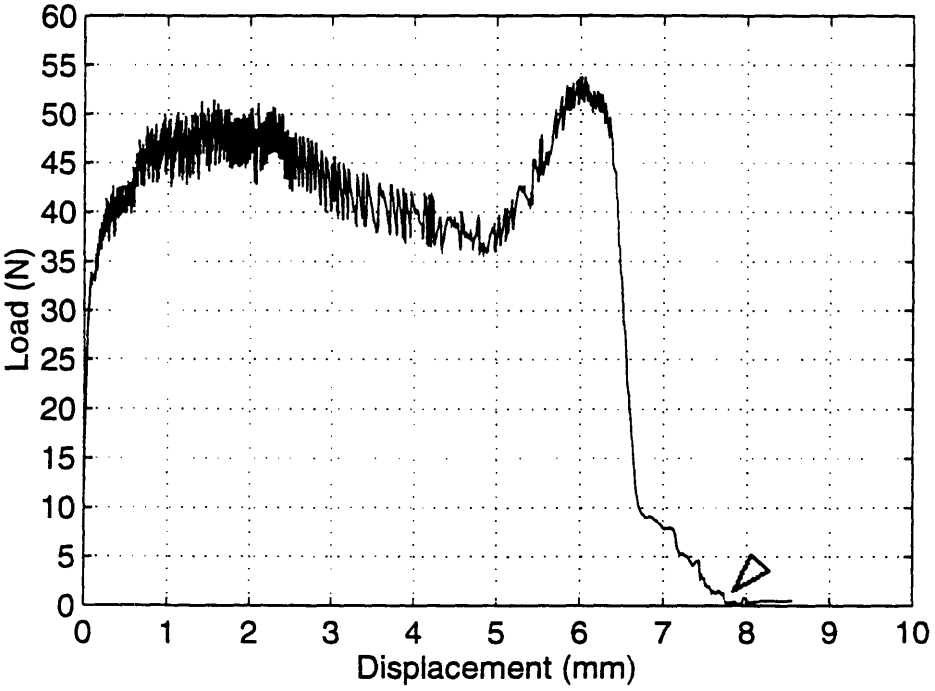

Figure 5.12: Pull-out curve for Series seven. specimen #2, Matrix: f'c = 5,000 psi, Fiber: F_y = 138,500 psi, Fiber Inclination: θ = sixty degrees

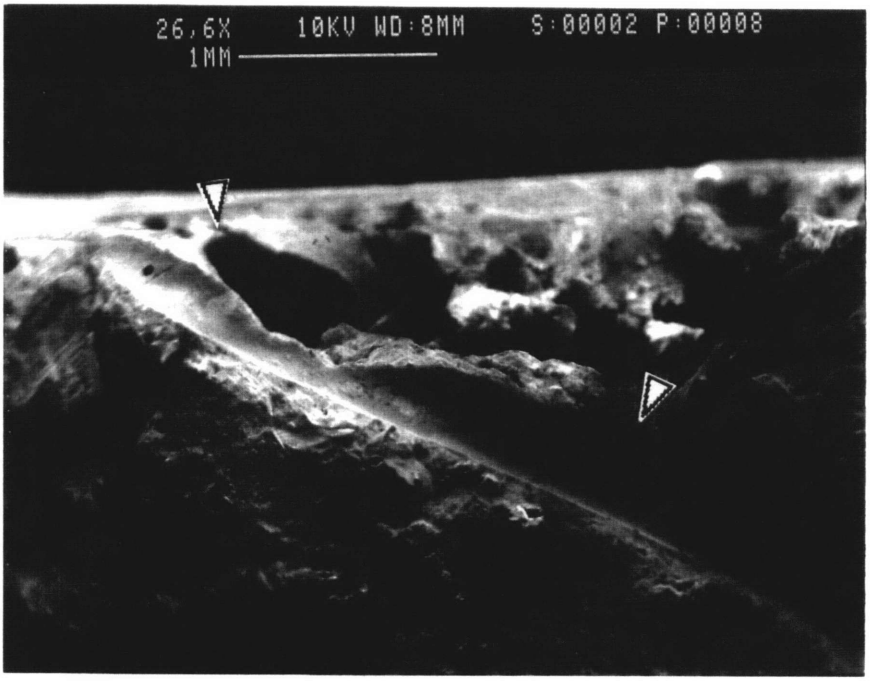

Figure 5.13: SEM micrograph of specimen #4, series four, corresponding to Figure 5.11, Spalling length was measured between arrows

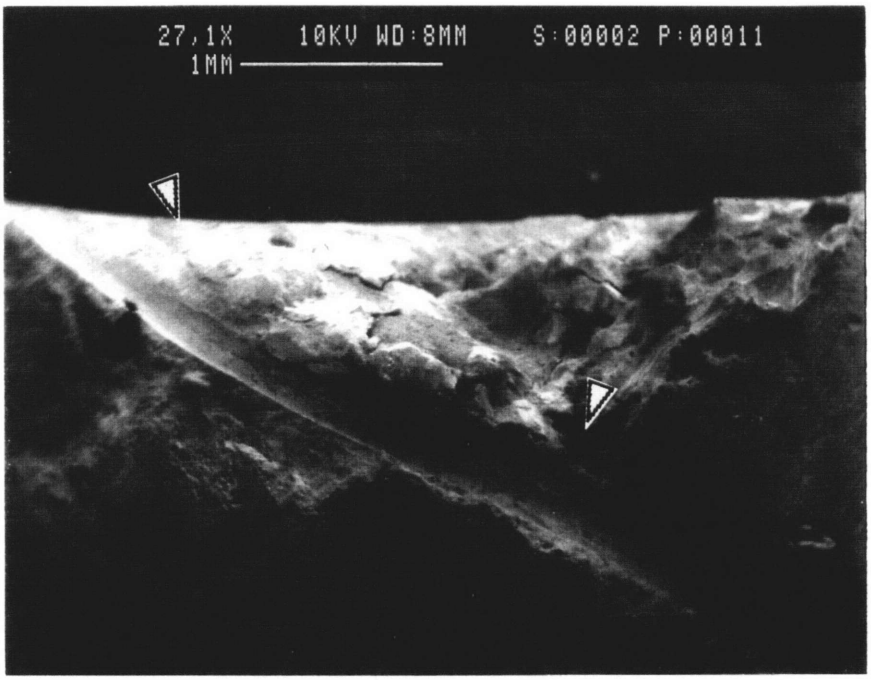

Figure 5.14: SEM micrograph of specimen #2, series seven,
corresponding to Figure 5.12, Spalling length is measured between arrows

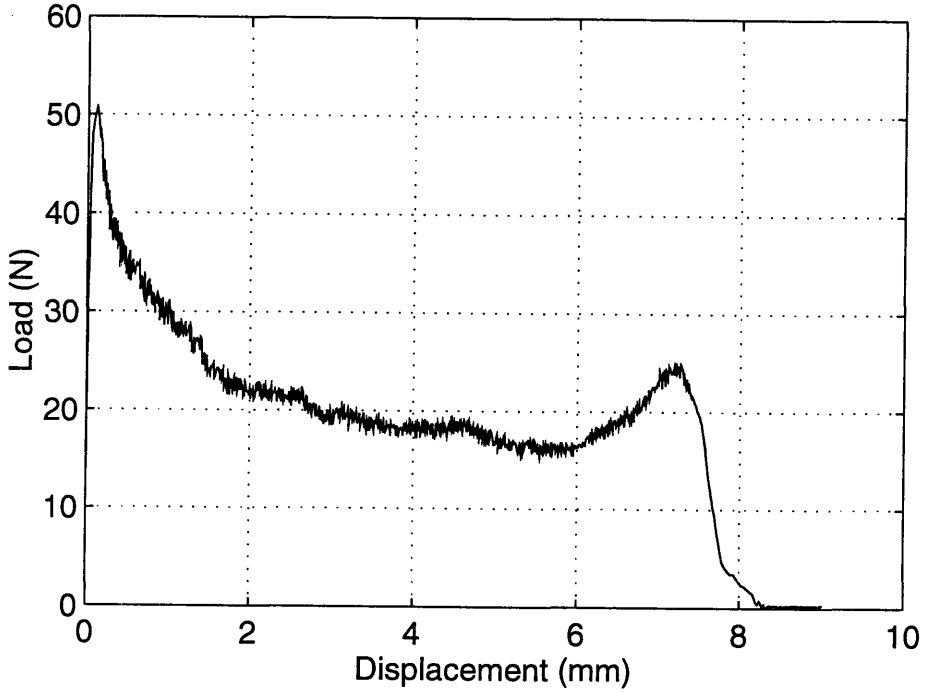

Figure 5.15: Pull-out curve for Series four, specimen # 6; Matrix: f'c = 5,000 psi, Fiber: F_y = 39,900 psi, Fiber Inclination: θ = thirty degrees

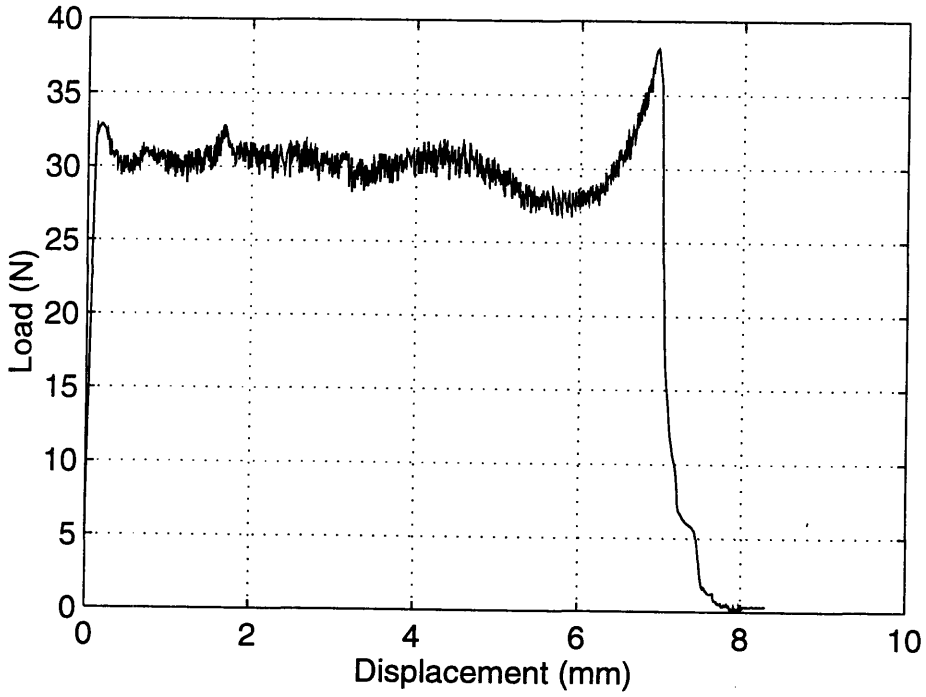

Figure 5.16: Pull-out curve for Series six, specimen #1; Matrix: f'c = 5,000 psi, Fiber: Fy = 92,200 psi, Fiber Inclination: θ = sixty degrees

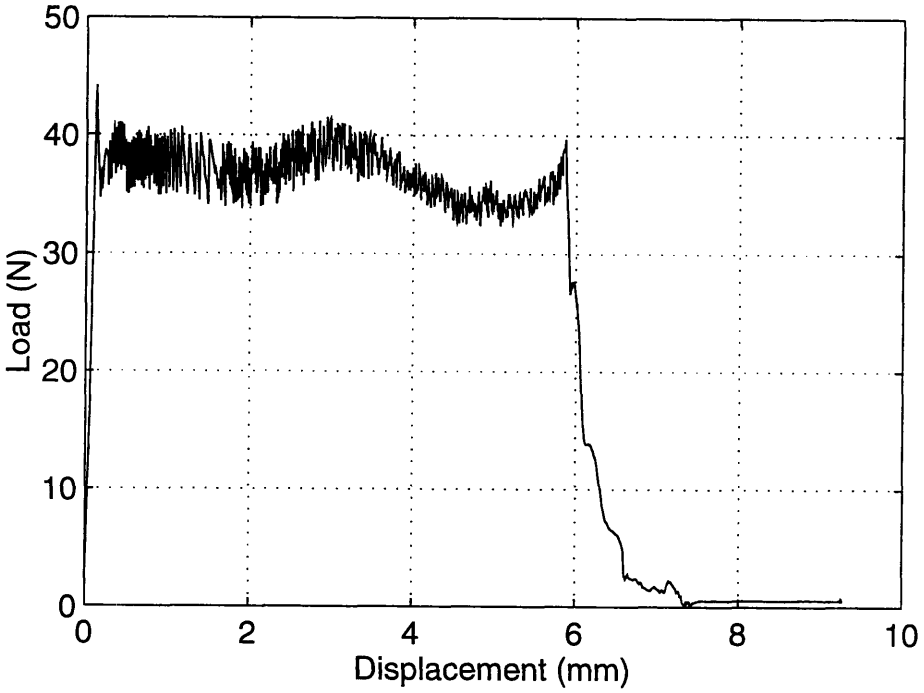

Figure 5.17: Pull-out curve for Series One, specimen #5; Matrix: f'c = 5,000 psi, Fiber: Fy = 170,000 psi, Fiber Inclination: θ = sixty degrees

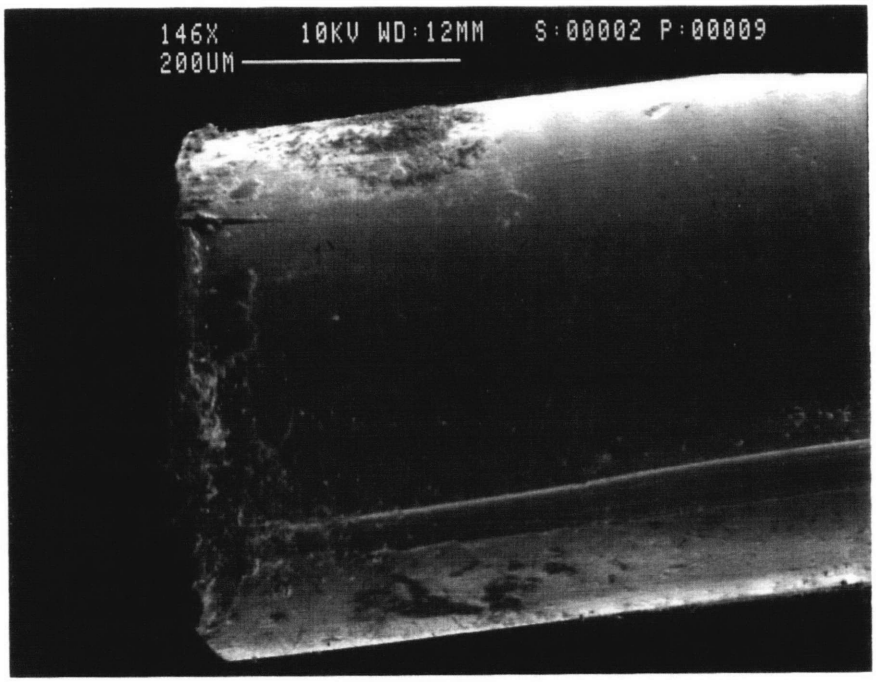

Figure 5.18: SEM micrograph of specimen #6, series four, corresponding to Figure 5.15, shows end of fiber after pullout with mortar on top edge

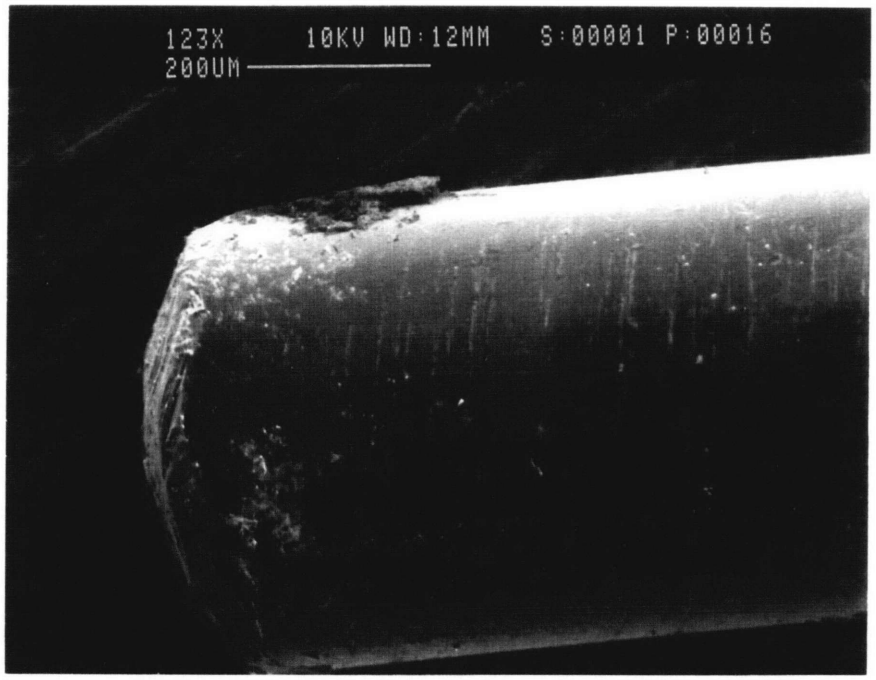

Figure 5.19: SEM micrograph of specimen #1, series six, corresponding to Figure 5.16, shows end of fiber after pullout with mortar on top edge

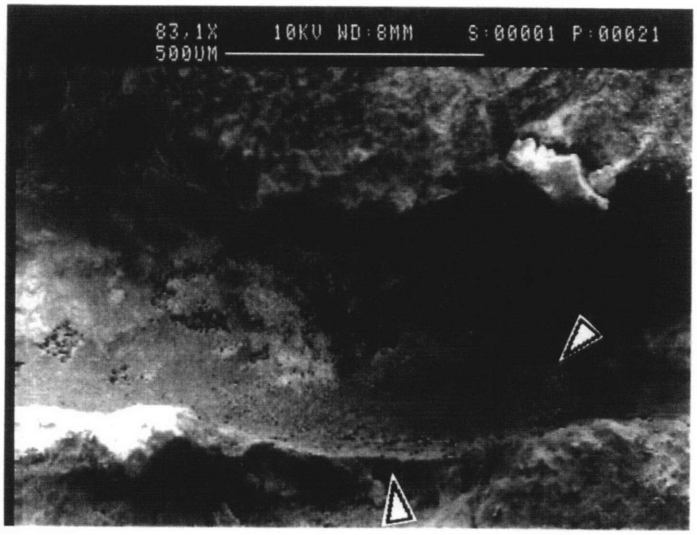

Figure 5.20: SEM micrograph of specimen #5, series one, corresponding to Figure 5.17, shows damage on bottom and left side of groove left by fiber

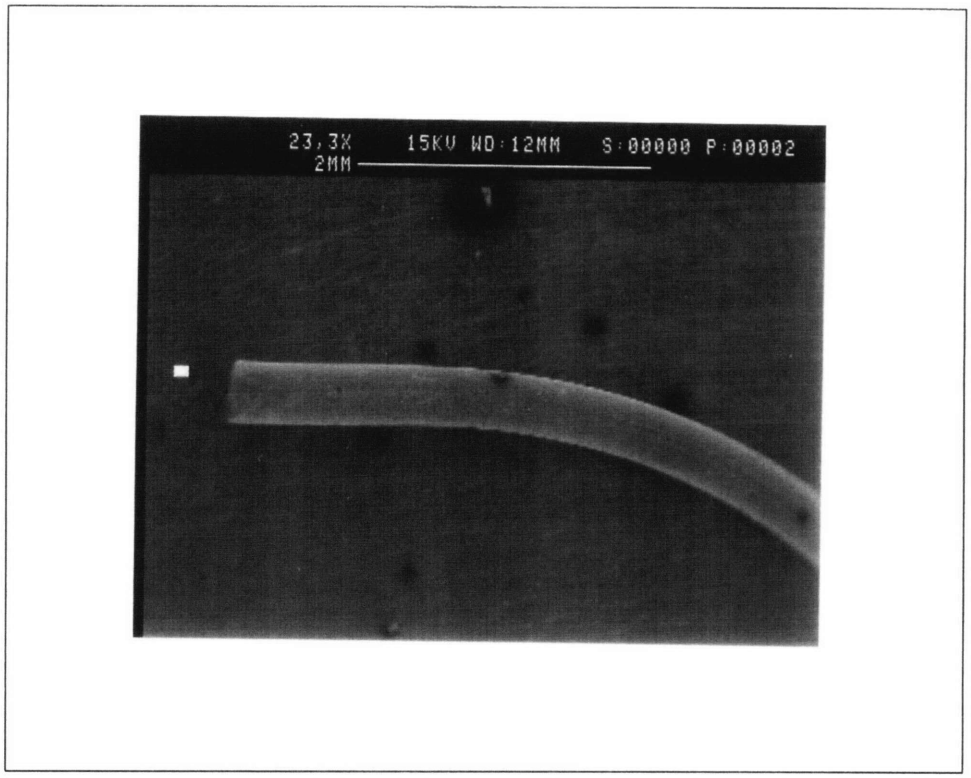

Figure 5.21: SEM micrograph of specimen #5, series one, shows that end of fiber was still straight after pullout

6.0 NUMERICAL ANALYSIS MODEL AND EXPERIMENTAL COMPARISON

6.1 INTRODUCTION

Various models have been developed to simulate the fiber pull out problem. Some models use a constant pull-out friction for the post debonding/slipping region. Others have tried to account for yielding in resin matrices. Leung and Chi have recently developed a model for fiber reinforced mortars which includes spalling, fiber yielding and bending, debonding and the effects of obliquely positioned fibers. However, the post peak friction is still assumed to be constant. In this work the model is modified by incorporating a multilinear drop in interfacial friction.

6.2 EXPLANATION OF MODEL

The model essentially simulated an elasto-plastic beam supported by an elastic foundation with varying elastic properties. For fibers laying at an angle to the crack face, the area of matrix under the fiber changes so the stiffness properties of the matrix had to change as well. Matrix spalling was modelled by removing elements of the matrix as they failed.

The fiber was broken down into a discrete number of elements. The fiber was pulled out a specified displacement and then the stiffness equations were solved. For angled fibers the fiber was tested for yielding.

Crack-bridging forces have two components, one, due to debonding and pull-out of the fiber and the other due to the bending of the fiber. Debonding and pull-out are a function of interfacial bonding and friction between the fiber and matrix. The bending component is a function of the fiber and matrix stiffnesses and strengths. Ideally a combination of fiber yield strength and matrix compressive strength could be used to optimize the peak bridging force and the pullout work.

The fiber is modelled as a beam with a circular cross-section. The load is applied axially and laterally due to debonding/pull-out and fiber bending, respectively. Fiber bridging force is given by:

$$\textbf{Bridging Force} = \mathbf{F_{Debonding/Pull\text{-}out}}(cos\ \theta) + \mathbf{F_{bending}}(sin\ \theta) \qquad (6.1)$$

A detailed description of the simulation can be found in Ref. [Chi 1992].

6.3 Model Parameters and Modifications

Parameters used in the model predictions were as follows: (1) Interfacial shear strength, τ_s; (2) frictional strength of the fiber-matrix interface, τ_i; (3) fiber embeddment length, l = 10 mm (0.3937 in); (4) fiber inclination angle, θ = 0°, 30°, and 60°; (5) fiber material properties including: Elastic Modulus of fibers, E_f = 200 GPa (29×10^6 psi); fiber diameter, d = 0.5 mm (0.02 in), and fiber yield strength, f_y; and (6) matrix material properties including: Elastic Modulus of the matrix, E_m; and matrix failure strength, f'_{sp}.

It was desired to model the pull-out load vs. fiber end displacement by a polylinear configuration following the initial peak crack bridging load. For this the first set of experiments were conducted with varying matrix compressive strengths and fiber angles normal to the crack face. From tests for zero fiber inclination angle the author was able to decern several distinct regions in the fiber pull-out history. It is quite clear that the interfacial friction degrades following debonding.

During debonding, the interfacial friction is assumed to be constant at the value of τ_s ($=\tau_i$), however in the pull-out region the friction changes as a function of the pull-out length, and crack opening. The pull-out behavior was modelled by specifying the interfacial friction at specific crack opening locations along the pull-out history. The micromechanical model developed by [Chi '92] was the basis for the revisions made in this thesis.

The values of interfacial friction were taken from the tests of each series with zero degrees. Each test within the series was plotted as a pull-out force vs. displacement graph. The results were then plotted on a log scale along the pull-out load axis to determine variations in interfacial friction. Several regions were noted where the friction was more or less linear in the post-peak region. The displacement values corresponding to the points where these regions changed were noted. Friction values at each of these displacement points were taken from each test in the series and averaged. The average values were used in the model and produced pull-out responses reflecting an average of the interfacial friction from the tests in each series.

Any differences between the model and the predictions in the frictional pull-out region are due to the assumptions that the friction varies linearly between two prescribed frictional values. Once the prediction was accurate enough for cases of zero degrees it was used to predict the pull-out response for corresponding cases with different fiber angles. The entire purpose of this model is to try and account for fiber angles greater than zero which includes matrix spalling, fiber bending and fiber yielding.

The major adjustments to the model only affected the constants used to calculate the crack bridging force at a specified pull out displacement. It has been shown previously that the interfacial friction degrades during slip therefore it could not be simulated as a constant.

Another factor which was looked at was the mortar spalling strength. This is important for fibers at an oblique angle to the crack face. During pull-out the mortar under the fiber experiences very high compressive forces from the bending component of the pull-out force. Normally concrete is an extremely brittle and relatively weak material in compression and in tension. This inherent weakness is caused by microcracks in the matrix, however, when looking at the small area under load by the fiber, the crack size is extremely small. With very small crack sizes the spalling strength of the mortar should be much higher than that of the macroscopic material. Because of this the mortar spalling strength is actually a fitting constant in this simulation.

Simulations were made of specimens with angled fibers and normal matrix strength. The matrix strength was then adjusted upward to try and fit the curve to the

experimental results. From this it was hoped that we could determine the spalling strength of the mortar specimens and better simulate pull-out for angled fibers.

6.4 Comparison of Model With Experimental Results

The purpose of the model was to predict crack bridging behavior for fibers at angles greater than zero degrees while accounting for mortar spalling. The model used the material properties, and interfacial properties for each case of fiber yield strength at zero degrees. Initialization of the model with properties from matrix-fiber interaction at zero degrees describes the debonding and pull-out phenomenom of the specimens. From this the model should predict changes in fiber angle. The simulation will be compared to the experimental results obtained from section two of the experimental program.

6.4.1 Observations

The Qualitative trend is in good agreement with experimental results, however, quantitatively the simulation deviates for fibers at angles. The model predicts pull-out behavior very well for fibers perpendicular to the crack face, (Figure 6.1, 6.4, 6.7, 6.10, 6.13).

At zero degrees the analysis is quite simple and straight forward. Concrete spalling is not taken into account and only friction is necessary to predict the pull-out behavior. However, for larger angles the simulated load decreases much faster after reaching the peak than the experimental results, (Figure 6.2). Figure 6.2 is a plot of load vs displacement of the average test results for series one, 5,000 psi mortar, f_y = 170,000

psi, and θ = 30 degrees, compared to four simulations with different matrix spalling strengths. The first plot, marked "A", was run with a strength of 5,000 psi, but it is evident that the load drops off suddenly, due to spalling of the matrix. The spalling strength was increased to 100 MPa then 200 MPa and finally 400 MPa which began to compare fairly well. However, an inspection of the data file shows that the entire length of the mortar under the fiber spalled which does not follow with the experiments. Figure 6.3 is a comparison of series one with an angle of 60 degrees, where the prepeak behavior is comparable but then it drops off as well. Figures 6.4 through 6.15 display simulations run for section two of the experimental program for each angle and fiber type. Again the zero degree cases are favorable.

6.4.2 Explanation of Inconsistencies

Inconsistencies were noted between the experimental results and the prediction of the crack-bridging force model. These deviations can be explained due to effects which were not included in the current model. It has been shown that the model predicts the bridging force for zero degree angles very well, however, three mechanisms were not taken into account in this model were: "Snubbing", P-δ effect, and the plausible presence of friction along the spalled part of the matrix groove.

As the fiber is bent, the axial force along the embedded part is no longer in line with the axial force at the midlle of the crack. The resulting P-δ effect will lead to an increase in the force required to bend the fiber through a given displacement.

Snubbing is normally observed for synthetic fibers. Li, Wang and Backer (1990) reported that for increasing angles the normalized pull-out load, with respect to zero degrees, increased. Their findings showed that the effect of snubbing can be characterized by a "snubbing" coefficient. For steel fiber of small diameter, the snubbing effect can also be important.

6.6 OVERVIEW OF COMPARISON

The behavior of the model had mixed results mostly due to fiber angle changes. The results for zero degree specimens compared favorably to the experimental results. This is not surprising since the interfacial properties for the model came from the experimental results. The model for zero degrees is not complicated by mortar spalling, or the P-δ effect.

However, the model prediction for angles thirty and sixty degrees did not compare well. The crack bridging force was under estimated in the post-peak region. One reason for this could be due to the fact that the model does not take in to account the P-δ effect.

The optimization did not compare well with the experimental results. From the tests, the fiber with f_y = 138,500 psi had similar maximum pull-out loads with that of the fiber with f_y = 170,000 psi. But from the simulations, a fiber of f_y = 170,000 psi gives the largest loads for both 30 and 60 degrees, where as the 138,500 psi fiber gives much lower loads for both angles. Figure 6.16 is a plot of maximum pull-out load vs fiber angle for results from the simulations. A comparison of maximum pull-out values for 30° and 60° from the model and from tests show that most are very close to the actual loads, except

the f_y = 138,500 psi fiber where the discrepancy is much larger than for any of the other fibers, (Figure 6.17a,b,c and 6.18a,b).

6.7 PROGRAM SOURCE CODE AND INPUT FILES[1]

A portion of the model source code can be found in Appendix E. This portion is the modified function which calculates the crack bridging force. For the complete source code see [Chi 1992]. Copies of the input files for each series is listed in Appendix E as well. The input files vary only in fiber yield strength, mortar failure strength and interfacial friction values.

[1] Chi, J. C., "Micromechanical Modeling of Ductile-Fiber-Reinforced Ceramics",

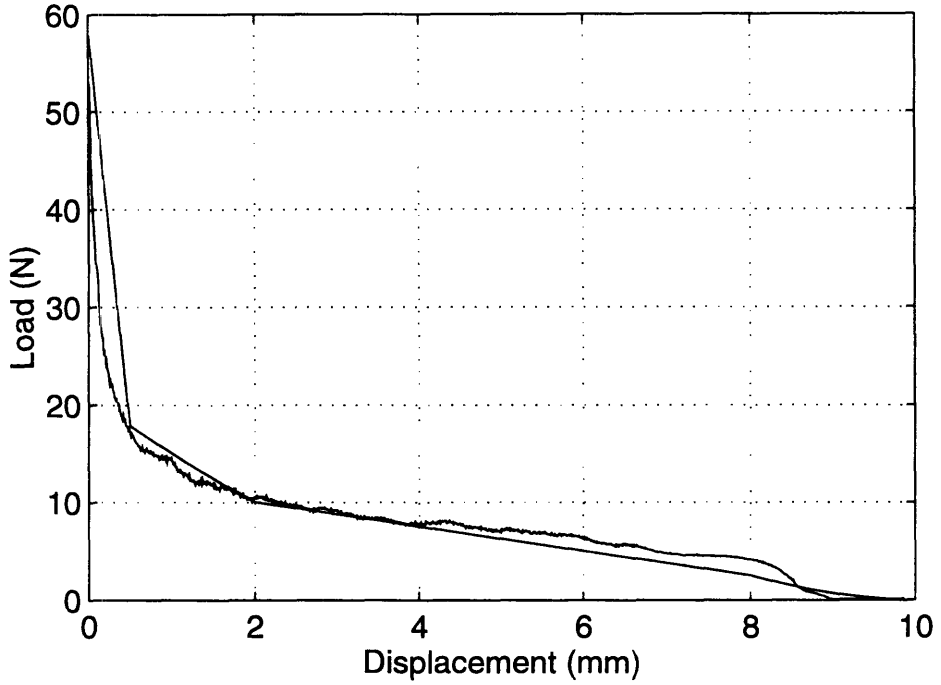

Figure 6.1: Simulation comparison for Series One; Matrix: f'c = 5,000 psi, Fiber: Fy = 170,000 psi, Fiber Inclination: θ = zero degrees

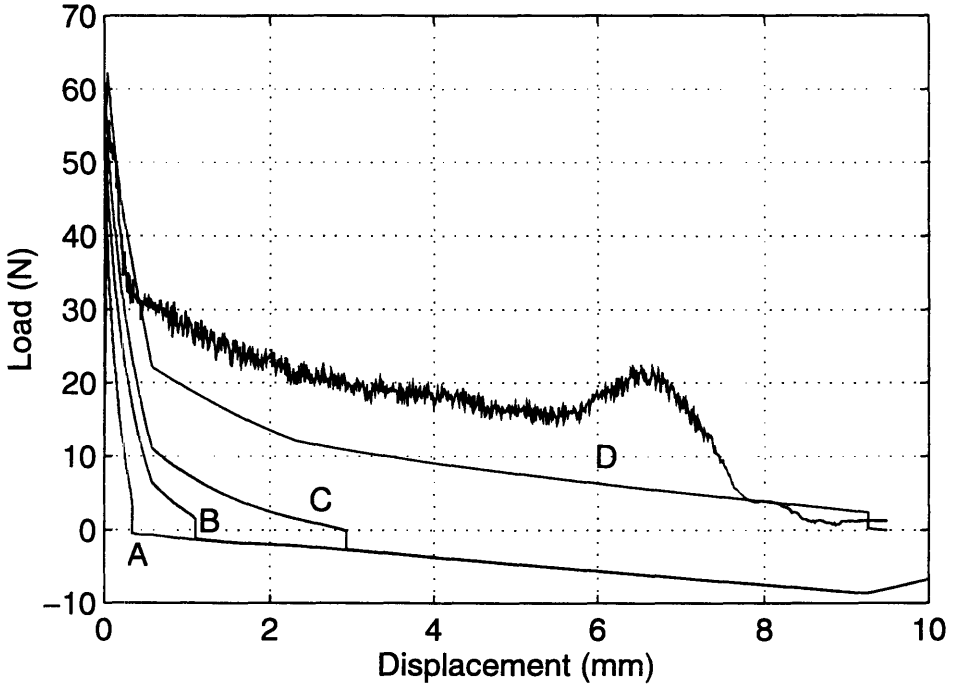

Figure 6.2: Simulation comparison for Series One; Matrix: f'c = 5,000 psi, Fiber: Fy = 170,000 psi, Fiber Inclination: θ = thirty degrees

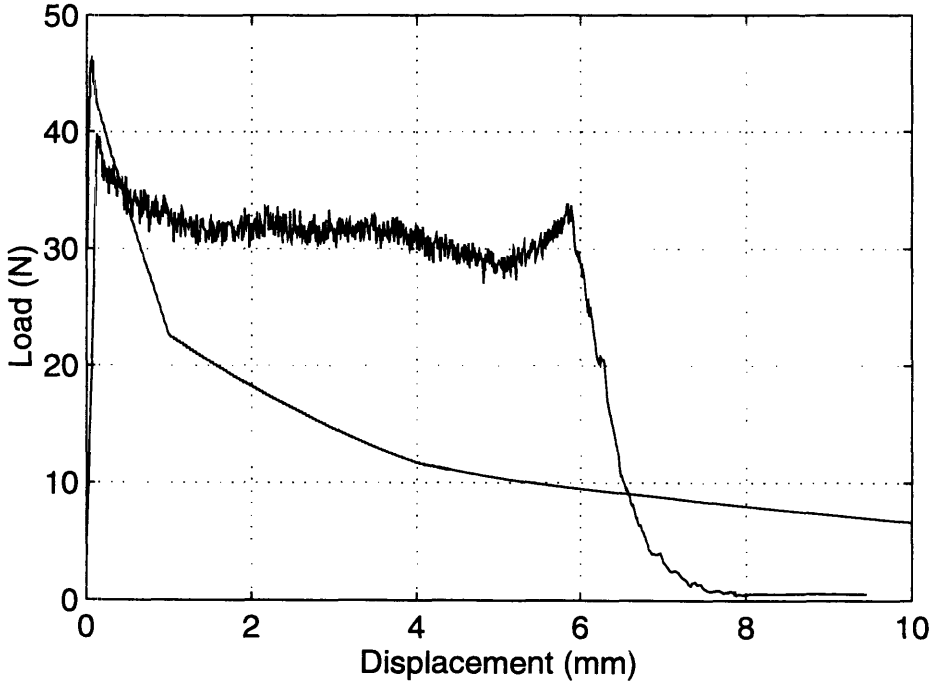

Figure 6.3: Simulation comparison for Series One; Matrix: f'c = 5,000 psi, Fiber: Fy = 170,000 psi, Fiber Inclination: θ = sixty degrees

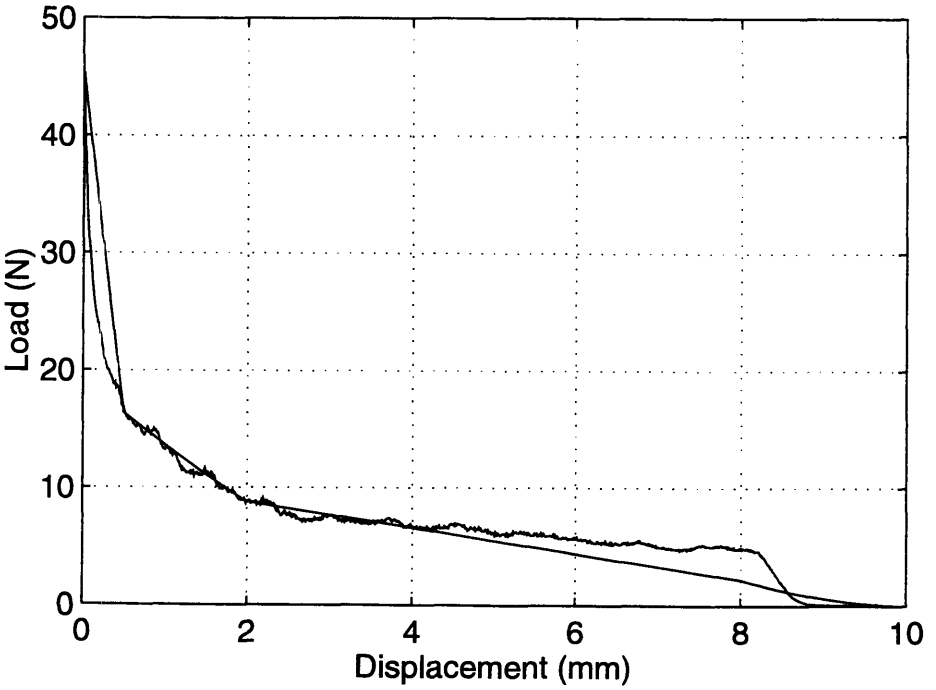

Figure 6.4: Simulation comparison for Series Four; Matrix: f'c = 5,000 psi, Fiber: Fy = 39,900 psi, Fiber Inclination: θ = zero degrees

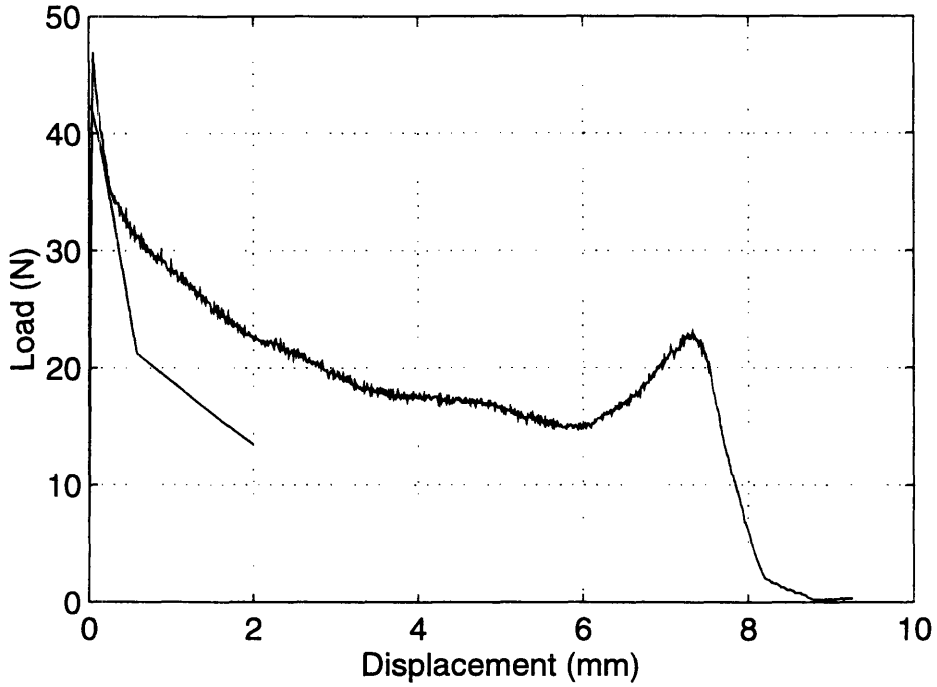

Figure 6.5: Simulation comparison for Series Four; Matrix: f'c = 5,000 psi, Fiber: Fy = 39,900 psi, Fiber Inclination: θ = thirty degrees

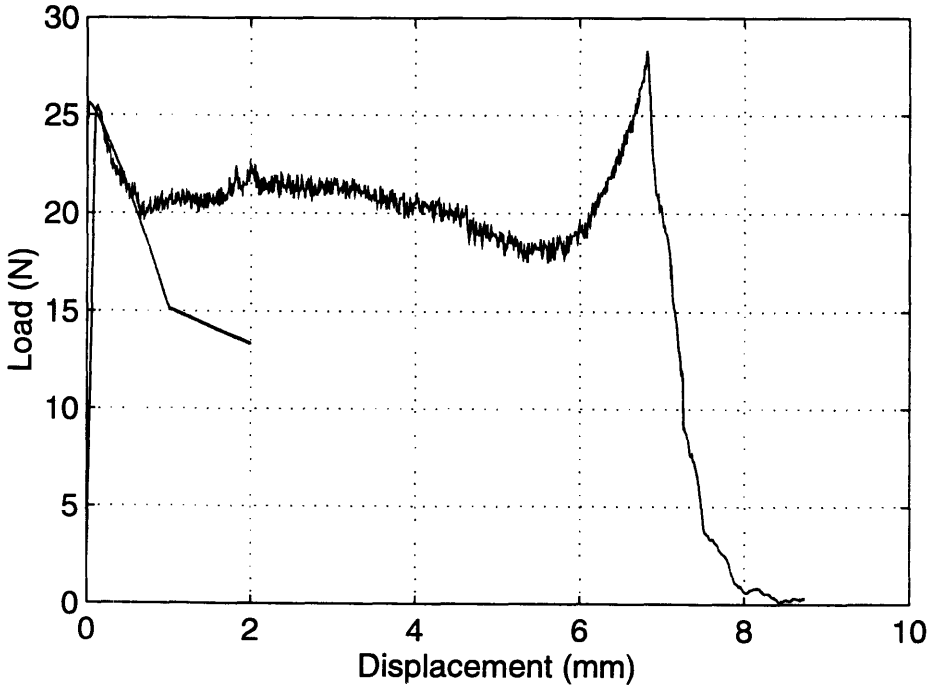

Figure 6.6: Simulation comparison for Series Four; Matrix: f'c = 5,000 psi, Fiber: Fy = 39,900 psi, Fiber Inclination: θ = sixty degrees

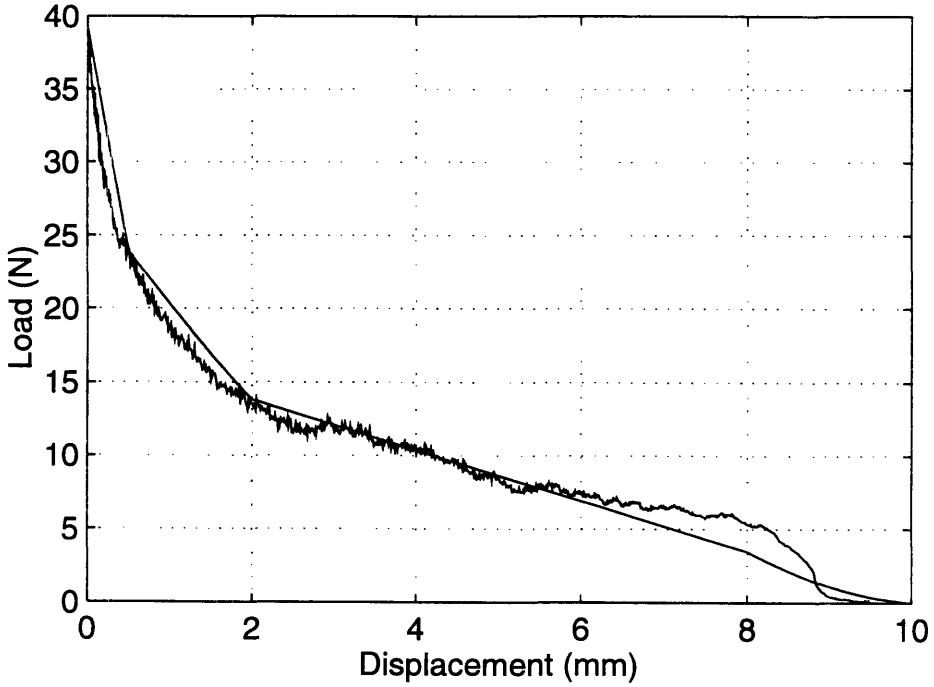

Figure 6.7: Simulation comparison for Series Seven; Matrix: f'c = 5,000 psi, Fiber: Fy = 138,500 psi, Fiber Inclination: θ = zero degrees

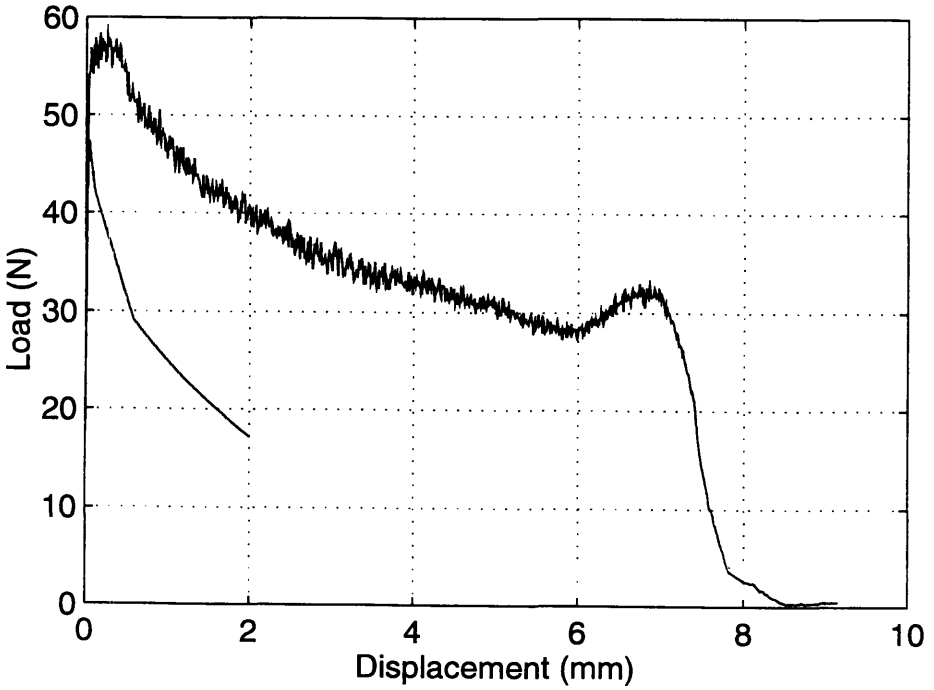

Figure 6.8: Simulation comparison for Series Seven; Matrix: f'c = 5,000 psi, Fiber: Fy = 138,500 psi, Fiber Inclination: θ = thirty degrees

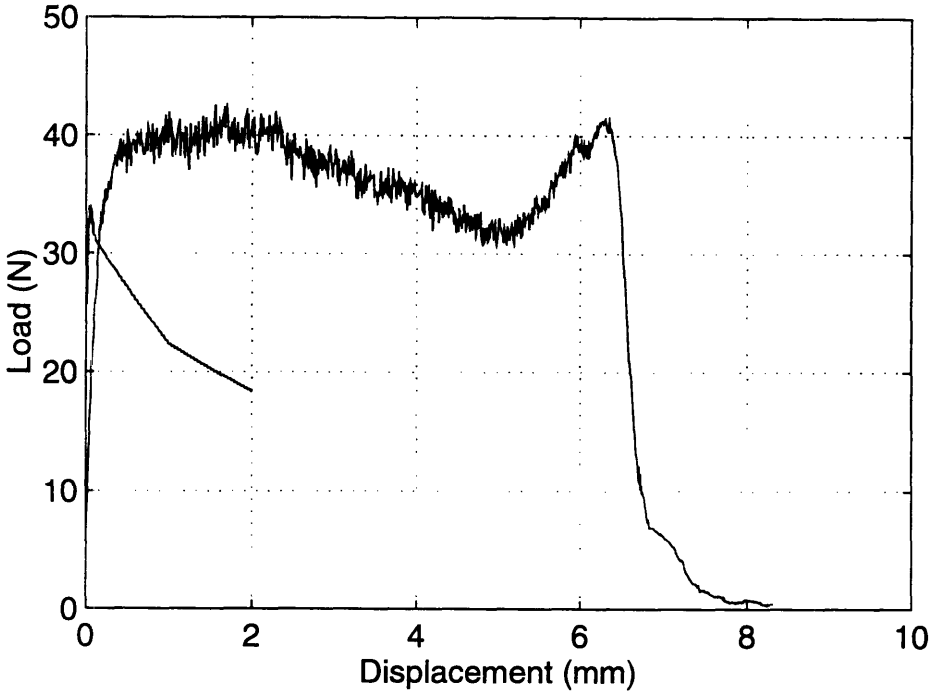

Figure 6.9: Simulation comparison for Series Seven; Matrix: f'c = 5,000 psi, Fiber: Fy = 138,500 psi, Fiber Inclination: θ = sixty degrees

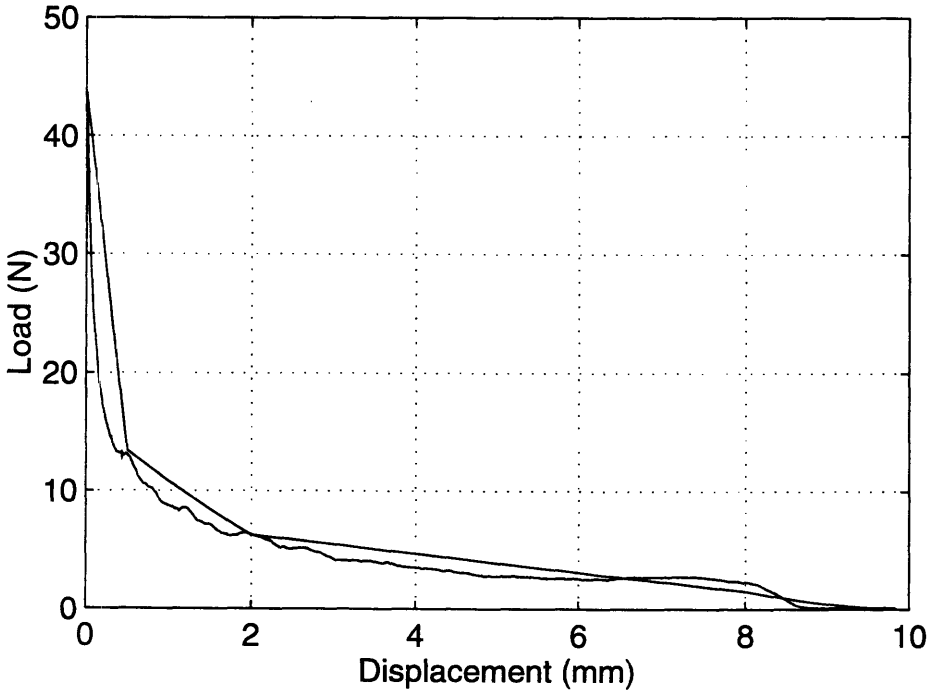

Figure 6.10: Simulation comparison for Series Five; Matrix: f'c = 5,000 psi, Fiber: Fy = 68,100 psi, Fiber Inclination: θ = zero degrees

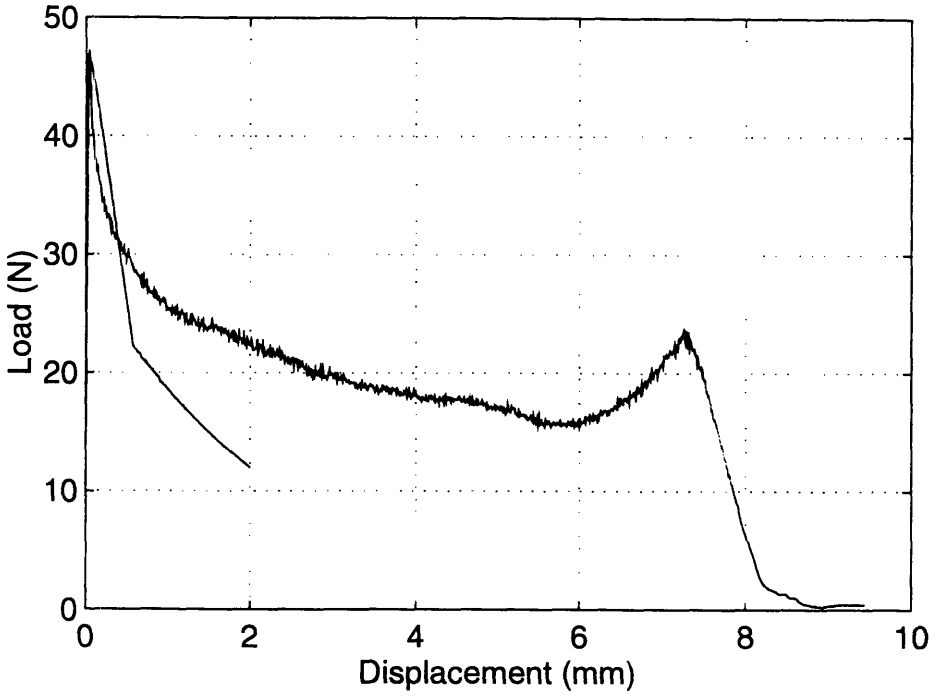

Figure 6.11: Simulation comparison for Series Five; Matrix: f'c = 5,000 psi, Fiber: Fy = 68,100 psi, Fiber Inclination: θ = thirty degrees

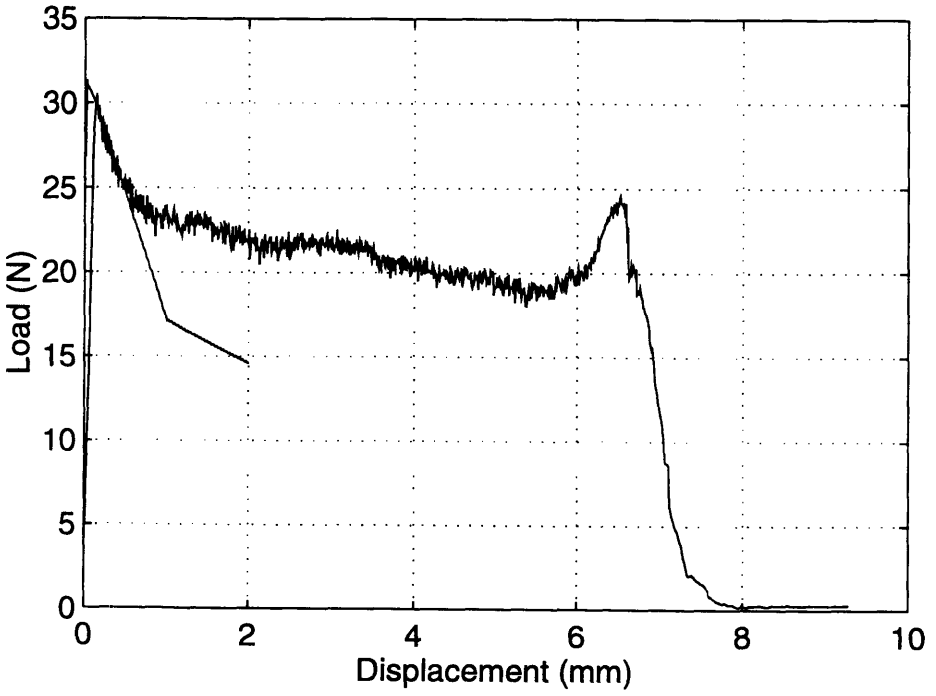

Figure 6.12: Simulation comparison for Series Five; Matrix: f'c = 5,000 psi, Fiber: Fy = 68,100 psi, Fiber Inclination: θ = sixty degrees

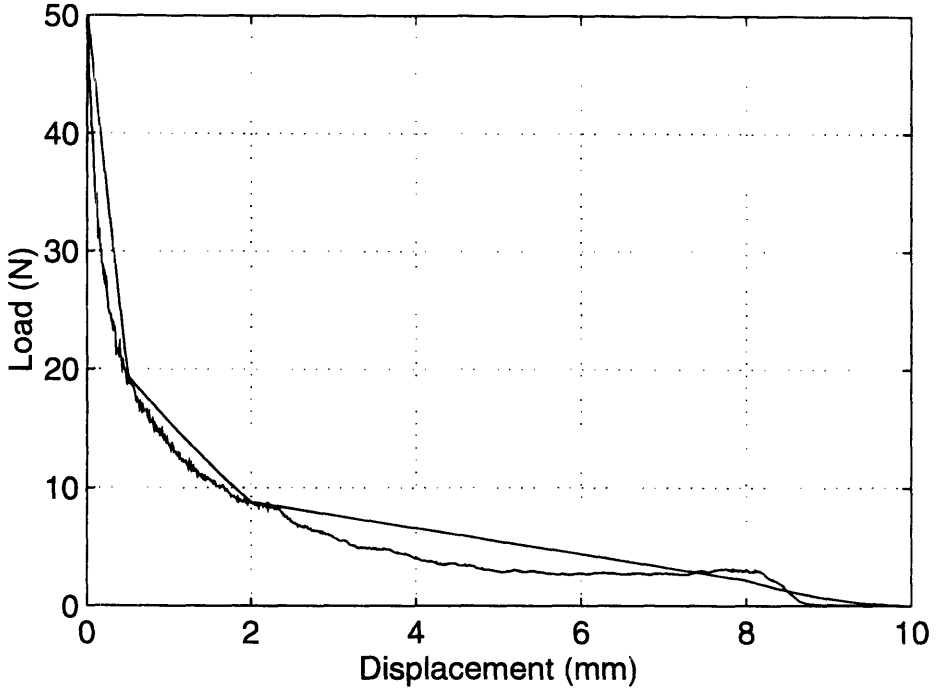

Figure 6.13: Simulation comparison for Series Six; Matrix: f'c = 5,000 psi, Fiber: Fy = 92,200 psi, Fiber Inclination: θ = zero degrees

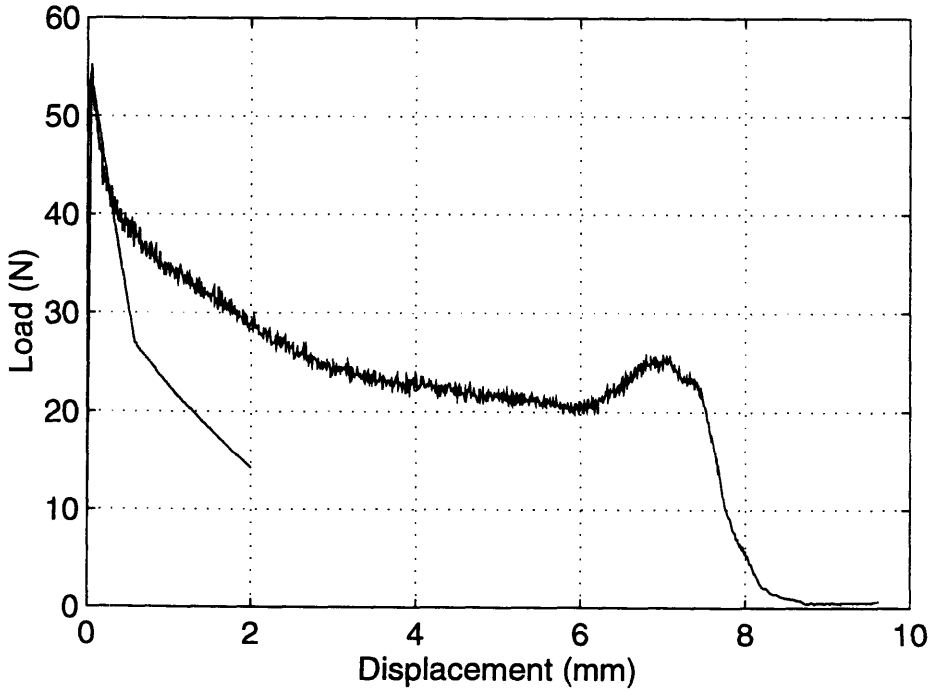

Figure 6.14: Simulation comparison for Series Six; Matrix: f'c = 5,000 psi, Fiber: Fy = 92,200 psi, Fiber Inclination: θ = thirty degrees

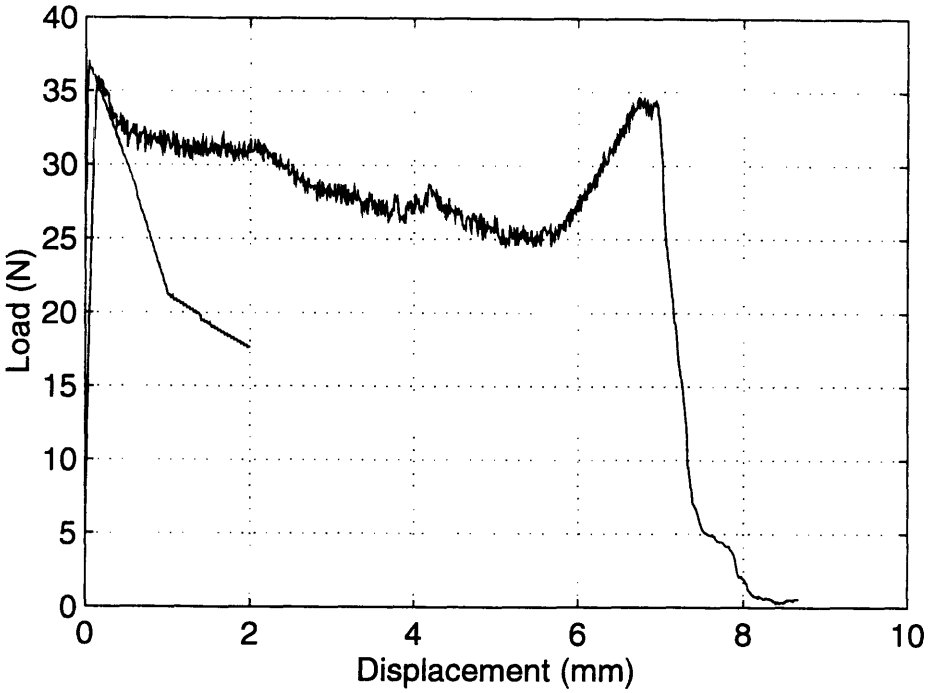

Figure 6.15: Simulation comparison for Series Six; Matrix: f'c = 5,000 psi, Fiber: Fy = 92,200 psi, Fiber Inclination: θ = sixty degrees

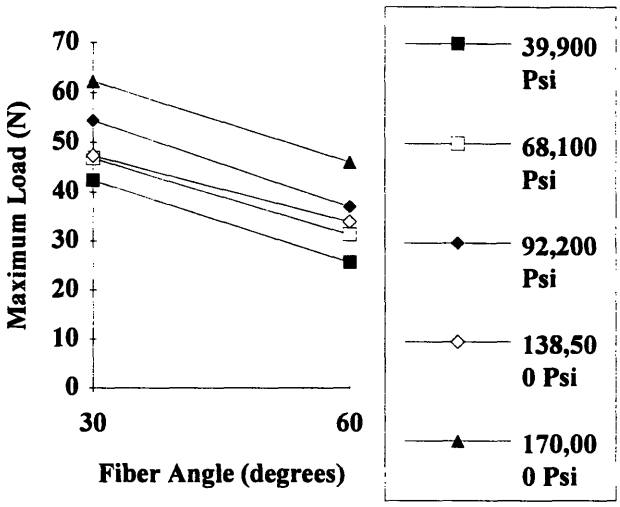

Figure 6.16: Maximum Pull-out Load from simulation for varying fiber yield strengths

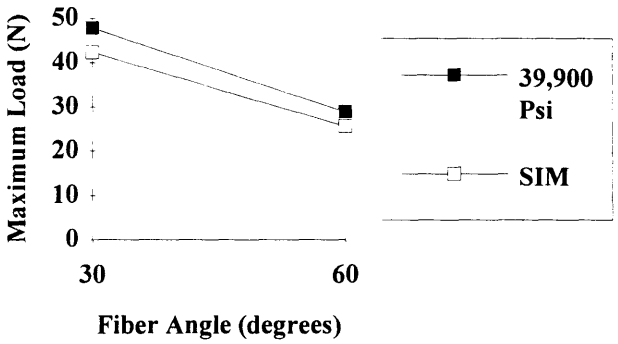

(a)

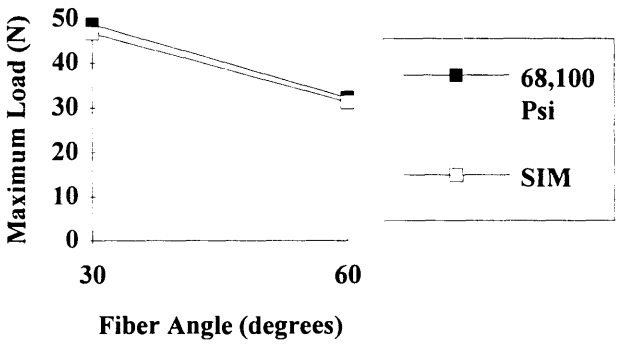

(b)

Figure 6.17: Simulation versus experimental Maximum Load for Fiber: (a) f_y = 39,900 psi and (b) f_y = 68100 psi

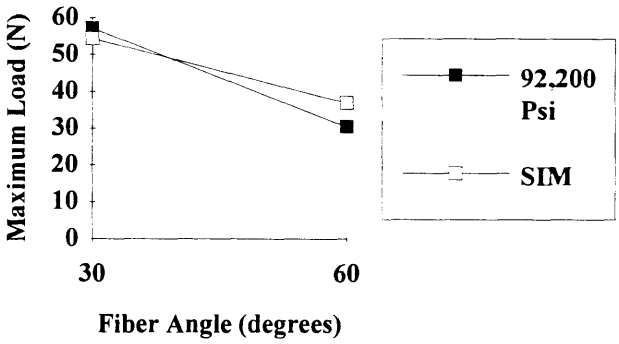

(a)

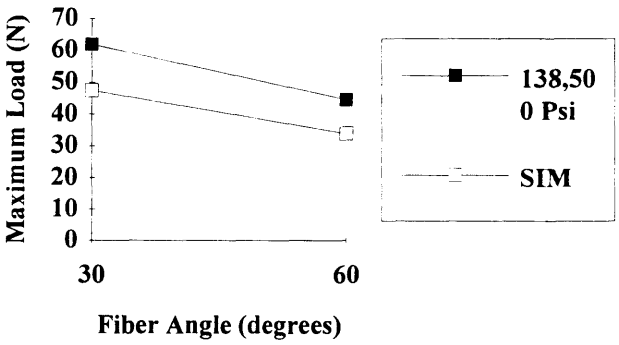

(b)

Figure 6.18: Simulation versus experimental Maximum Load for Fiber: (a) f_y = 92,200 psi and (b) f_y = 138,500 psi

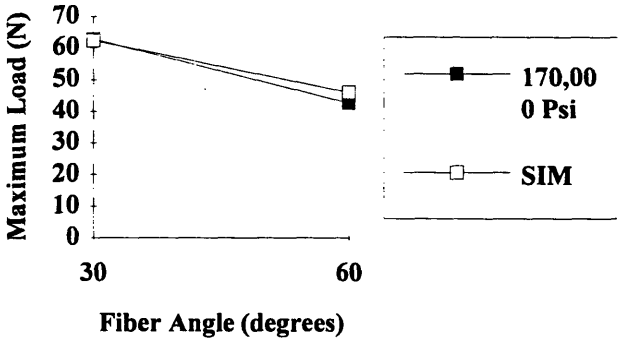

Figure 6.19: Simulation versus experimental Maximum Load for Matrix: 5,000 psi, Fiber: f_y = 170,000 psi

7 RESULTS AND CONCLUSION

7.1 SUMMARY OF EXPERIMENTAL RESULTS

Fiber pull-out behavior is affected by mortar strength and fiber angle were studied in the first part of the program. It was found that for increasing mortar strength the maximum pull-out load increased as well. When the fiber angle was increased the maximum pull-out load decreased while the work done to pullout the fiber was highest at about 30°.

For the second part of the program several fibers were compared to see which yield strength provided the best crack bridging behavior. For maximum pullout load two fibers were comparable for 30° and 60°, 170,000 psi and 138,500 psi yield strength wire. However for bending components of pullout force the 138,500 psi fiber was clearly the best, attaining maximum values at 30° and 60°. For total pullout work this fiber also gave the best results. Spalling length for the 138,500 psi fiber was comparable to most of the other fibers except for the highest strength fiber (170,000 psi) which had the greatest spalling.

7.1.1 CONCLUSIONS

The experimental procedure which was developed for this study yielded valuable information on the crack bridging behavior of fiber reinforced concrete. The test method was such that it approximated as best as possible actual crack opening across a fiber.

Within the samples of this work an optimal fiber yield strength was found for maximum pull-out work and energy absorption during crack opening. For high fiber strength, the amount of matrix spalling was found to increase. The results confirm that the mechanism of matrix spalling set a limit to the fiber yield strength for maximum reinforcement efficiency. It also implies that for a stronger matrix, the optimal yield strength will also be higher.

7.2 IMPROVEMENTS OF MODEL

An existing computer model was adjusted by incorporating a multilinear frictional drop so that the predicted curve for zero degree fibers more closely resembled that of actual pull-out tests. The predictions of the model for 0° were very close but for angles greater than that the model gave fair prediction of the peak load but severely underestimate the post-peak bridging force. It also fails to predict the occurrence of optimal behavior at σ_y = 138,5000 psi.

7.3 FURTHER RESEARCH TOPICS

Further study of the optimal fiber yield strength with respect to matrix strength should be carried out.

Additional modifications should be made to the simulation to account for the P-δ effect and snubbing effect.

APPENDIX A

Mortar Compressive Strength ~5,000 Psi					
Specimen	**Batch 1**	**Batch 2**	**Batch 3**	**Batch 4**	**Batch 5**
	(psi)	**(psi)**	**(psi)**	**(psi)**	**(psi)**
1	5115	6009	5273	5107	5107
2	5184	5859	5093	5096	5096
3	5393	6252	5096	5290	5290
4		6280	5168	5386	5386
Best of 3:	5200	6000	5100	5200	5200
Specimen	**Batch 6**	**Batch 7**	**Batch 8**	**Batch 9**	
	(psi)	**(psi)**	**(psi)**	**(psi)**	
1	4967	5479	5836	5121	
2	4748	5286	5744	5475	
3	4613	5123	5687	5326	
4	4741	5693	5836	4789	
Best of 3:	4800	5300	5800	5100	
Mean:				5300	
% Error:				6.0	

Table A.1: Compressive strength test results for 5,000 psi mortar

Mortar Compressive Strength ~10,000 Psi			
Specimen	**Batch 1**	**Batch 2**	**Batch 3**
	(psi)	**(psi)**	**(psi)**
1	10175	9659	10006
2	10041	10638	9894
3	10472	10220	10341
4	10589	10811	9604
Best of 3:	10200	10200	10100
Mean:			10200
% Error:			2.0

Table A.2: Compressive strength test results for 5,000 psi mortar

Mortar Compressive Strength ~12,000 Psi			
Specimen	**Batch 1**	**Batch 2**	**Batch 3**
	(psi)	**(psi)**	**(psi)**
1	11605	10952	12003
2	12339	11847	11692
3	11398	11466	12104
4	11259	12035	11852
Best of 3:	11400	11400	11800
Mean:			11500
% Error:			4.2

Table A.3: Compressive strength test results for 12,000 psi mortar

APPENDIX B

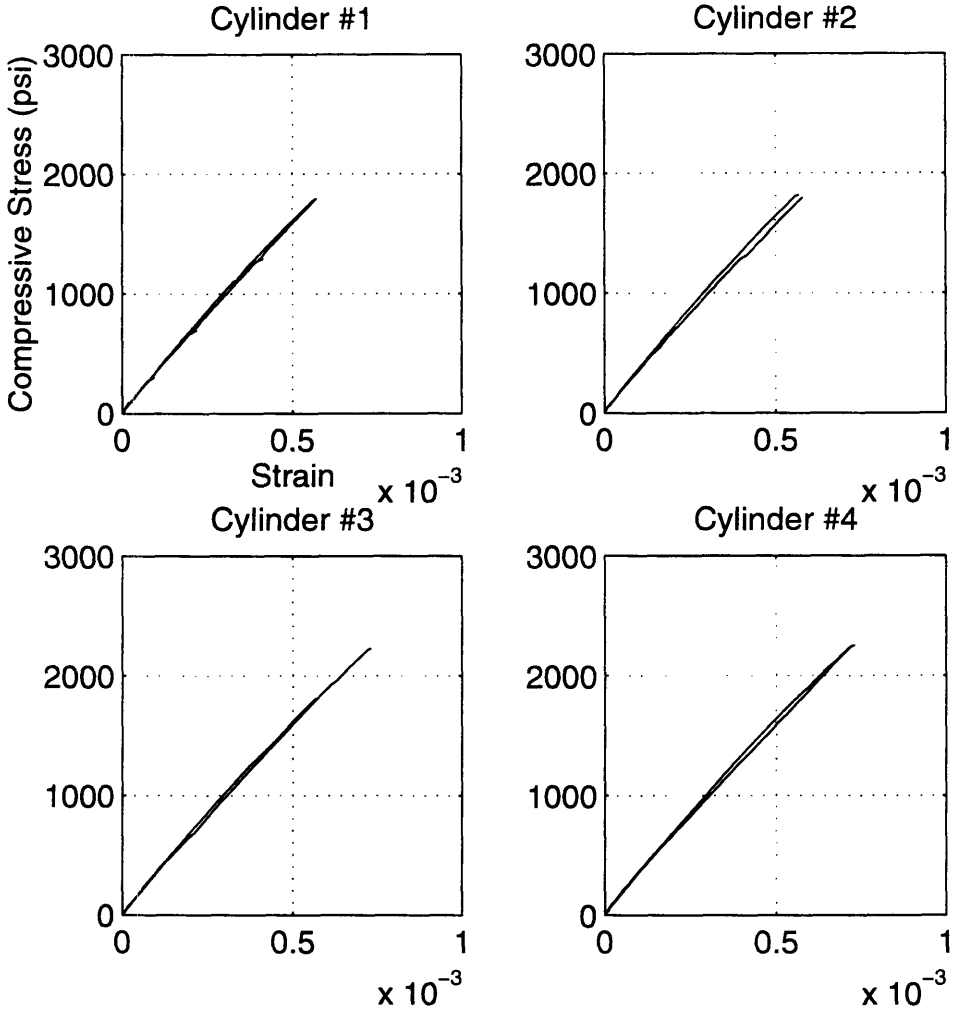

(a)

Elastic Modulus, 5,000 Psi Mortar			
Cylinder	**Trial 1**	**Trial 2**	**Average**
1	4.60E+06	4.55E+06	4.60E+06
2	4.80E+06	4.75E+06	4.80E+06
3	4.60E+06	4.55E+06	4.60E+06
4	4.75E+06	4.65E+06	4.70E+06
Mean:		(Psi)	4.70E+06
Batch 1		(GPa)	32.4

(b)

Elastic Modulus, 5,000 Psi Mortar			
Cylinder	**Trial 1**	**Trial 2**	**Average**
1	3.15E+06	3.10E+06	3.15E+06
2	3.20E+06	3.05E+06	3.15E+06
3	3.20E+06	3.10E+06	3.15E+06
4	3.20E+06	3.15E+06	3.20E+06
Mean:		(Psi)	3.15E+06
Batch 2		(GPa)	21.7

(c)

Figure B.1: (a) Sample Plots from Elastic Modulus Test for f'_c = 5,000 psi, Batch 2. Two trials per cylinder for four cylinders: (b) Elastic Modulus test results for f'_c = 5,000 psi, Batch 1; (c) Elastic Modulus test results for f'_c = 5,000 psi, Batch 2

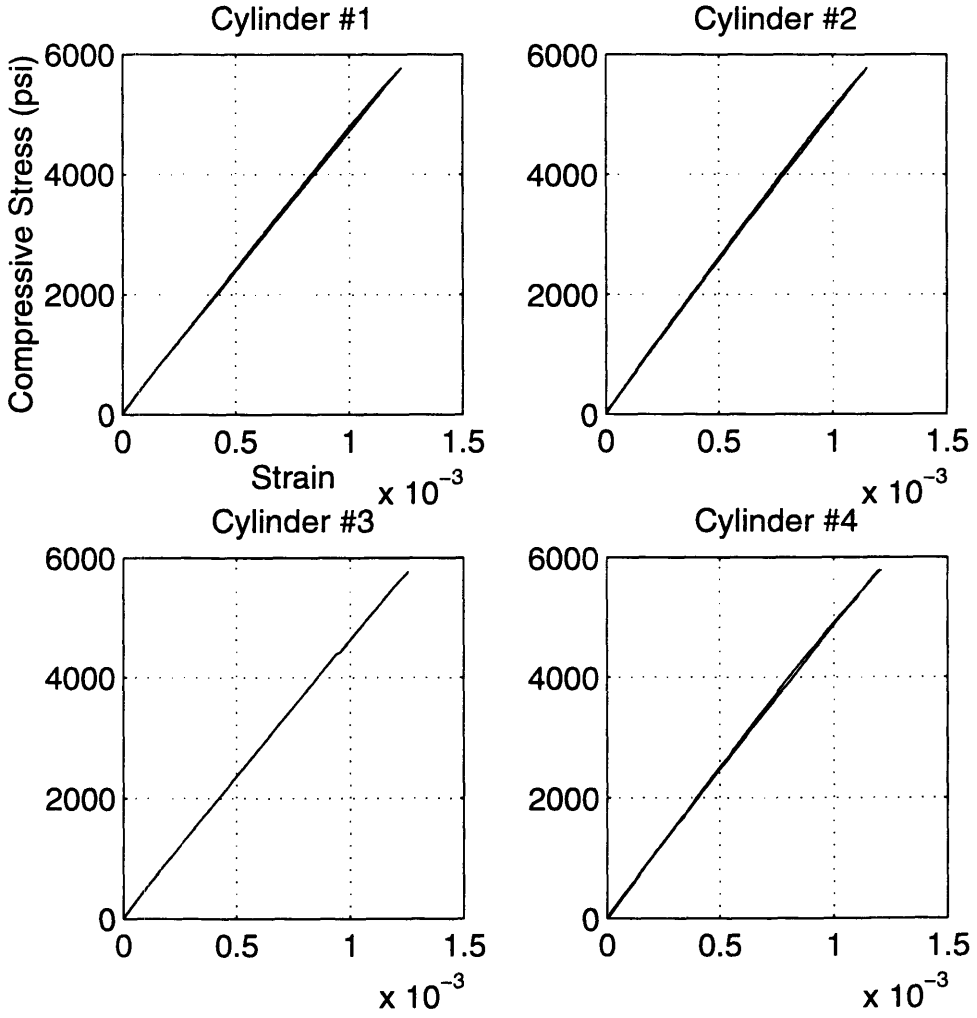

(a)

Elastic Modulus, 10,000 Psi Mortar			
Cylinder	**Trial 1**	**Trial 2**	**Average**
1	4.60E+06	4.50E+06	4.55E+06
2	4.55E+06	4.55E+06	4.55E+06
3	4.65E+06	4.60E+06	4.65E+06
4	4.65E+06	4.60E+06	4.65E+06
Mean:		(Psi)	4.60E+06
Batch 1		(GPa)	31.7

(b)

Elastic Modulus, 10,000 Psi Mortar			
Cylinder	**Trial 1**	**Trial 2**	**Average**
1	4.55E+06	4.55E+06	4.55E+06
2	4.65E+06	4.65E+06	4.65E+06
3	4.45E+06	4.50E+06	4.50E+06
4	4.55E+06	4.50E+06	4.55E+06
Mean:		(Psi)	4.55E+06
Batch 2		(GPa)	31.3

(c)

Figure B.2: (a) Sample Plots from Elastic Modulus Test for f'_c = 10,000 psi, Batch 2. Two trials per cylinder for four cylinders; (b) Elastic Modulus test results for f'_c = 10,000 psi, Batch 1; (c) Elastic Modulus test results for f'_c = 10,000 psi, Batch 2

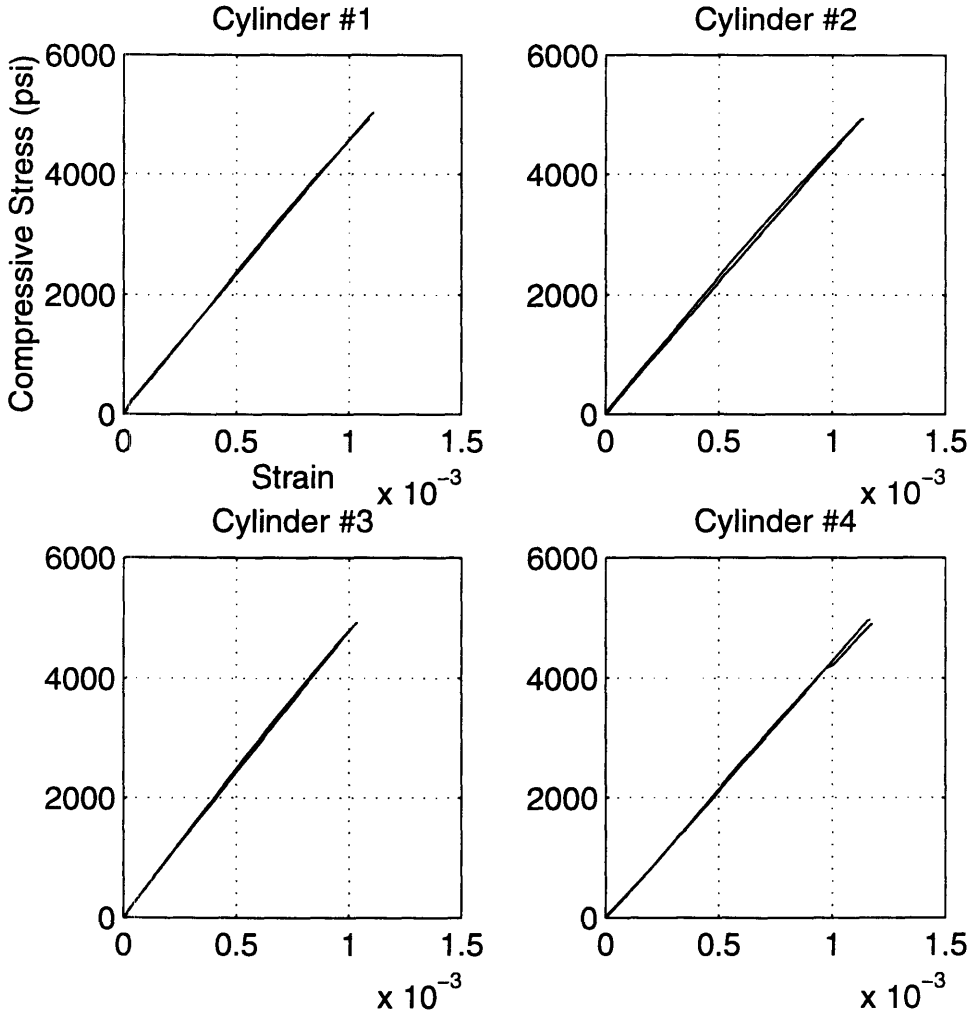

(a)

Elastic Modulus, 10,000 Psi Mortar			
Cylinder	**Trial 1**	**Trial 2**	**Average**
1	4.45E+06	4.40E+06	4.45E+06
2	4.80E+06	4.80E+06	4.80E+06
3	4.65E+06	4.65E+06	4.65E+06
4	4.55E+06	4.50E+06	4.55E+06
Mean:		(Psi)	4.60E+06
Batch 3		(GPa)	31.7

(b)

Elastic Modulus, 10,000 Psi Mortar			
Cylinder	**Trial 1**	**Trial 2**	**Average**
1	4.65E+06	4.55E+06	4.60E+06
2	4.45E+06	4.40E+06	4.45E+06
3	4.85E+06	4.80E+06	4.85E+06
4	4.35E+06	4.30E+06	4.35E+06
Mean:		(Psi)	4.55E+06
Batch 4		(GPa)	31.3

(c)

Figure B.3: (a) Sample Plots from Elastic Modulus Test for f'_c = 10,000 psi, Batch 3. Two trials per cylinder for four cylinders; (b) Elastic Modulus test results for f'_c = 10,000 psi, Batch 3; (c) Elastic Modulus test results for f'_c = 10,000 psi, Batch 4

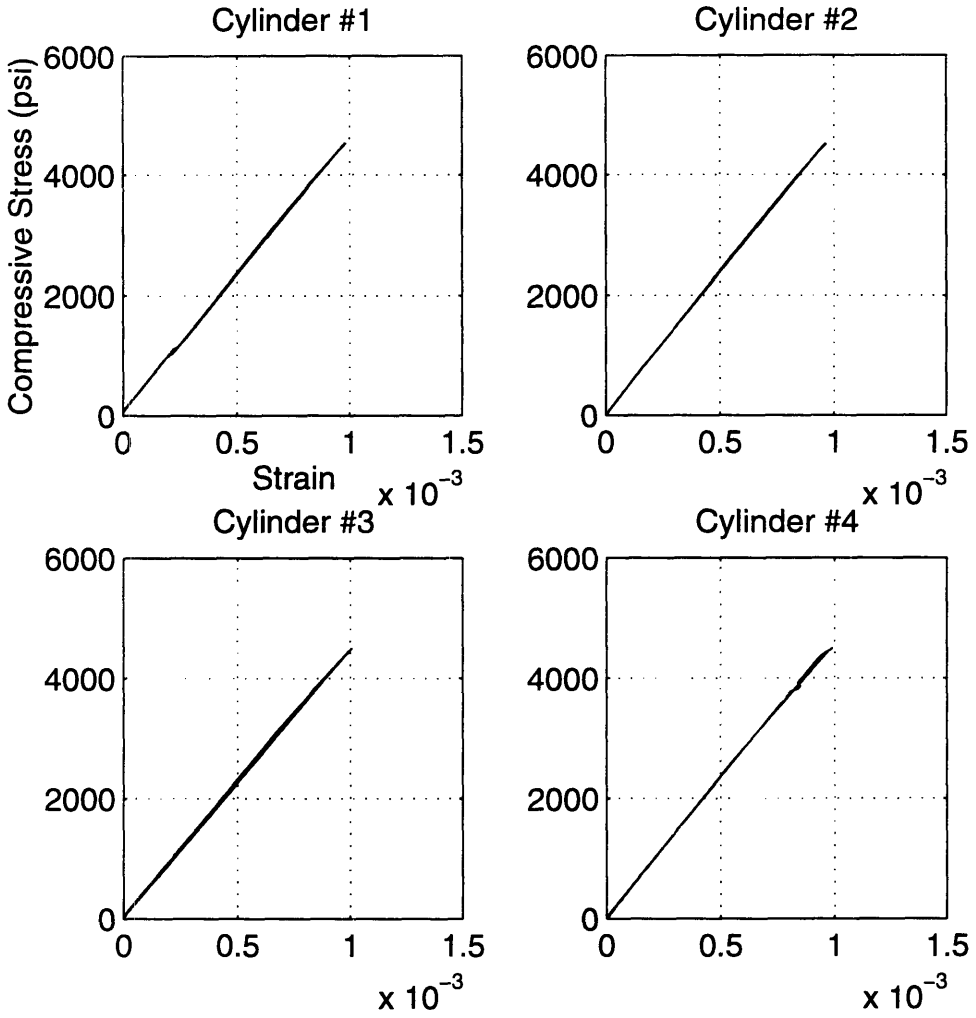

(a)

Elastic Modulus, 12,000 Psi Mortar			
Cylinder	**Trial 1**	**Trial 2**	**Average**
1	4.95E+06	4.90E+06	4.95E+06
2	4.60E+06	4.55E+06	4.60E+06
3	4.95E+06	4.90E+06	4.95E+06
4	4.85E+06	4.75E+06	4.80E+06
Mean:		(Psi)	4.85E+06
Batch 1		(GPa)	33.4

(b)

Elastic Modulus, 12,000 Psi Mortar			
Cylinder	**Trial 1**	**Trial 2**	**Average**
1	4.80E+06	4.70E+06	4.75E+06
2	5.15E+06	5.05E+06	5.10E+06
3	4.60E+06	4.60E+06	4.60E+06
4	4.95E+06	4.90E+06	4.95E+06
Mean:		(Psi)	4.85E+06
Batch 2		(GPa)	33.4

(c)

Figure B.4: (a) Sample Plots from Elastic Modulus Test for f'_c = 12,000 psi, Batch 2. Two trials per cylinder for four cylinders; (b) Elastic Modulus test results for f'_c = 12,000 psi, Batch 1; (c) Elastic Modulus test results for f'_c = 12,000 psi, Batch 2

Elastic Modulus, 12,000 Psi Mortar			
Cylinder	**Trial 1**	**Trial 2**	**Average**
1	4.95E+06	4.85E+06	4.90E+06
2	5.05E+06	5.00E+06	5.05E+06
3	5.25E+06	5.10E+06	5.20E+06
4	5.30E+06	5.15E+06	5.25E+06
Mean:		(Psi)	5.10E+06
Batch 3		(GPa)	35.1

(a)

Elastic Modulus, (Psi)			
	Mortar Compressive Strength		
	5,000 Psi	**10,000 Psi**	**12,000 Psi**
Batch 1	4.70E+06	4.60E+06	4.85E+06
Batch 2	3.15E+06	4.55E+06	4.85E+06
Batch 3		4.60E+06	5.10E+06
Batch 4		4.55E+06	
Mean:	3.95E+06	4.60E+06	4.95E+06

(b)

Elastic Modulus, (GPa)			
	Mortar Compressive Strength		
	34.5 MPa	**68.9 MPa**	**82.7 MPa**
Batch 1	32.4	31.7	33.4
Batch 2	21.7	31.3	33.4
Batch 3		31.7	35.1
Batch 4		31.3	
Mean:	27.1	31.5	34.0

(c)

Figure B.5: (a) Elastic Modulus test results for f'_c = 12,000 psi, Batch 3; (b) Final values of Elastic Modulus for mortar specimens in units of (psi); (c) Final values of Elastic Modulus for mortar specimens in units of (GPa)

APPENDIX C

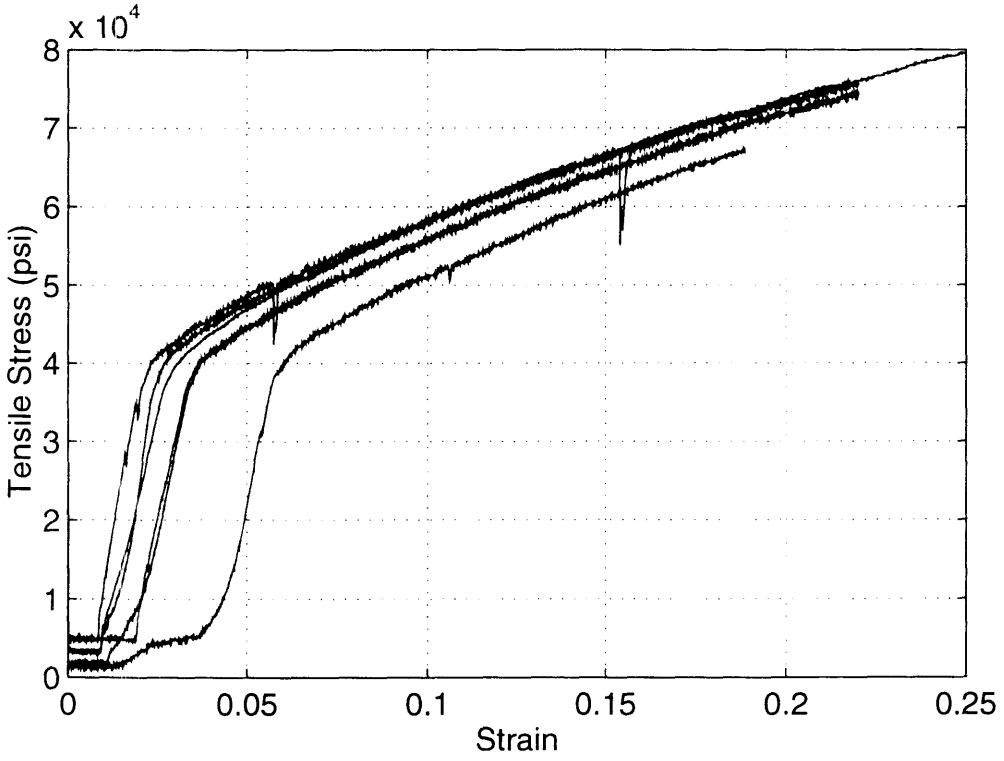

(a)

Central Wire, 0.2% Offset Yield					
Material Type	**Diameter**	**Elongation**	**Breaking Strength**	**Stress @ max load**	**Yield Stress @ 2% Offset**
S304	**(in)**	**(%)**	**(lbs)**	**(psi)**	**(psi)**
1	0.01978	N.A.	N.A.	N.A.	39,000
2	0.01978	N.A.	N.A.	N.A.	40,000
3	0.01978	N.A.	N.A.	N.A.	39,500
4	0.01978	N.A.	N.A.	N.A.	40,000
5	0.01978	N.A.	N.A.	N.A.	40,000
6	0.01978	N.A.	N.A.	N.A.	41,000
Mean:	0.01978	N.A.	N.A.	N.A.	39,900

(b)

Figure C.1: (a) Stress-strain diagram for fiber with f_y = 39,900 psi (b) Yield strength data for fiber with f_y = 39,900 psi

Baird Industries Inc., 60/70 ksi					
Material Type	Diameter	Elongation	Breaking Strength	Stress @ max load	Yield Stress @ 2% Offset
S304	(in)	(%)	(lbs)	(Kpsi)	(Kpsi)
1	0.02000	33.50	35.50	113.0	67.75
2	0.02000	36.17	35.75	113.8	67.94
3	0.02000	34.33	35.71	113.7	68.40
4	0.02000	34.83	35.57	113.2	67.95
5	0.01995	35.67	35.57	113.8	68.39
Mean:	0.01999	34.90	35.62	113.5	68.09

(a)

Baird Industries Inc., 90/100 ksi					
Material Type	Diameter	Elongation	Breaking Strength	Stress @ max load	Yield Stress @ 2% Offset
S304	(in)	(%)	(lbs)	(Kpsi)	(Kpsi)
1	0.02075	28.33	41.42	122.5	92.18
2	0.02060	30.00	41.44	124.3	94.04
3	0.02075	28.00	41.38	122.4	91.08
4	0.02080	29.17	41.30	121.6	91.45
Mean:	0.02073	28.88	41.39	122.7	92.19

(b)

Figure C.2: (a) Yield strength data for fiber with f_y = 68,100 psi (b) Yield strength data for fiber with f_y = 92,200 psi

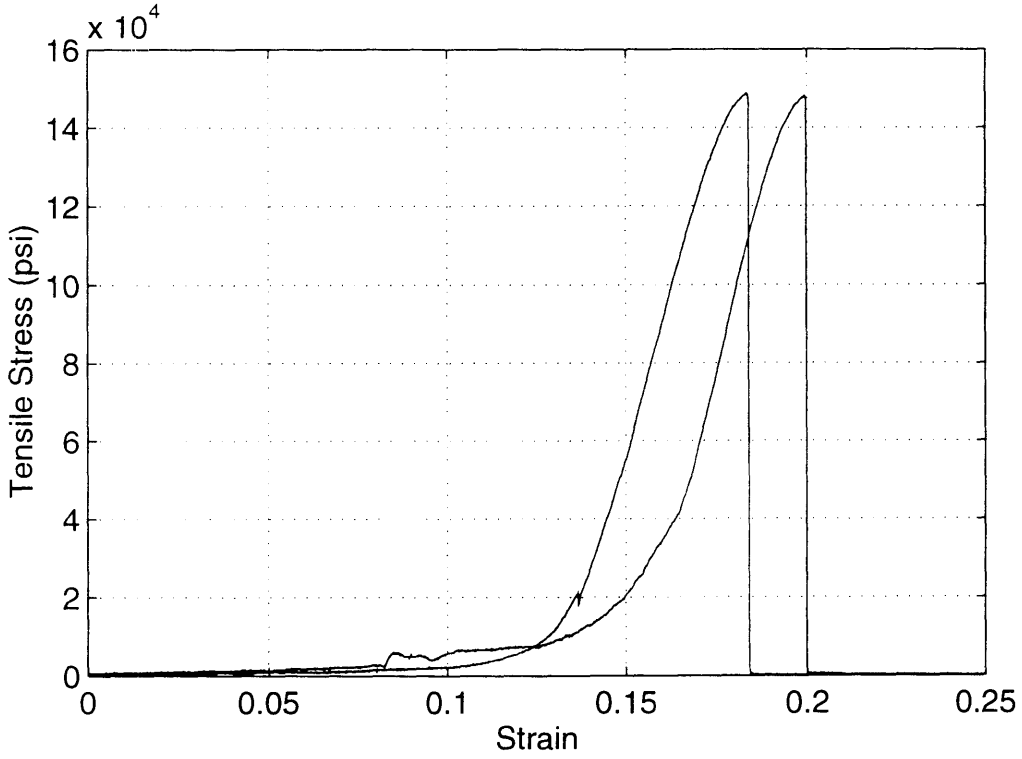

(a)

Central Wire, 1.5 Dies Hard					
Material Type	**Diameter**	**Elongation**	**Breaking Strength**	**Stress @ max load**	**Yield Stress @ 2% Offset**
S304	**(in)**	**(%)**	**(lbs)**	**(psi)**	**(psi)**
1	0.02004	19.9	186.60	147,900	139,000
2	0.02004	18.3	187.48	148,600	138,000
Mean:	0.02004	19.1	187.04	148,300	138,500

(b)

Figure C.3: (a) Stress-strain diagram for fiber with f_y = 138,500 psi (b) Yield strength data for fiber with f_y = 138,500 psi

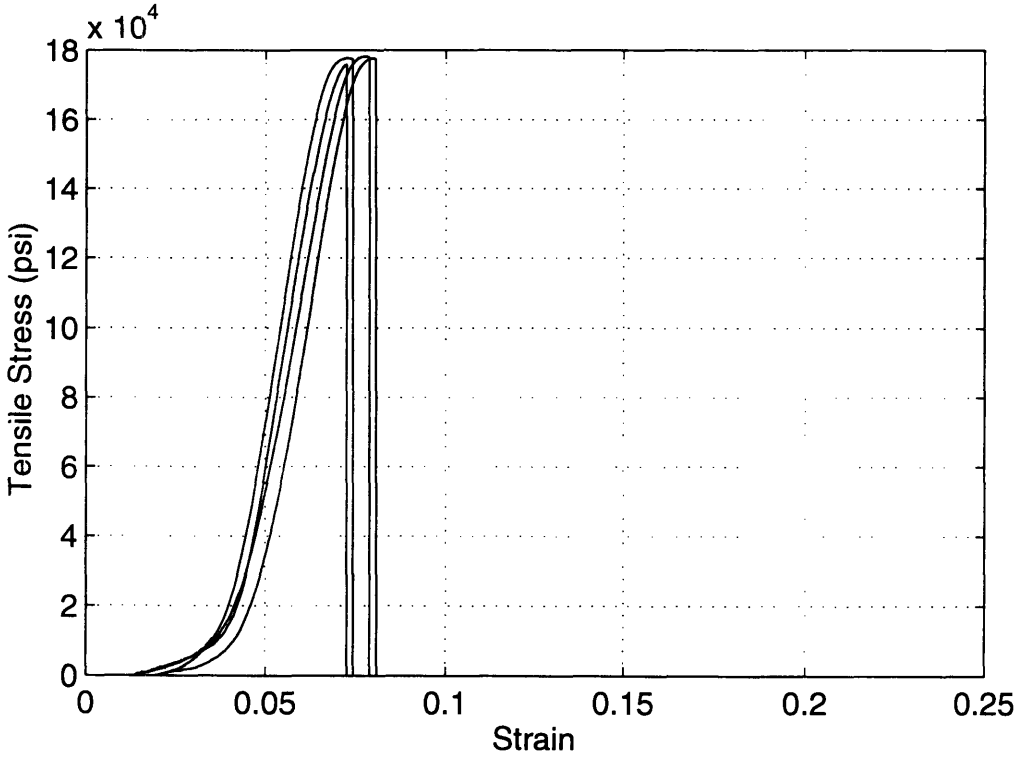

(a)

Bekaert, DRAMIX Fiber					
Material Type	**Diameter**	**Elongation**	**Breaking Strength**	**Stress @ max load**	**Yield Stress @ 2% Offset**
Low Carbo	**(in)**	**(%)**	**(lbs)**	**(psi)**	**(psi)**
1	0.01970	8.0	216.53	177,600	168,000
2	0.01970	7.8	217.27	178,200	172,500
3	0.01970	7.2	215.80	177,000	171,000
4	0.01970	7.2	214.34	175,800	168,000
Mean:	0.01970	7.6	215.99	177,200	170,000

(b)

Figure C.4: (a) Stress-strain diagram for fiber with f_y = 170,000 psi (b) Yield strength data for fiber with f_y = 170,000 psi

APPENDIX D

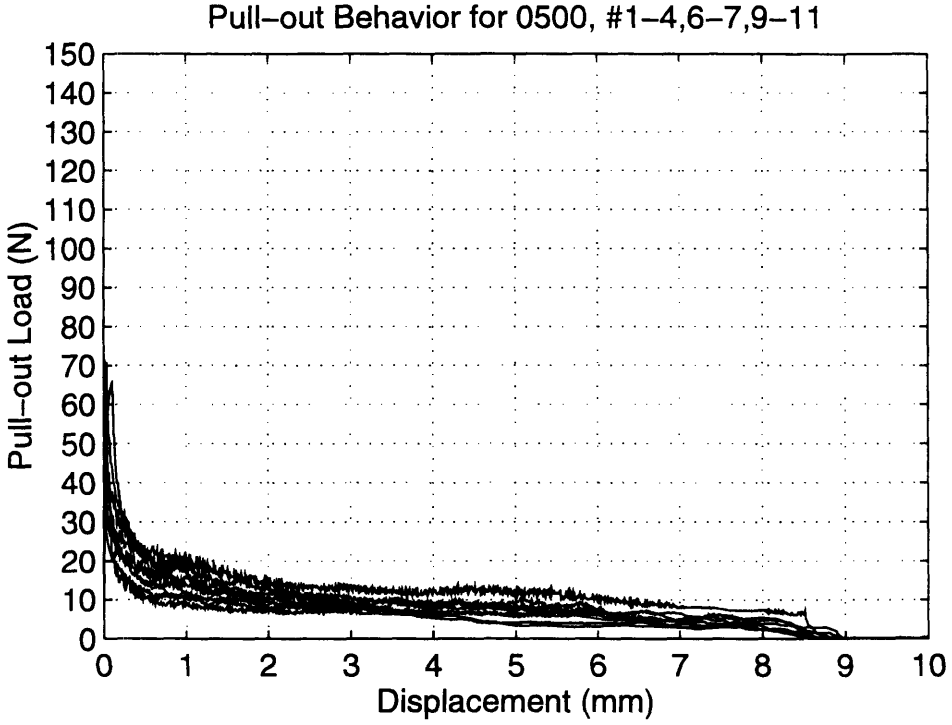

Figure D.1: Pull-out curves for Series One; Matrix: f'c = 5,000 psi, Fiber: Fy = 170,000 psi, Fiber Inclination: θ = zero degrees

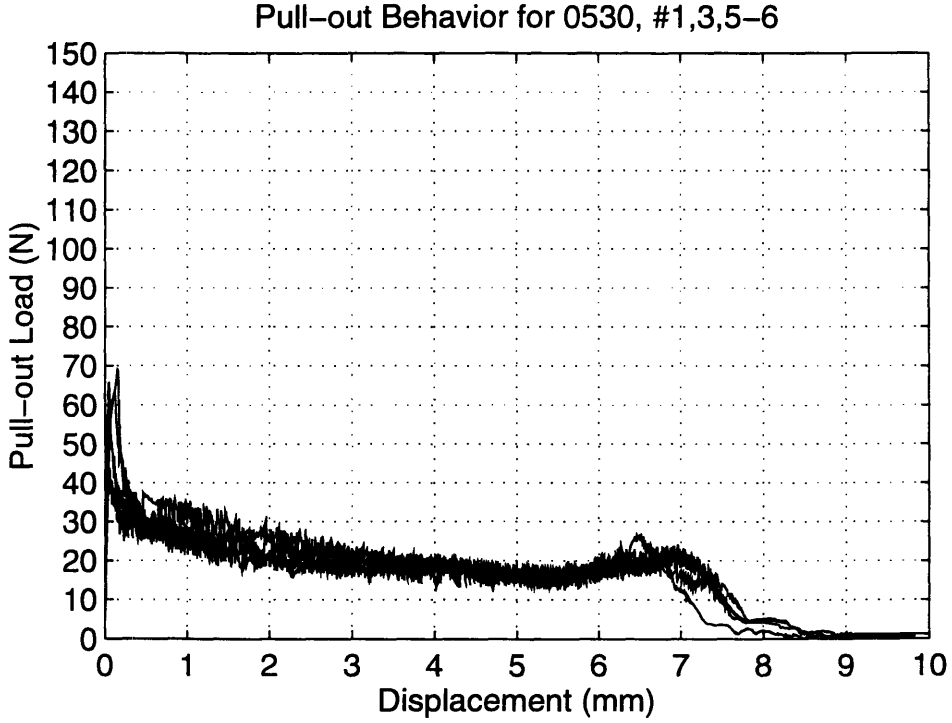

Figure D.2: Pull-out curves for Series One; Matrix: f'c = 5,000 psi, Fiber: Fy = 170,000 psi, Fiber Inclination: θ = thirty degrees

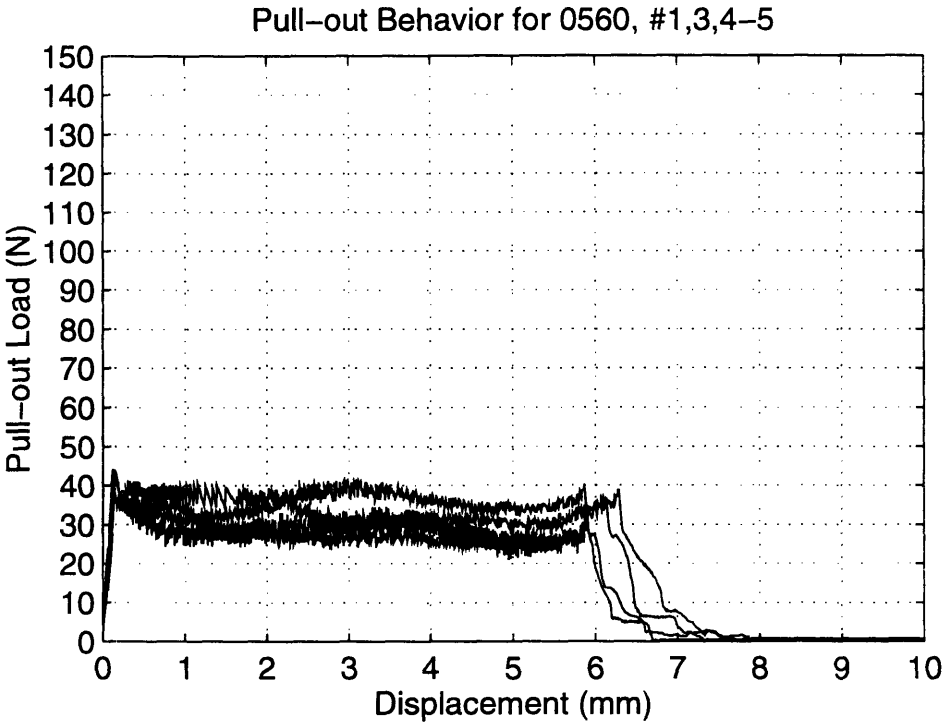

Figure D.3: Pull-out curves for Series One; Matrix: f'c = 5,000 psi, Fiber: Fy = 170,000 psi, Fiber Inclination: θ = sixty degrees

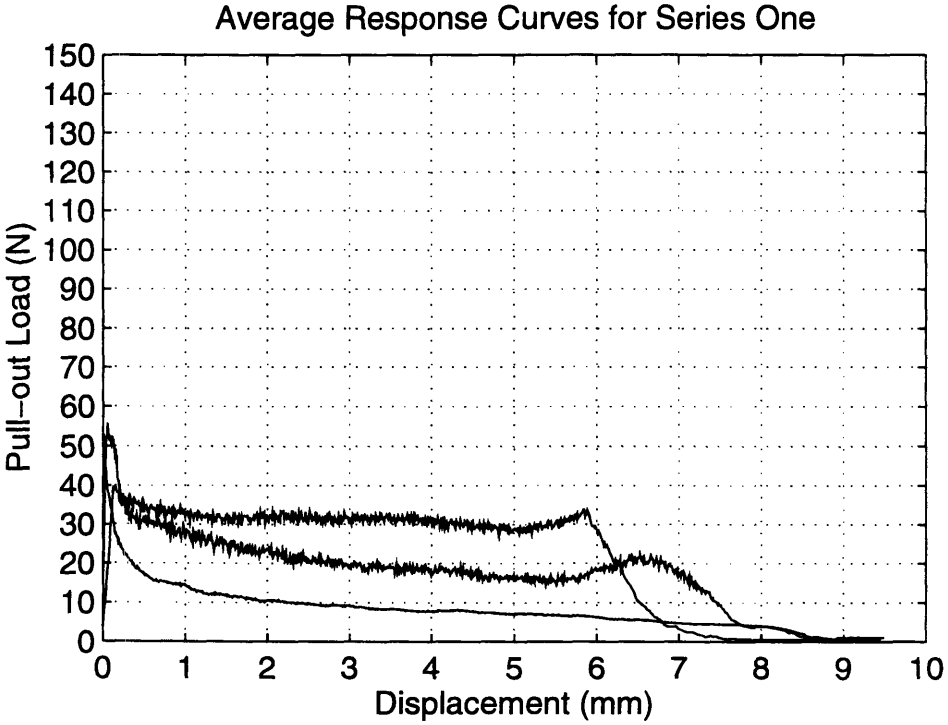

Figure D.4: Average pull-out curves for Series One; Matrix: f'c = 5,000 psi, Fiber: Fy = 170,000 psi, Fiber Inclination: θ = 0°, 30°, 60°

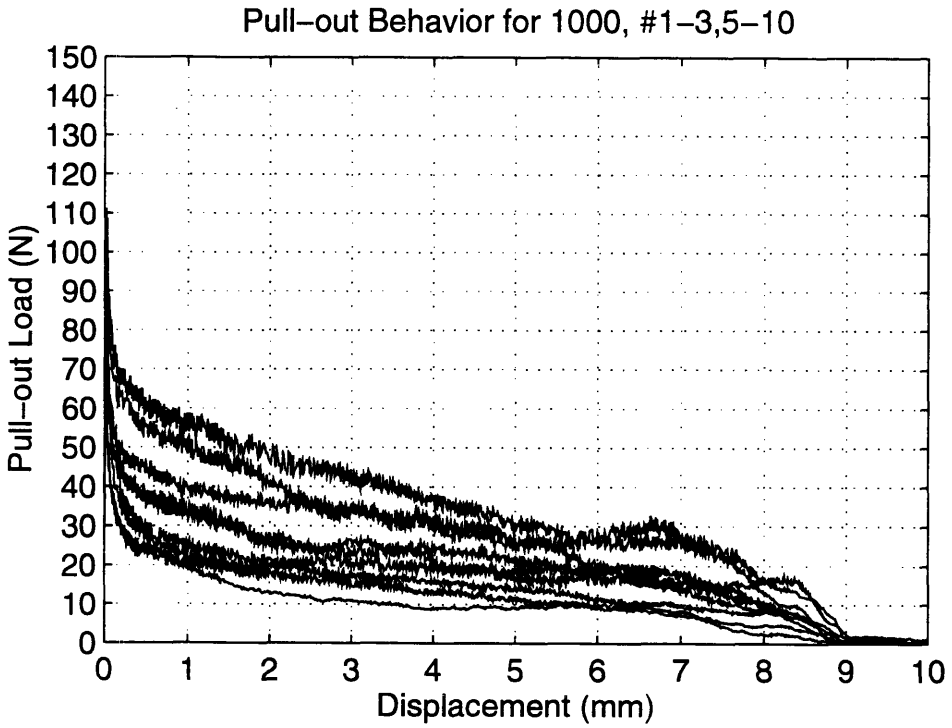

Figure D.5: Pull-out curves for Series Two; Matrix: f'c = 10,000 psi, Fiber: Fy = 170,000 psi, Fiber Inclination: θ = zero degrees

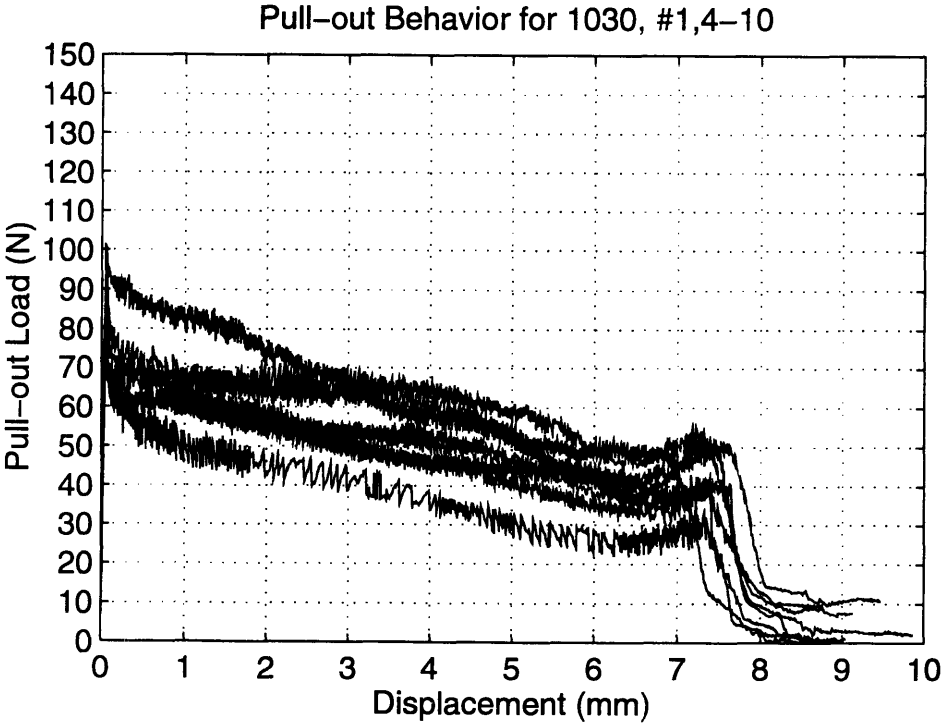

Figure D.6: Pull-out curves for Series Two; Matrix: f'c = 10.000 psi, Fiber: Fy = 170,000 psi, Fiber Inclination: θ = thirty degrees

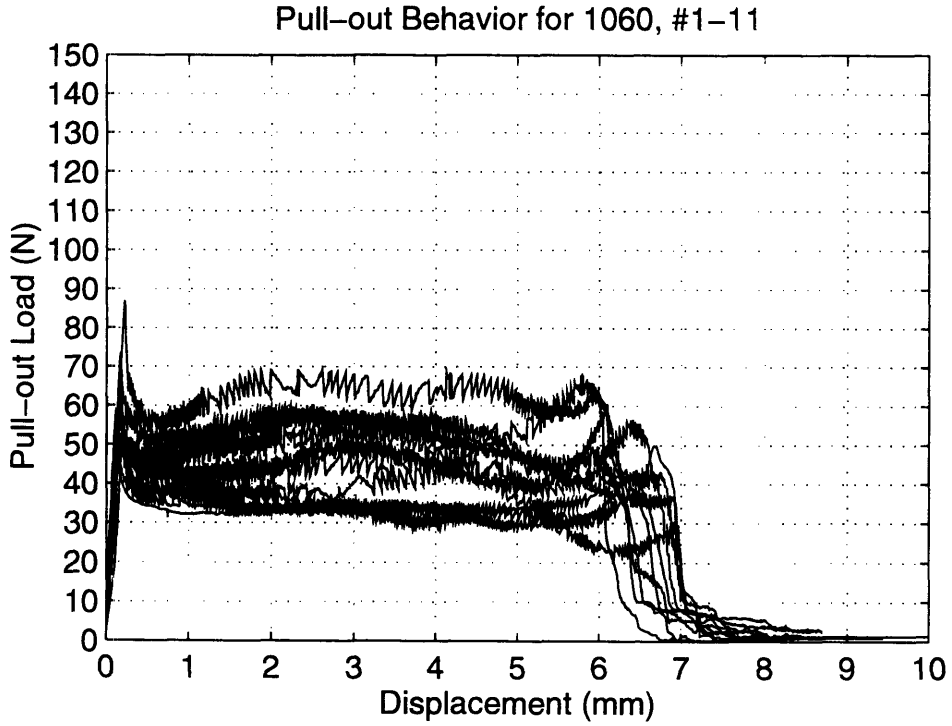

Figure D.7: Pull-out curves for Series Two; Matrix: f'c = 10.000 psi, Fiber: Fy = 170,000 psi, Fiber Inclination: θ = sixty degrees

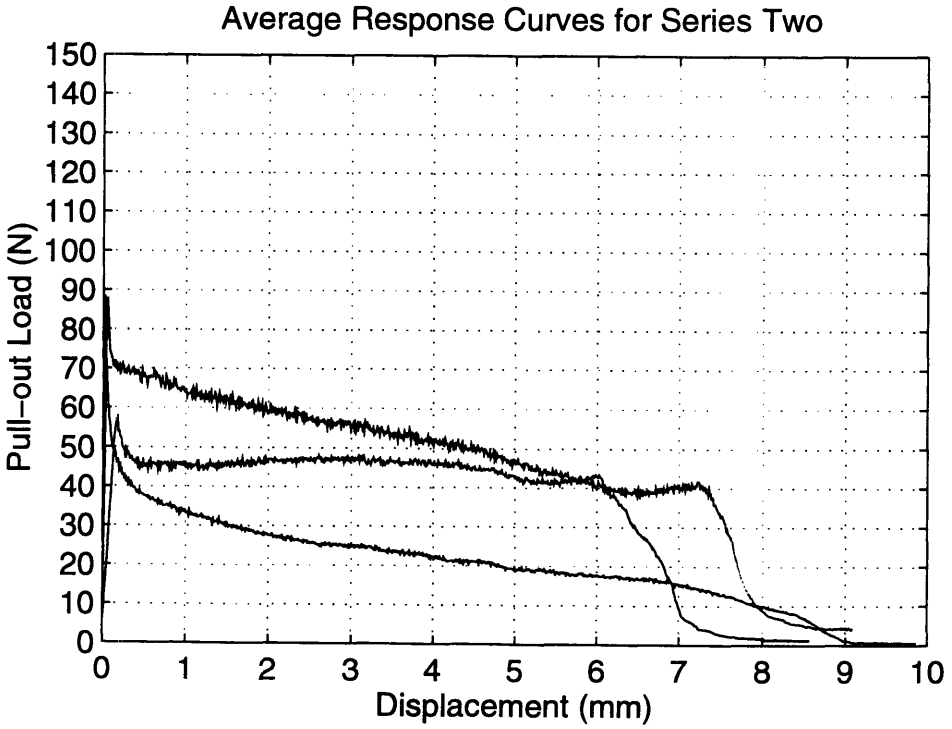

Figure D.8: Average pull-out curves for Series Two; Matrix: f'c = 10,000 psi, Fiber: Fy = 170,000 psi, Fiber Inclination: θ = 0°, 30°, 60°

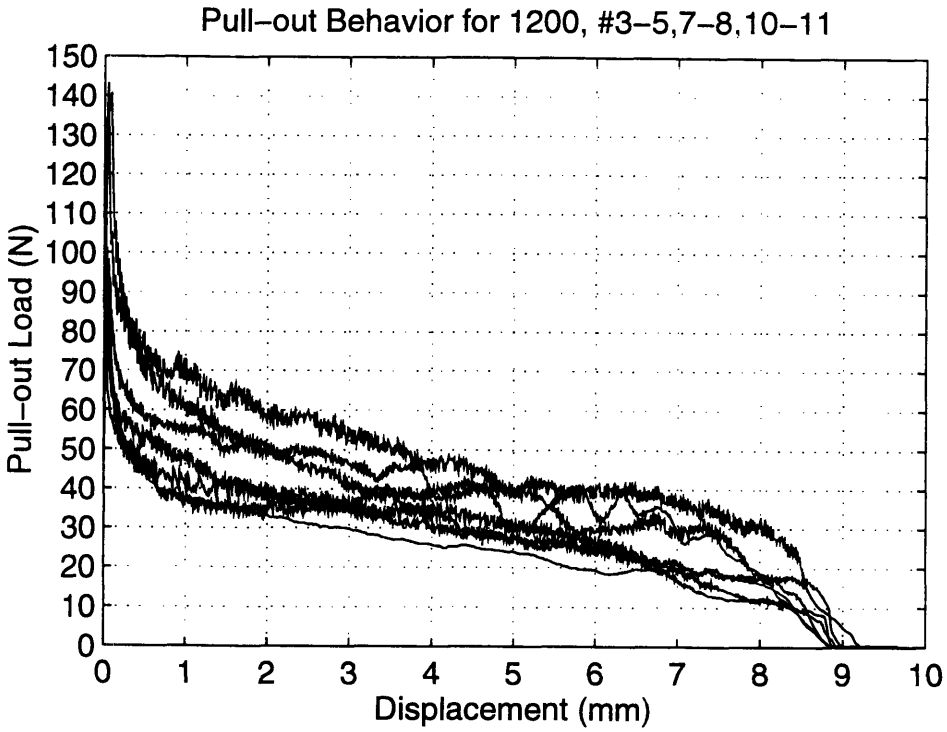

Figure D.9: Pull-out curves for Series Three; Matrix: f'c = 12,000 psi, Fiber: Fy = 170,000 psi, Fiber Inclination: θ = zero degrees

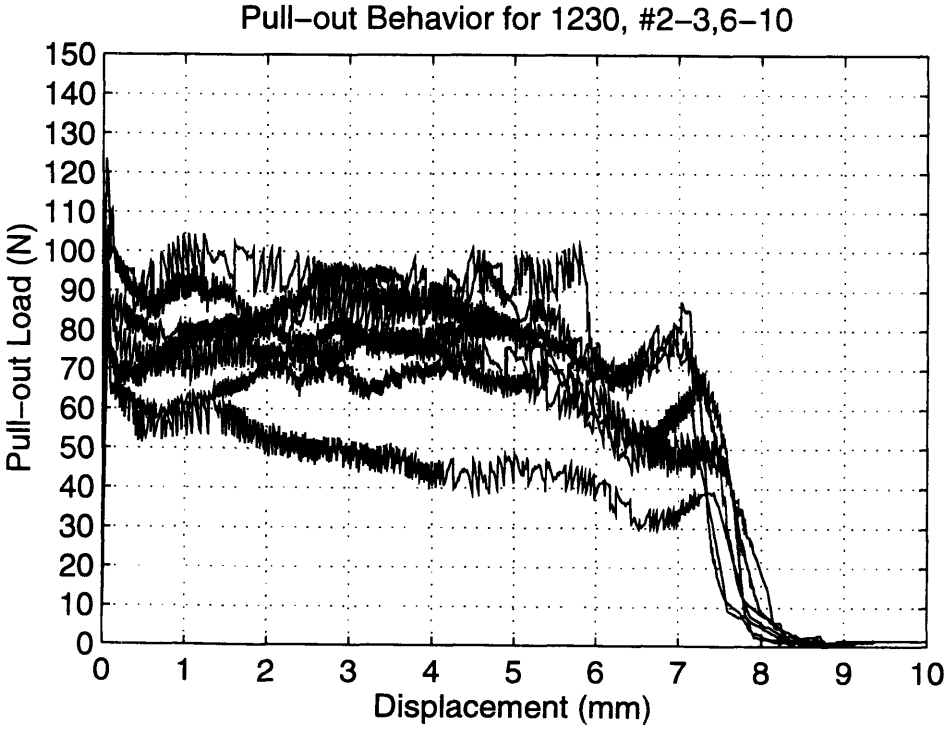

Figure D.10: Pull-out curves for Series Three; Matrix: f'c = 12,000 psi, Fiber: Fy = 170,000 psi, Fiber Inclination: θ = thirty degrees

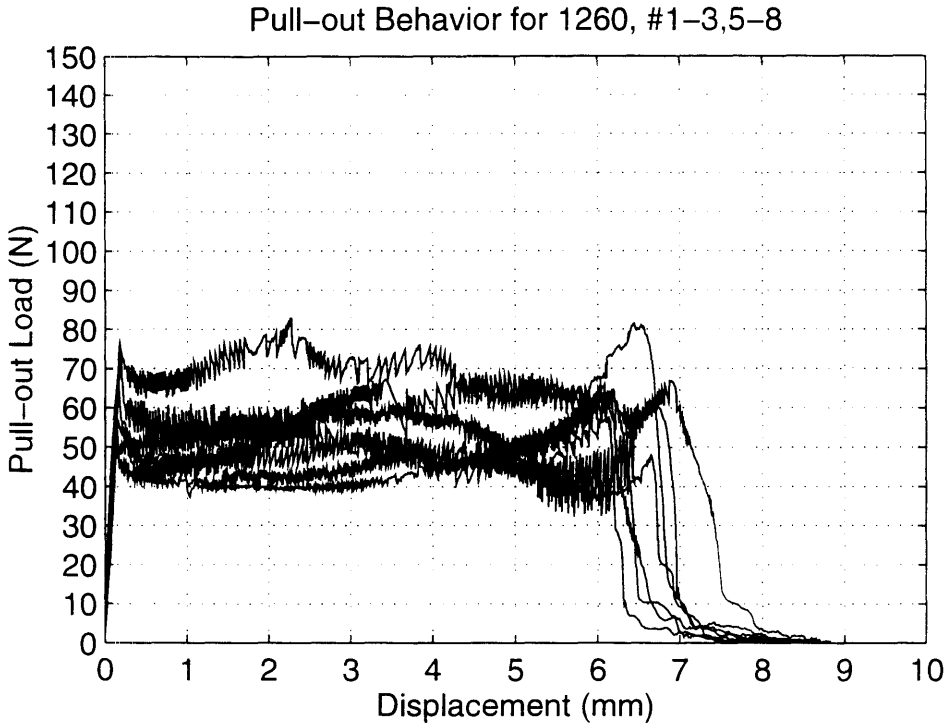

Figure D.11: Pull-out curves for Series Three; Matrix: f'c = 12,000 psi, Fiber: Fy = 170,000 psi, Fiber Inclination: θ = sixty degrees

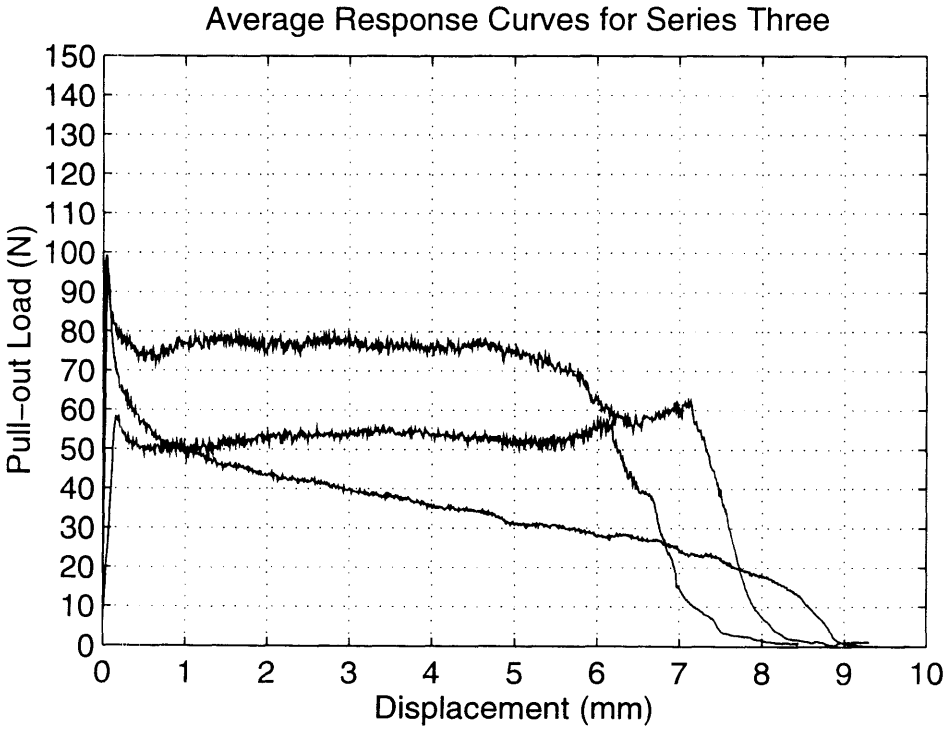

Figure D.12: Average pull-out curves for Series Three; Matrix: f'c = 12,000 psi, Fiber: Fy = 170,000 psi, Fiber Inclination: θ = 0°, 30°, 60°

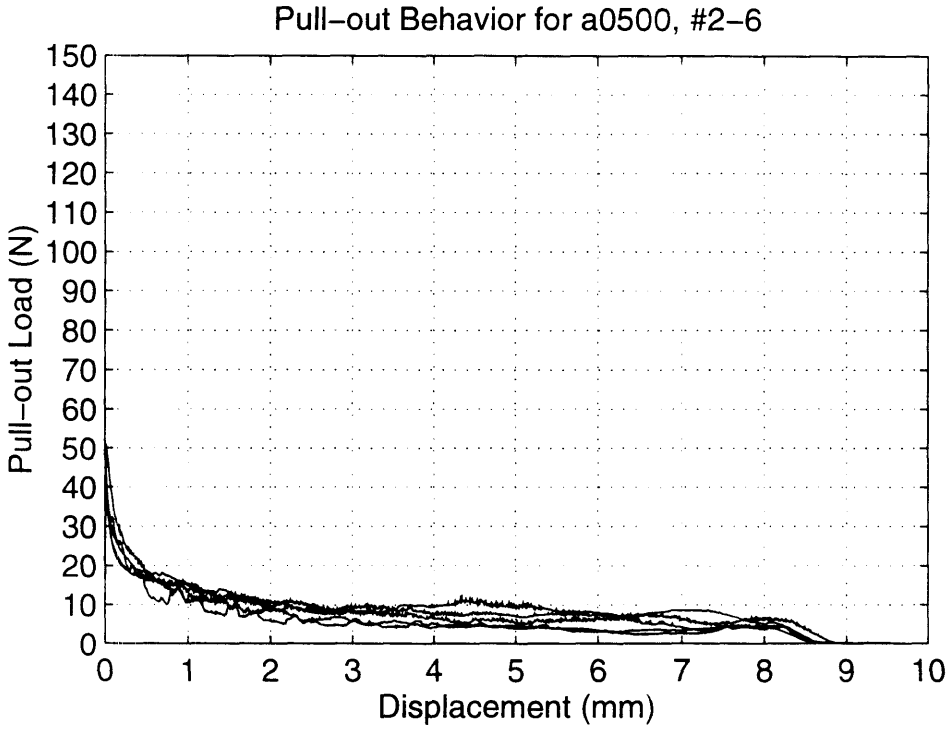

Figure D.13: Pull-out curves for Series Four; Matrix: f'c = 5,000 psi, Fiber: Fy = 39,900 psi, Fiber Inclination: θ = zero degrees

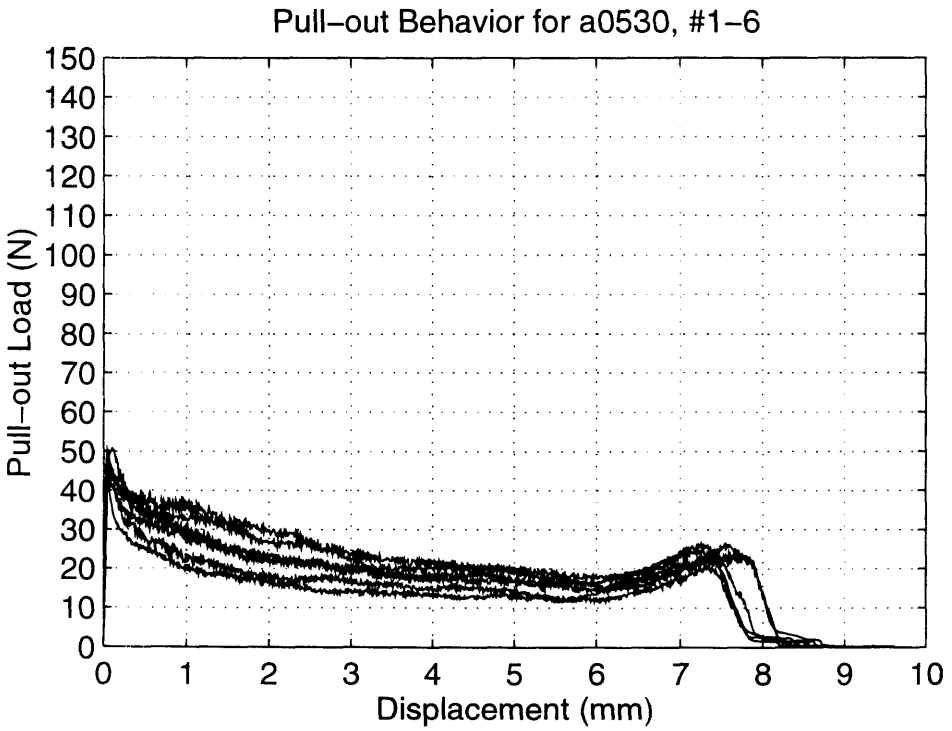

Figure D.14: Pull-out curves for Series Four; Matrix: f'c = 5,000 psi, Fiber: Fy = 39,900 psi, Fiber Inclination: θ = thirty degrees

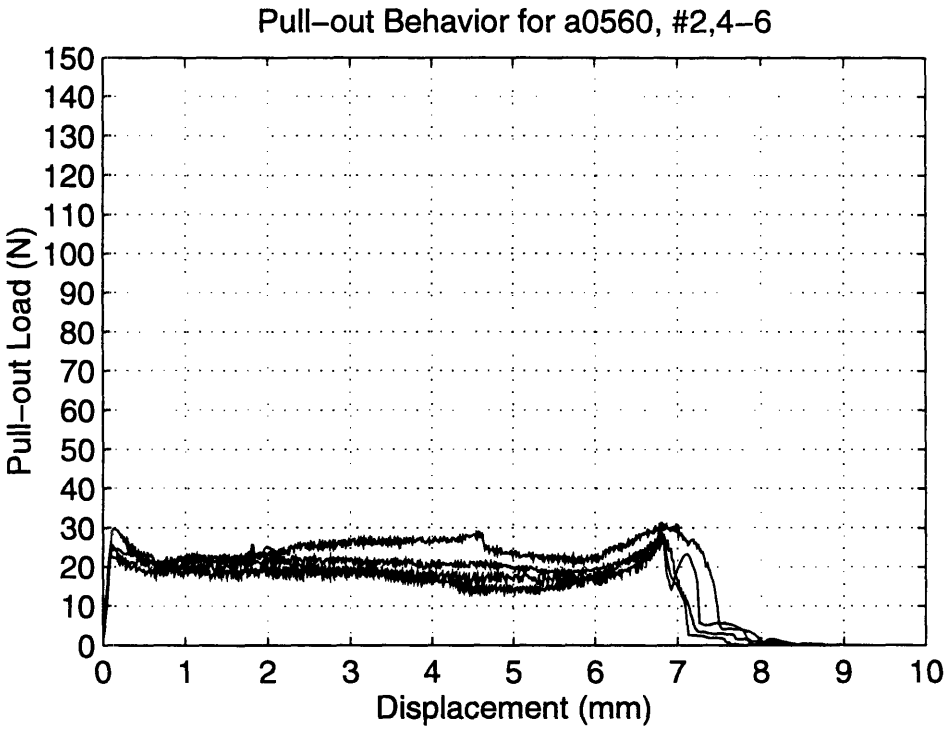

Figure D.15: Pull-out curves for Series Four; Matrix: f'c = 5,000 psi, Fiber: Fy = 39,900 psi, Fiber Inclination: θ = sixty degrees

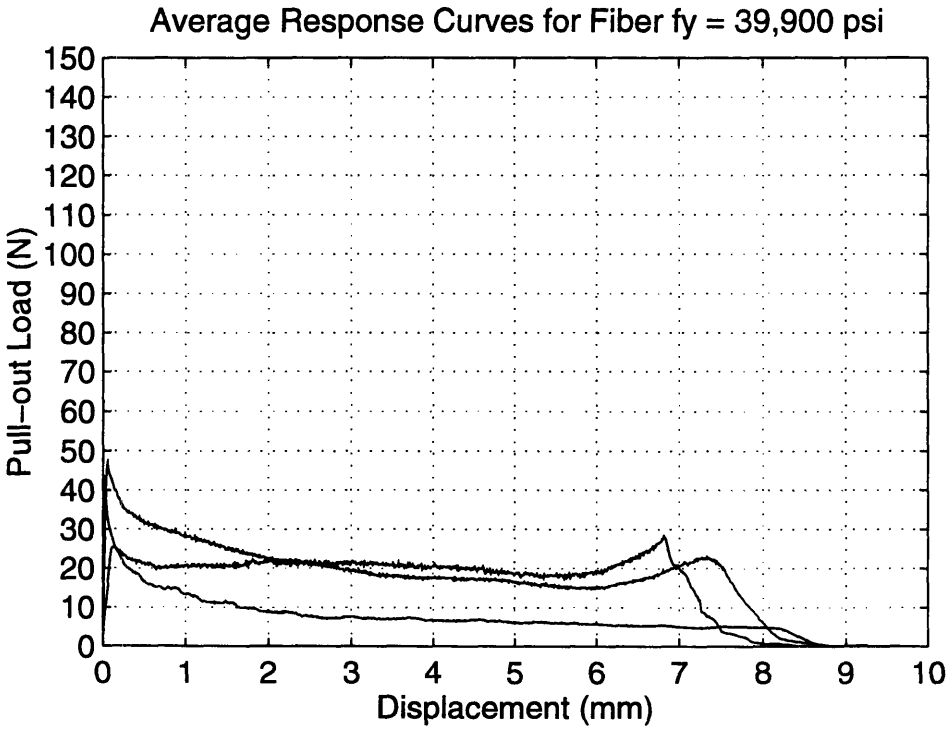

Figure D.16: Average pull-out curves for Series Four; Matrix: f'c = 5,000 psi, Fiber: Fy = 39,900 psi, Fiber Inclination: θ = 0°, 30°, 60°

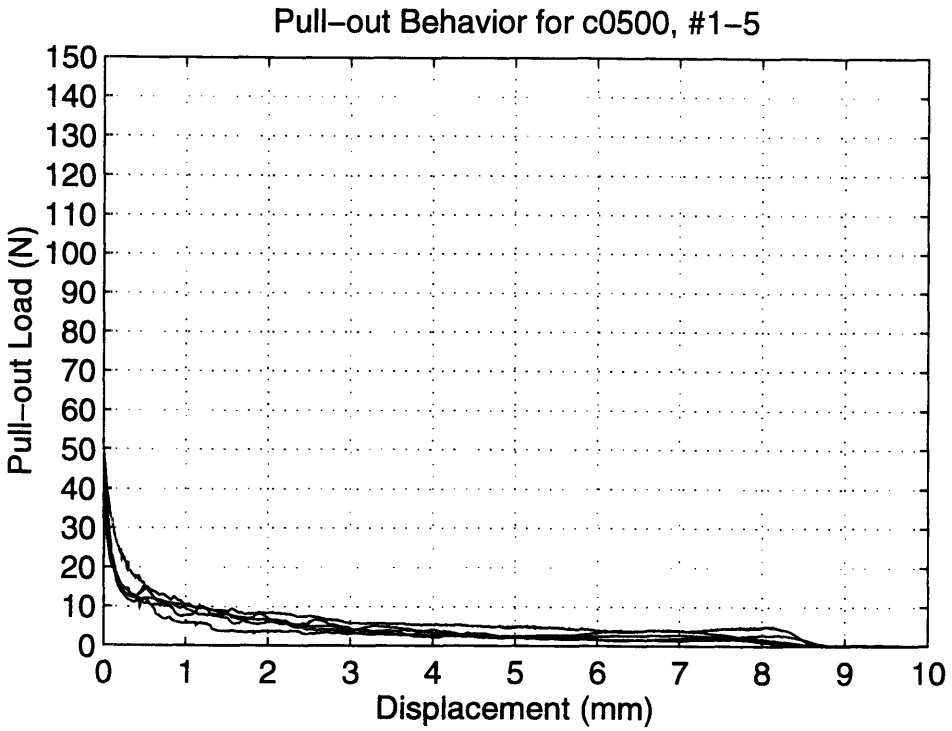

Figure D.17: Pull-out curves for Series Five; Matrix: f'c = 5,000 psi, Fiber: Fy = 68,100 psi, Fiber Inclination: θ = zero degrees

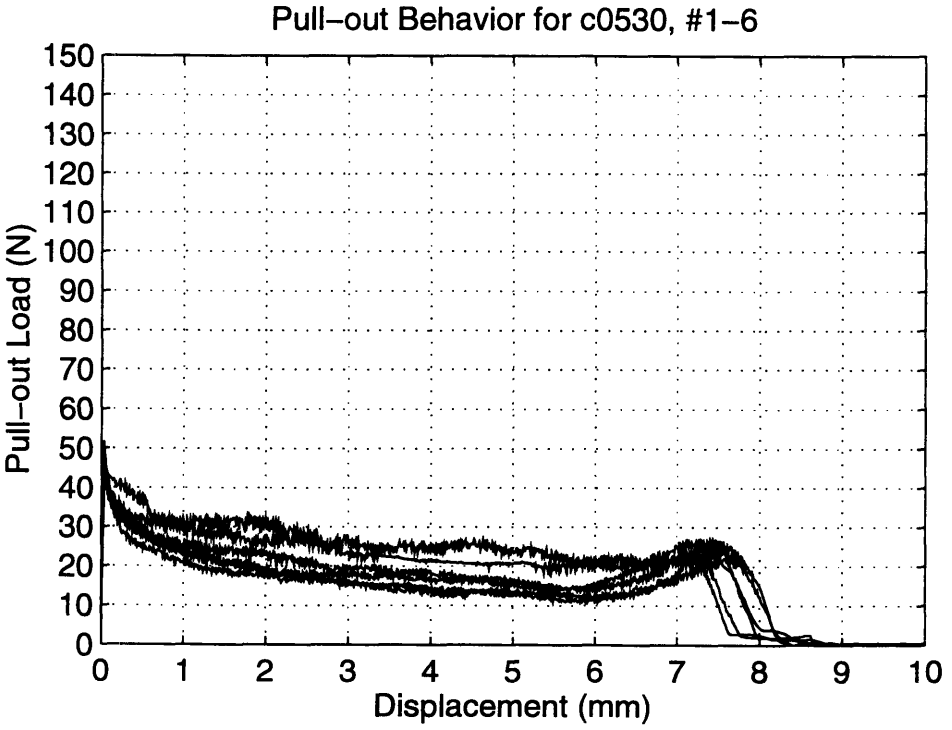

Figure D.18: Pull-out curves for Series Five; Matrix: f'c = 5,000 psi, Fiber: Fy = 68,100 psi, Fiber Inclination: θ = thirty degrees

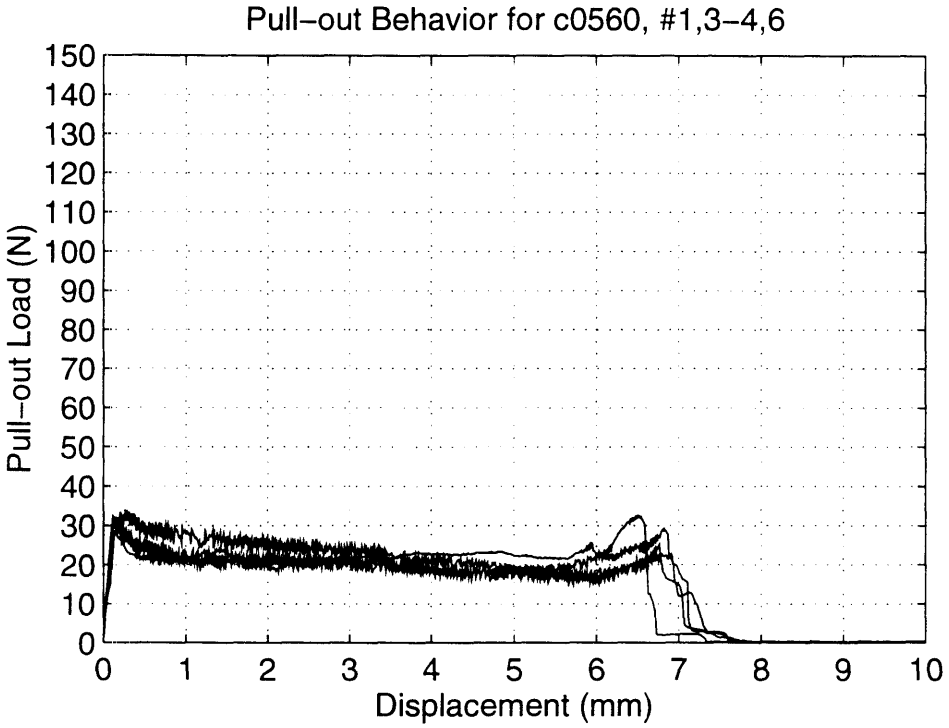

Figure D.19: Pull-out curves for Series Five; Matrix: f'c = 5,000 psi, Fiber: Fy = 68,100 psi, Fiber Inclination: θ = sixty degrees

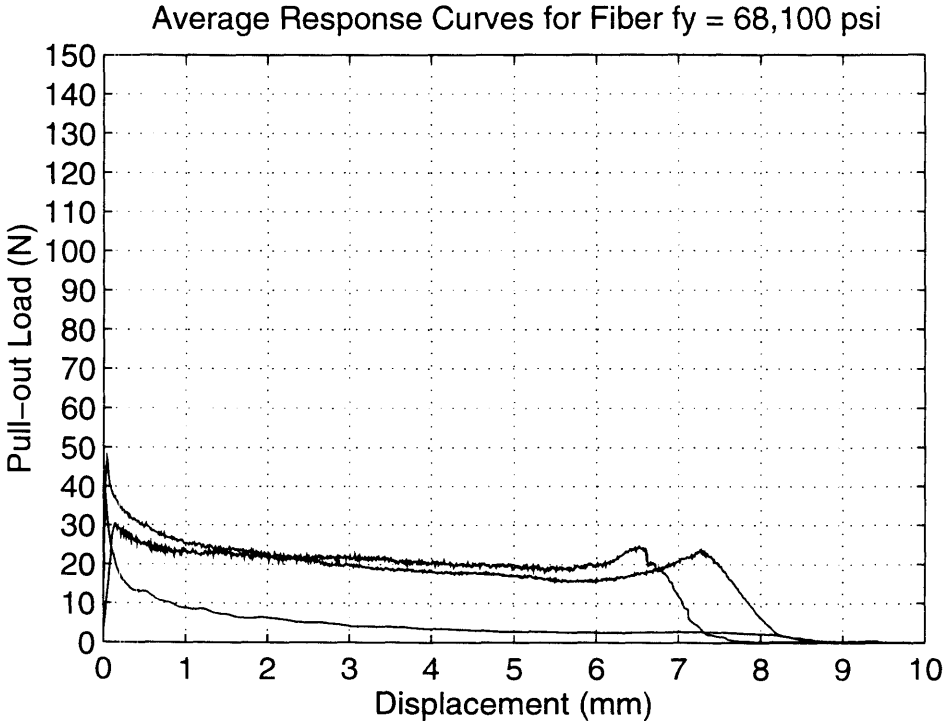

Figure D.20: Average pull-out curves for Series Five; Matrix: f'c = 5,000 psi, Fiber: Fy = 68,100 psi, Fiber Inclination: θ = 0°, 30°, 60°

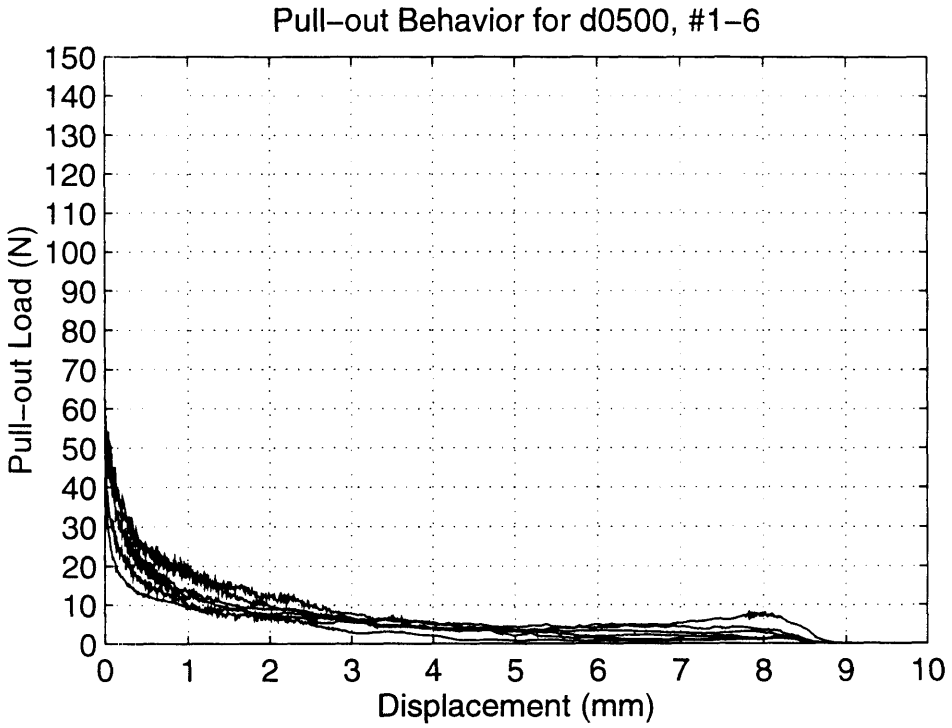

Figure D.21: Pull-out curves for Series Six; Matrix: f'c = 5,000 psi, Fiber: Fy = 92,200 psi, Fiber Inclination: θ = zero degrees

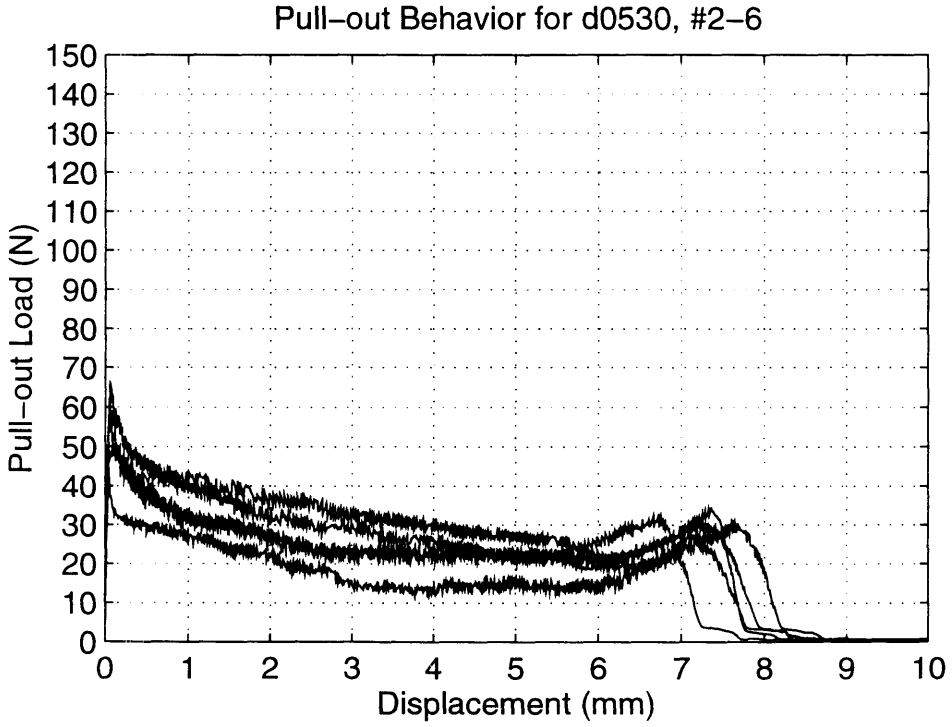

Figure D.22: Pull-out curves for Series Six; Matrix: f'c = 5,000 psi, Fiber: Fy = 92,200 psi, Fiber Inclination: θ = thirty degrees

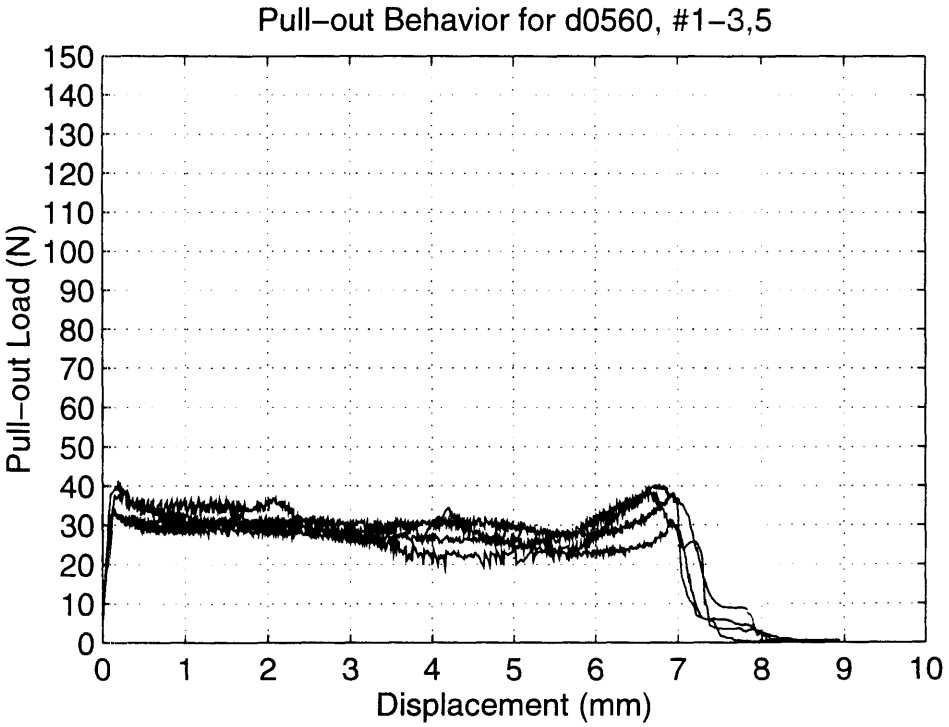

Figure D.23: Pull-out curves for Series Six; Matrix: f'c = 5,000 psi, Fiber: Fy = 92,200 psi, Fiber Inclination: θ = sixty degrees

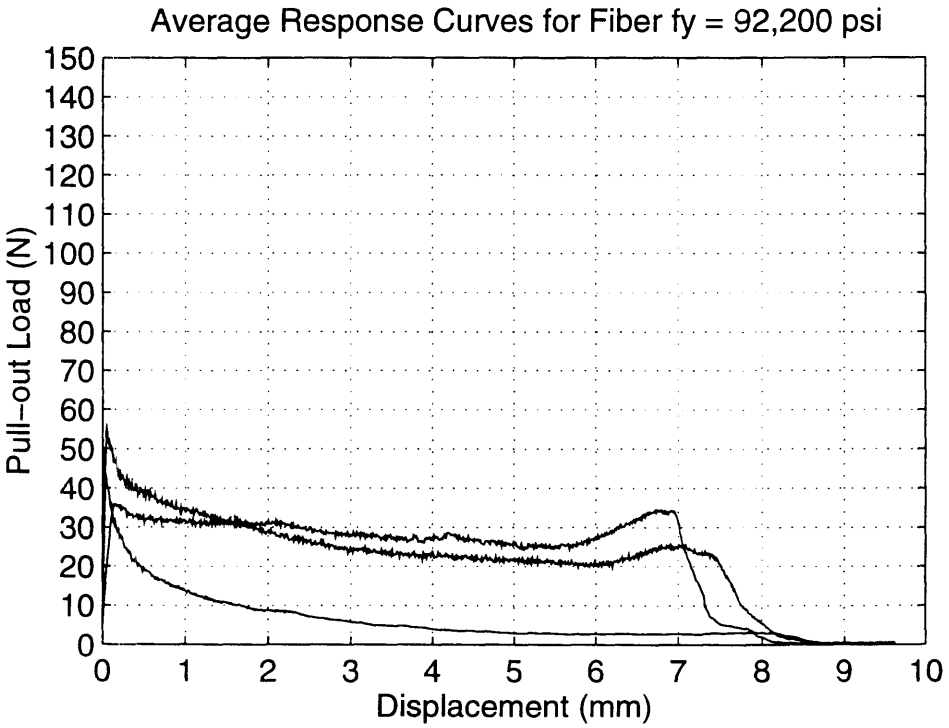

Figure D.24: Average pull-out curves for Series Six; Matrix: f'c = 5,000 psi, Fiber: Fy = 92,200 psi, Fiber Inclination: θ = 0°, 30°, 60°

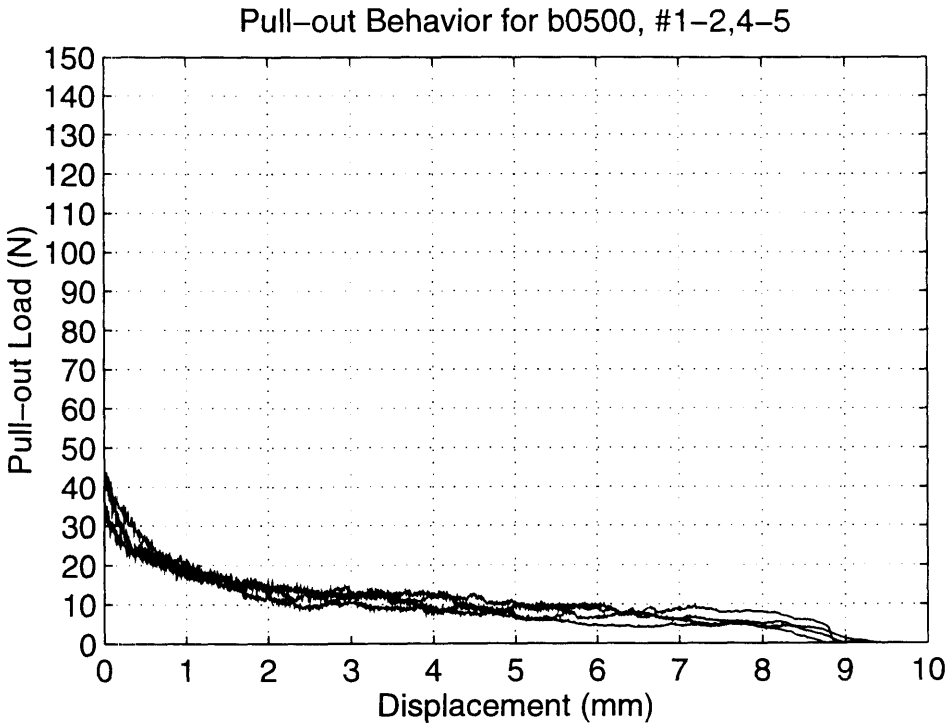

Figure D.25: Pull-out curves for Series Seven; Matrix: f'c = 5,000 psi, Fiber: Fy = 138,500 psi, Fiber Inclination: θ = zero degrees

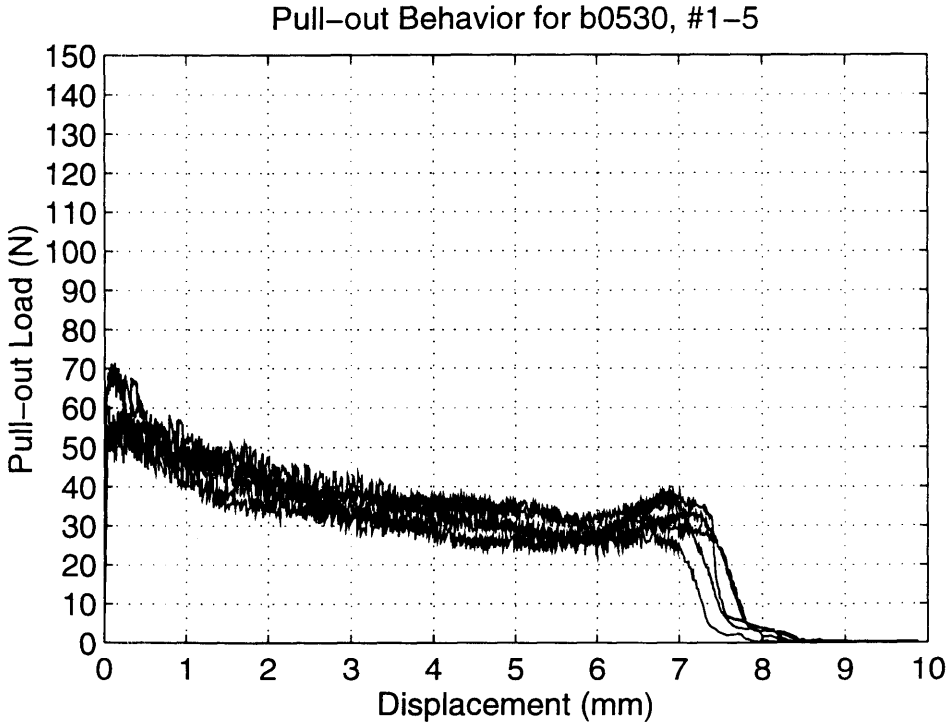

Figure D.26: Pull-out curves for Series Seven; Matrix: f'c = 5,000 psi, Fiber: Fy = 138,500 psi, Fiber Inclination: θ = thirty degrees

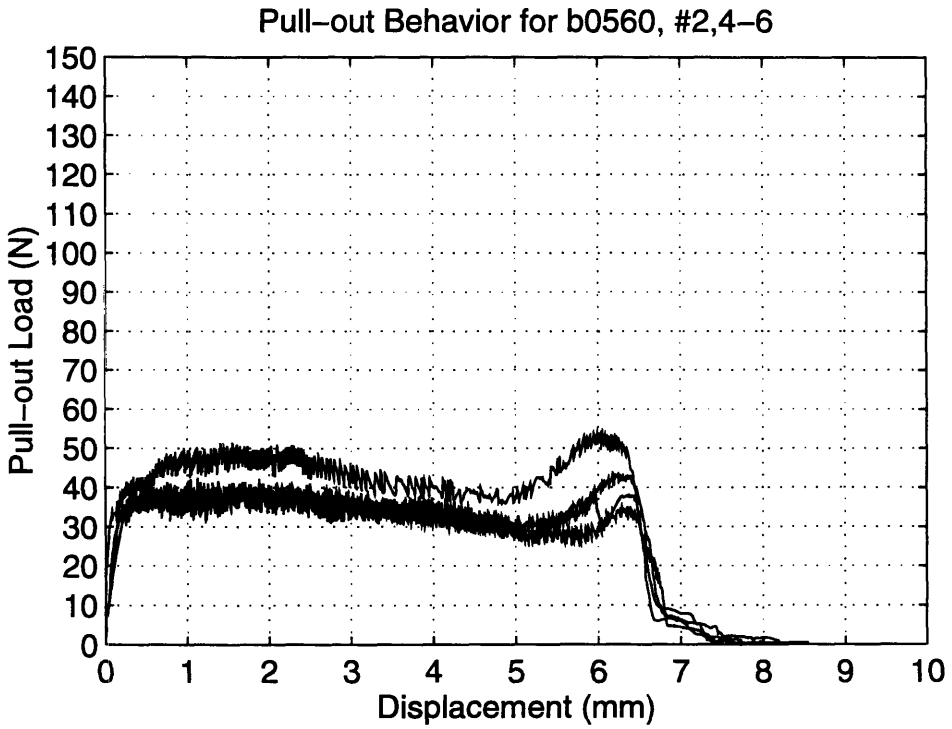

Figure D.27: Pull-out curves for Series Seven; Matrix: f'c = 5,000 psi, Fiber: Fy = 138,500 psi, Fiber Inclination: θ = sixty degrees

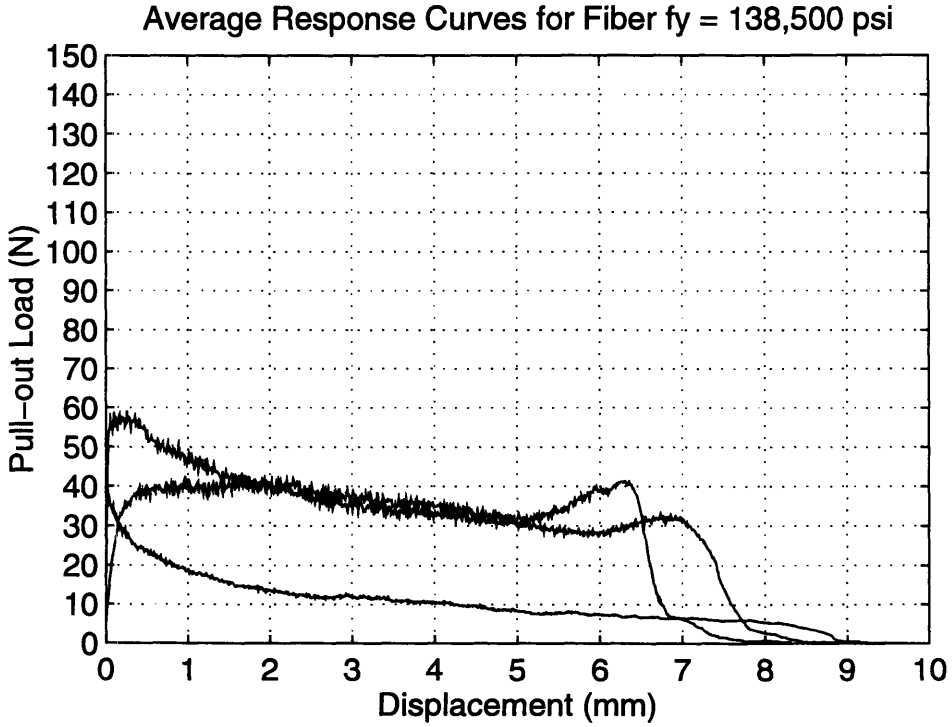

Figure D.28: Average pull-out curves for Series Seven; Matrix: f'c = 5,000 psi, Fiber: Fy = 138,500 psi, Fiber Inclination: θ = 0°, 30°, 60°

APPENDIX E

Figure E.1: Simulation Input File for Series One f'_c = 5,000 psi (34.5 Gpa), f_y = 170,000 psi (1.171 GPa)

```
40.                          ;EMBEDD LENGTH/RADIUS FOR THE FIBER
0.00001                      ;FIBER INCLINATION ANGLE (IN DEGREE)
200.0, 0., 250.0, 1.171      ;FIBER E (GPa), G (GPa), R (Micron) AND Sy (GPa)
26.8, 34.5                   ;MATRIX E (GPa) AND FAILURE STRESS (MPa)
3.7e-3,1.2e-3,8e-4,8e-4,1e-4 ;FRICTION COEFFICIENT TAUi, TAU2, TAU3, TAU4 AND TAU5
                             (GPa)
1000                         ;ELEMENTS ALONG THE LENGTH OF THE FIBER
1000                         ;NO. OF DIFF. CRACK OPENING
1000*10.0                    ;INCREMENT IN OPENING  U (Micron?)
1000*0.0                     ;INCREMENT IN SHEARING V (Micron?)
11                           ;POINTS OF BOTTOM FOUNDATION (MUST BE ODD)
0.0,  0.0000, 0.0000         ;PRESCRIBED SPRING PROPERTIES
0.25, 0.19569, 0.4052        ;AT EACH POINT (HRI, RATIOKE, RATIOFRS)
0.5,  0.2338, 0.6692
0.75, 0.2623, 0.8716
1.0,  0.2807, 0.9803
2.0,  0.3308, 1.2066
4.0,  0.37408, 1.4686
10.0, 0.4273, 1.6849
16.0, 0.4532, 1.6949
22.0, 0.4671, 1.7421
33.0, 0.4773, 1.8034
3                            ;POINTS OF TOP FOUNDATION (MUST BE ODD)
1.0,  0.4152                 ;PRESCRIBED SPRING PROPERTIES
10.0, 0.4598                 ;AT EACH POINT (HRI, RATIOKE)
33.0, 0.49375
```

Figure E.2: Simulation Input File for Series Two f'_c = 10,000 psi (68.9 Gpa), f_y = 170,000 psi (1.171 GPa)

```
40.                                ;EMBEDD LENGTH/RADIUS FOR THE FIBER
0.00001                            ;FIBER INCLINATION ANGLE (IN DEGREE)
200.0, 0., 250.0, 1.171            ;FIBER E (GPa), G (GPa), R (Micron) AND Sy (GPa)
31.3, 68.9                         ;MATRIX E (GPa) AND FAILURE STRESS (MPa)
5.7e-3,2.5e-3,2.2e-3,2.2e-3,7e-4   ;FRICTION COEFFICIENT TAUi, TAU2, TAU3, TAU4 AND TAU5
                                   (GPa)
1000                               ;ELEMENTS ALONG THE LENGTH OF THE FIBER
1000                               ;NO. OF DIFF. CRACK OPENING
1000*10.0                          ;INCREMENT IN OPENING  U (Micron?)
1000*0.0                           ;INCREMENT IN SHEARING V (Micron?)
11                                 ;POINTS OF BOTTOM FOUNDATION (MUST BE ODD)
0.0,  0.0000, 0.0000               ;PRESCRIBED SPRING PROPERTIES
0.25, 0.19569, 0.4052              ;AT EACH POINT (HRI, RATIOKE, RATIOFRS)
0.5,  0.2338, 0.6692
0.75, 0.2623, 0.8716
1.0,  0.2807, 0.9803
2.0,  0.3308, 1.2066
4.0,  0.37408, 1.4686
10.0, 0.4273, 1.6849
16.0, 0.4532, 1.6949
22.0, 0.4671, 1.7421
33.0, 0.4773, 1.8034
3                                  ;POINTS OF TOP FOUNDATION (MUST BE ODD)
1.0,  0.4152                       ;PRESCRIBED SPRING PROPERTIES
10.0, 0.4598                       ;AT EACH POINT (HRI, RATIOKE)
33.0, 0.49375
```

Figure E.3: Simulation Input File for Series Three f'_c = 12,000 psi (82.7 Gpa), f_y = 170,000 psi (1.171 GPa)

```
40.                                 ;EMBEDD LENGTH/RADIUS FOR THE FIBER
0.00001                             ;FIBER INCLINATION ANGLE (IN DEGREE)
200.0, 0., 250.0, 1.171             ;FIBER E (GPa), G (GPa), R (Micron) AND Sy (GPa)
33.76, 82.7                         ;MATRIX E (GPa) AND FAILURE STRESS (MPa)
6.8e-3,3.8e-3,3.4e-3,3.4e-3,5.6e-4  ;FRICTION COEFFICIENT TAUi, TAU2, TAU3, TAU4 AND TAU5
                                    (GPa)
1000                                ;ELEMENTS ALONG THE LENGTH OF THE FIBER
1000                                ;NO. OF DIFF. CRACK OPENING
1000*10.0                           ;INCREMENT IN OPENING  U (Micron?)
1000*0.0                            ;INCREMENT IN SHEARING V (Micron?)
11                                  ;POINTS OF BOTTOM FOUNDATION (MUST BE ODD)
0.0,  0.0000, 0.0000                ;PRESCRIBED SPRING PROPERTIES
0.25, 0.19569, 0.4052               ;AT EACH POINT (HRI, RATIOKE, RATIOFRS)
0.5,  0.2338, 0.6692
0.75, 0.2623, 0.8716
1.0,  0.2807, 0.9803
2.0,  0.3308, 1.2066
4.0,  0.37408, 1.4686
10.0, 0.4273, 1.6849
16.0, 0.4532, 1.6949
22.0, 0.4671, 1.7421
33.0, 0.4773, 1.8034
3                                   ;POINTS OF TOP FOUNDATION (MUST BE ODD)
1.0,  0.4152                        ;PRESCRIBED SPRING PROPERTIES
10.0, 0.4598                        ;AT EACH POINT (HRI, RATIOKE)
33.0, 0.49375
```

Figure E.4: Simulation Input File for Series Four f'_c = 5,000 psi (34.5 Gpa), f_y = 39,900 psi (0.275 GPa)

```
40.                          ;EMBEDD LENGTH/RADIUS FOR THE FIBER
0.00001                      ;FIBER INCLINATION ANGLE (IN DEGREE)
200.0, 0., 250.0, 0.275      ;FIBER E (GPa), G (GPa), R (Micron) AND Sy (GPa)
26.8, 34.5                   ;MATRIX E (GPa) AND FAILURE STRESS (MPa)
2.9e-3,1.1e-3,7e-4,7e-4,1e-4 ;FRICTION COEFFICIENT TAUi, TAU2, TAU3, TAU4 AND TAU5
                             (GPa)
1000                         ;ELEMENTS ALONG THE LENGTH OF THE FIBER
1000                         ;NO. OF DIFF. CRACK OPENING
1000*10.0                    ;INCREMENT IN OPENING  U (Micron?)
1000*0.0                     ;INCREMENT IN SHEARING V (Micron?)
11                           ;POINTS OF BOTTOM FOUNDATION (MUST BE ODD)
0.0,  0.0000, 0.0000         ;PRESCRIBED SPRING PROPERTIES
0.25, 0.19569, 0.4052        ;AT EACH POINT (HRI, RATIOKE, RATIOFRS)
0.5,  0.2338, 0.6692
0.75, 0.2623, 0.8716
1.0,  0.2807, 0.9803
2.0,  0.3308, 1.2066
4.0,  0.37408, 1.4686
10.0, 0.4273, 1.6849
16.0, 0.4532, 1.6949
22.0, 0.4671, 1.7421
33.0, 0.4773, 1.8034
3                            ;POINTS OF TOP FOUNDATION (MUST BE ODD)
1.0,  0.4152                 ;PRESCRIBED SPRING PROPERTIES
10.0, 0.4598                 ;AT EACH POINT (HRI, RATIOKE)
33.0, 0.49375
```

Figure E.5: Simulation Input File for Series Five f'_c = 5,000 psi (34.5 Gpa), f_y = 68,100 psi (0.469 GPa)

```
40.                          ;EMBEDD LENGTH/RADIUS FOR THE FIBER
0.00001                      ;FIBER INCLINATION ANGLE (IN DEGREE)
200.0, 0., 250.0, 0.469      ;FIBER E (GPa), G (GPa), R (Micron) AND Sy (GPa)
26.8, 34.5                   ;MATRIX E (GPa) AND FAILURE STRESS (MPa)
2.8e-3,9e-4,5e-4,5e-4,1e-4   ;FRICTION COEFFICIENT TAUi, TAU2, TAU3, TAU4 AND TAU5
                             (GPa)
1000                         ;ELEMENTS ALONG THE LENGTH OF THE FIBER
1000                         ;NO. OF DIFF. CRACK OPENING
1000*10.0                    ;INCREMENT IN OPENING  U (Micron?)
1000*0.0                     ;INCREMENT IN SHEARING V (Micron?)
11                           ;POINTS OF BOTTOM FOUNDATION (MUST BE ODD)
0.0,  0.0000, 0.0000         ;PRESCRIBED SPRING PROPERTIES
0.25, 0.19569, 0.4052        ;AT EACH POINT (HRI, RATIOKE, RATIOFRS)
0.5,  0.2338, 0.6692
0.75, 0.2623, 0.8716
1.0,  0.2807, 0.9803
2.0,  0.3308, 1.2066
4.0,  0.37408, 1.4686
10.0, 0.4273, 1.6849
16.0, 0.4532, 1.6949
22.0, 0.4671, 1.7421
33.0, 0.4773, 1.8034
3                            ;POINTS OF TOP FOUNDATION (MUST BE ODD)
1.0,  0.4152                 ;PRESCRIBED SPRING PROPERTIES
10.0, 0.4598                 ;AT EACH POINT (HRI, RATIOKE)
33.0, 0.49375
```

Figure E.6: Simulation Input File for Series Six f'_c = 5,000 psi (34.5 Gpa), f_y = 92,200 psi (0.636 GPa)

```
40.                          ;EMBEDD LENGTH/RADIUS FOR THE FIBER
60.0                         ;FIBER INCLINATION ANGLE (IN DEGREE)
200.0, 0., 250.0, 0.636      ;FIBER E (GPa), G (GPa), R (Micron) AND Sy (GPa)
26.8, 34.5                   ;MATRIX E (GPa) AND FAILURE STRESS (MPa)
3.2e-3,1.3e-3,7e-4,7e-4,1e-4 ;FRICTION COEFFICIENT TAUi, TAU2, TAU3, TAU4 AND TAU5
                             (GPa)
1000                         ;ELEMENTS ALONG THE LENGTH OF THE FIBER
1000                         ;NO. OF DIFF. CRACK OPENING
1000*10.0                    ;INCREMENT IN OPENING  U (Micron?)
1000*0.0                     ;INCREMENT IN SHEARING V (Micron?)
11                           ;POINTS OF BOTTOM FOUNDATION (MUST BE ODD)
0.0,  0.0000, 0.0000         ;PRESCRIBED SPRING PROPERTIES
0.25, 0.19569, 0.4052        ;AT EACH POINT (HRI, RATIOKE, RATIOFRS)
0.5,  0.2338, 0.6692
0.75, 0.2623, 0.8716
1.0,  0.2807, 0.9803
2.0,  0.3308, 1.2066
4.0,  0.37408, 1.4686
10.0, 0.4273, 1.6849
16.0, 0.4532, 1.6949
22.0, 0.4671, 1.7421
33.0, 0.4773, 1.8034
3                            ;POINTS OF TOP FOUNDATION (MUST BE ODD)
1.0,  0.4152                 ;PRESCRIBED SPRING PROPERTIES
10.0, 0.4598                 ;AT EACH POINT (HRI, RATIOKE)
33.0, 0.49375
```

Figure E.7: Simulation Input File for Series Seven f'_c = 5,000 psi (34.5 Gpa), f_y = 138,500 psi (0.955 GPa)

```
40.                              ;EMBEDD LENGTH/RADIUS FOR THE FIBER
0.00001                          ;FIBER INCLINATION ANGLE (IN DEGREE)
200.0, 0., 250.0, 0.955          ;FIBER E (GPa), G (GPa), R (Micron) AND Sy (GPa)
26.8, 34.5                       ;MATRIX E (GPa) AND FAILURE STRESS (MPa)
2.5e-3,1.6e-3,1.1e-3,1.1e-3,3e-4 ;FRICTION COEFFICIENT TAUi, TAU2, TAU3, TAU4 AND TAU5
                                 (GPa)
1000                             ;ELEMENTS ALONG THE LENGTH OF THE FIBER
1000                             ;NO. OF DIFF. CRACK OPENING
1000*10.0                        ;INCREMENT IN OPENING  U (Micron?)
1000*0.0                         ;INCREMENT IN SHEARING V (Micron?)
11                               ;POINTS OF BOTTOM FOUNDATION (MUST BE ODD)
0.0,  0.0000, 0.0000             ;PRESCRIBED SPRING PROPERTIES
0.25, 0.19569, 0.4052            ;AT EACH POINT (HRI, RATIOKE, RATIOFRS)
0.5,  0.2338, 0.6692
0.75, 0.2623, 0.8716
1.0,  0.2807, 0.9803
2.0,  0.3308, 1.2066
4.0,  0.37408, 1.4686
10.0, 0.4273, 1.6849
16.0, 0.4532, 1.6949
22.0, 0.4671, 1.7421
33.0, 0.4773, 1.8034
3                                ;POINTS OF TOP FOUNDATION (MUST BE ODD)
1.0,  0.4152                     ;PRESCRIBED SPRING PROPERTIES
10.0, 0.4598                     ;AT EACH POINT (HRI, RATIOKE)
33.0, 0.49375
```

Figure E.8: Tensile Load Function in Simulation Source Code: Adapted function to account for shape of pull-out behavior

```
FUNCTION TENSILE(I,UOPEN,VOPEN,THETA,TAU,TAU2,TAU3,TAU4,
   *     TAU5,NELEMT,RFIBER,RATIO_LR,NSPAL,XSPAL)
C*************************************************************************
C        CALCULATE TENSILE LOAD FOR GIVEN OPENING
C        CANNOT DEAL WITH FIBER COMPRESSION LOADING
C*************************************************************************
    IMPLICIT REAL*8(A-H,O-Z)
    COMMON GK(6000,4),F(6000),U(6000),ELELNTH(3000),FKNOW(3000),
   *    XIBEAM,EFIBER,GFBEAM
    COMMON /CONST/SFIBER
    PI = 3.14159265
    A  = PI*(RFIBER**2)
C*************************************************************************
C        U2,U3,U4,U5 IN UNITS OF MICROMETERS
C        U2,U3,U4,U5 DEFINE THE PULL-OUT REGION IN WHICH TO USE A NEW TAU
C*************************************************************************
    U2 = 500
    U3 = 2000
    U4 = 8000
    U5 = (RATIO_LR*RFIBER)
    IF(I.GT.NELEMT) I = NELEMT
C*************************************************************************
C        DEFINING THE CERTAIN CONSTANTS
C*************************************************************************
    PMAX    = 2.0*PI*RFIBER*TAU*(RATIO_LR*RFIBER)
    DELTAMAX = (PMAX**2)/(4*PI**2*RFIBER**3*EFIBER*TAU)
C*************************************************************************
C        DETERMINE THE CASE
C*************************************************************************
    DELTA   = UOPEN*COS(THETA) + VOPEN*SIN(THETA)
    IF( DELTA .LT. 0.0) THEN
      WRITE(*,*) 'FIBER COMPRESSION OCCURS'
      STOP 2222
    ENDIF
    IF(DELTA.LT.DELTAMAX) THEN
C*************************************************************************
C        PRE-PEAK
C*************************************************************************
      PY = SQRT(4*PI**2*RFIBER**3*EFIBER*TAU*DELTA)
      ZEROLEN = PY/(2*PI*RFIBER*TAU)
      IF(BLENGTH(1,I).LT.(RATIO_LR*RFIBER-DELTA-ZEROLEN-XSPAL))THEN
        X = 0
```

```
      ELSE
        X = (BLENGTH(1,I)-(RATIO_LR*RFIBER-DELTA-ZEROLEN-XSPAL))
     *       /ZEROLEN
      ENDIF
      IF(X.GT.1.0) THEN
        X = 1.0
      ENDIF
     TENSILE = PY*X
     ELSE
C*************************************************************************
C        POST-PEAK :   CHOOSE BETWEEN FOUR DIFFERENT TAUS DEPENDING ON
C                      CRACK OPENING
C*************************************************************************
      IF(DELTA.GT.DELTAMAX.AND.DELTA.LE.U2)THEN
        TAUI=(TAU2-TAU)/(U2-DELTAMAX)*(DELTA-U2)+TAU2
        IF(BLENGTH(1,I).GT.(RATIO_LR*RFIBER-DELTA-XSPAL))THEN
          PY = TAUI*2*PI*RFIBER*(RATIO_LR*RFIBER-DELTA-XSPAL)
        ELSE
          PY = TAUI*2*PI*RFIBER*BLENGTH(1,I)
        ENDIF
      ELSE IF(DELTA.GT.U2.AND.DELTA.LE.U3)THEN
        TAUI=(TAU3-TAU2)/(U3-U2)*(DELTA-U3)+TAU3
        IF(BLENGTH(1,I).GT.(RATIO_LR*RFIBER-DELTA-XSPAL))THEN
          PY = TAUI*2*PI*RFIBER*(RATIO_LR*RFIBER-DELTA-XSPAL)
        ELSE
          PY = TAUI*2*PI*RFIBER*BLENGTH(1,I)
        ENDIF
      ELSE IF(DELTA.GT.U3.AND.DELTA.LE.U4)THEN
        TAUI=(TAU4-TAU3)/(U4-U3)*(DELTA-U4)+TAU4
        IF(BLENGTH(1,I).GT.(RATIO_LR*RFIBER-DELTA-XSPAL))THEN
          PY = TAUI*2*PI*RFIBER*(RATIO_LR*RFIBER-DELTA-XSPAL)
        ELSE
          PY = TAUI*2*PI*RFIBER*BLENGTH(1,I)
        ENDIF
      ELSE IF(DELTA.GT.U4.AND.DELTA.LE.U5)THEN
        TAUI=(TAU5-TAU4)/(U5-U4)*(DELTA-U5)+TAU5
        IF(BLENGTH(1,I).GT.(RATIO_LR*RFIBER-DELTA-XSPAL))THEN
          PY = TAUI*2*PI*RFIBER*(RATIO_LR*RFIBER-DELTA-XSPAL)
        ELSE
          PY = TAUI*2*PI*RFIBER*BLENGTH(1,I)
        ENDIF
      ENDIF
      TENSILE = PY
     ENDIF
     RETURN
     END
```

REFERENCES

ACI, "Refractory Concrete", ACI Publication SP-57, San Diego, 1977

ACI Committee 506, "State-of-the-Art Report on Fiber Reinforced Shotcrete", ACI 506.1R-84, 1984, pp.1-11,.

ACI Committee 363, "State-of-the-Art Report on High Strength Concrete", ACI 363R-92.

Alwan, J. M., Naaman, A. E., Hansen, W., "Pull-out Work of Steel Firbers from Cemetitious Composites: Analytical Investigation", Cement & Concrete Composites, Elsevier Science Publishers Ltd, England, 1992
American Iron and Steel Institute, "Designers Handbook: Steel Wire Committee of Rod and Drawn Wire Producers".

ASTM C 305 - 91, "Standard Practice for Mechanical Mixing of Hydraulic Cement Pastes and Mortars of Plastic Consistency

ASTM C 469 - 87a, "Standard Test Method for Static Modulus of Elasticity and Poisson's Ratio of Concrete in Compression"

ASTM C 39 - 86, "Standard Test Method for Compression Strength of Cylindrical Concrete Specimens"

ASTM C 136 - 92, "Standard Test Method for Sieve Analysis of Fine and Coarse Aggregates"

ASTM E 8M - 93, "Standard Test Methods for Tension Testing of Metallic Materials [Metric]"

ASTM (1987), "Standard Test Method for Static Modulus of Elasticity and Poisson's Ratio of Concrete in Compression" Standard C469 - 87a, Annual Book of ASTM Standards, Vol. , pp. 247 - 250.

ASTM (1993), "Standard Test Methods for Tension Testing of Metallic Materials [Metric]" Standard E8M - 93, Annual Book of ASTM Standards, Vol. , pp. 150 - 168.

ASTM (1991), "Standard Practice for Mechanical Mixing of Hydraulic Cement Pastes and Mortars of Plastic Consistency" Standard C305 - 91, Annual Book of ASTM Standards, Vol. , pp. 201 - 203.

ASTM (1986), "Standard Test Method for Compressive Strength of Cylindrical Concrete Specimens" Standard C39 - 86$^{\varepsilon}$, Annual Book of ASTM Standards, Vol. , pp. 20 - 23.

ASTM (1992),"Standard Test Method for Sieve Analysis of Fine and Coarse Aggregates" Standard C136 - 92, Annual Book of ASTM Standards, Vol. , pp. 79 - 81.

ASTM, "Standard Specification for Concrete Aggregates" Standard C33 - 92a, Annual Book of ASTM Standards, Vol. , 1992, pp. 10 - 11.

ASTM A 820 - 90, "Standard Specification for Steel Fibers for Fiber Reinforced Concrete"

ASTM C 511 - 85,"Standard Specification for Moist Cabinets, Moist Rooms, and Water Storage Tanks Used in the Testing of Hydraulic Cements and Concretes"

Bakker, W. T., "Refractory Concretes: Past, Present, and Future", ACI Publication SP-57, pp.12.

Bernstein, I. M., Peckner, D., "Handbook of Stainless Steels", McGraw-Hill, Inc., 1977.

Bentur, A., Mindness, S., "Fibre Reinforced Cementitious Composites", Elsevier Applied Science, New York, 1990.

Chi, J., "Micromechanical Modeling of Ductile-Fiber Reinforced Ceramics", 1992

Collings, E.W., King, H. W., "The Metal Science of Stainless Steels", The Metallurgical Society of AIME, Conference Proceedings, 107th AIME Annual Meeting in Denver, Colorado, March 2, 1978.

Gopalaratnum, A. M., Shah, S. P., "Tensile Failure of Steel Fiber-Reinforced Mortar", Journal of Engineering Mechanics, Vol. 113, No. 5, May, 1987.

Hurd, M. K., "Shotcrete restores Fire Island Light", Concrete Construction, April 1989, pp.400-401.

Kosmatka, S. H., & Panarese, W. C., "Design and Control of Concrete Mixtures", Thirteenth Edition, Portland Cement Association, 1988.

Lankard, D. R.., "Steel Fiber Reinforced Refractory Concrete", ACI Publication SP-57.

Leung, C. K. Y., Li, V. C., "Strength-based and Fracture based Approaches in the Analysis of Fiber Debonding", Journal of Material Science Letters, Vol. 9, pp. 1140-1142.

Leung, K. Y., Chi, J., "Derivation of Crack Bridging Force in Random Fiber Reinforced Brittle Matrix Composites through Micromechanics", to appear in ASCE Journal of Engineering Mechanics, 1995.

Li, V. C., Wang, Y., Backer, S., "Effect of inclining angle, bundling and surface treatment on synthetic fibre pull-out from a cement matrix", Composites, Vol. 21, No. 2, March 1990, pp.132-139.

Lydon, F.D., "Concrete Mix Design", Applied Science Publishers Ltd., 1982.

Marshall, P., "Austenitic Stainless Steels: Microstructure and Mechanical Properties", Elsevier Applied Science publishers, New york, 1984.

Mitchell Fibercon, "9th & Penn Parking Garage Renovation", On The Job, CSL 100 2M 0790.

Mitchell Fibercon, "Fibercon Strengthens I-10", On The Job, CSL 001 8/93

Morton, J., Groves, G. W., "The cracking of composites consisting of discontinuous ductile fibres in a brittle matrix - effect of fibre orientation", Journal of Materials Science, vol. 9, 1974, pp. 1436-1445.

Neville, A.M. & Brooks, J.J., "Concrete Technology", John Wiley & Sons, Inc., 1987.

Piggott, M. R., "Toughness in Obliquely-Stressed Fibrous Composites", J. Mech. Phys. Solids, 1974, Vol. 22, pp.457-468.

Portland Concrete Association, "High Strength Concrete", PCA Publication EB114.

Robinson, C., Colasanti, A., Boyd G., "Steel Fibers Reinforce Auto Assembly Plant Floor", Concrete International, April 1991

Robson, T. D., "Refractory Concretes: Past, Present, and Future", ACI Publication SP-57.

Schneider, B., "Development of Sifcon Through Applications", High Performance Fiber Reinforced Cement Composites, edtors Reinhardt, H. W., Naaman, A. E., RILEM 1992, pp.177-194.

Shah, S. P., Ouyang, C., "Mechanical Behavior of Fiber-Reinforced Cement-Based Composites", Journal of The American Ceramic Society, Vol. 74, no. 11, Nov. 1991, pp.2727-2738, 2947-2953

Stang, H., Li, Z., Shah, S. P., "Pullout Problem: Stress versus Fracture Mechanical Approach", Journal of Engineering Mechanics, Vol. 116, No. 10, October, 1990.

Swamy, R. N., Barr, B., "Fibre Reinforced Cements and Concretes: Recent Developments", Elsevier Applied Science, London, 1989
Wallis, S., "Fibrecrete at Cumberland Gap advances NATM in the US", Tunnels & Tunnelling, June 1992, pp.23-26.